Monitoring Pharmacological Manipulations in the Brain by fMRI in Combination with Neurochemistry and Electrophysiology: Setting the Technical Prerequisites for the Use of fMRI in Drug Screening and Diagnostics

Dissertation

der Mathematisch-Naturwissenschaftlichen Fakultät
der Eberhard Karls Universität Tübingen
zur Erlangung des Grades eines
Doktors der Naturwissenschaften
(Dr. rer. nat.)

vorgelegt von
MSc Veronika von Pföstl
aus Meran, Südtirol, Italien

Tübingen
2012

The research work described herein, was conducted under the supervision of Dr. med. Alexander Rauch, Prof. Dr. Stefan Laufer and Prof. Dr. Nikos Logothetis in the Department of Physiology of Cognitive Processes, Max Planck Institute for Biological Cybernetics, Tübingen from the 29.01.09 to the 31.07.12.

Tag der mündlichen Qualifikation:	25.07.2012
Dekan:	Prof. Dr. Wolfgang Rosenstiel
1. Berichterstatter:	Prof. Dr. Nikos Logothetis
2. Berichterstatter:	Prof. Dr. Stefan Laufer

Acknowledgments

I would like to express my gratitude to those people that gave me the support and encouragement to start, conduct and complete this thesis. My thanks go to my family, colleagues and friends who accompanied me during this work, in particular...

- I am very grateful to my supervisor, Prof. Dr. Nikos Logothetis for his support in all phases of this work and for the excellent opportunity of being a PhD student in his department.

- Dr. Alexander Rauch for his supervision, constant encouragement, support and inspiration.

- Prof. Dr. Stefan Laufer for his advice and suggestions

- Our team: Juan Li, Sneha Viswanath, Ulrike Passlack, Nadine Serr and Daniel Zaldivar for the support and good cooperation and the fun during the experiments

- Simon Musall and Dr. Kevin Whittingstall for the good collaboration and helpful discussions

- Dr. Jozien Goense and Yvette Bohraus for all the suggestions and help, in particular for scanning and setting up the FAIR protocols

- Dr. Xiaozhe Zhang for his collaboration and support

- the members of my defense committee Prof. Dr. Michael Lemmerhofer and Prof. Dr. Peter Ruth, for their time to go through my dissertation and taking part of my final exam.

- The technicians in the department for their support:
    - Mark Augath and Thomas Steudel for running the fMRI scanners
    - Deniz Ipek, Golda Wendel and Mirko Lindig for their support during animal preparation and anesthesia
    - Our system administrators: Joachim Werner, Michael Schnabel
    - The animal caretakers Marcel, Hannes and Alex and our vet Pedro Douay
    - All the members of our two workshops
    - Axel Oeltermann for his helpful suggestions
    - Conchy Moya

Veronika von Pföstl

Table of contents

1. Abbreviations:

fMRI	Functional magnetic resonance imaging
phMRI	Pharmacological functional magnetic resonance imaging
BOLD signal	Blood oxygenation level dependent signal
EEG	electroencephalography
CBF	Cerebral blood flow
CBV	Cerebral blood volume
$CMRO_2$	Cerebral metabolic rate of oxygen
AD	Alzheimer's disease
EBF	Extracellular brain fluid
BBB	Blood brain barrier
MUA	Multiunit activity
LFP	Local field potential
V1	Primary visual cortex, visual area 1
ROI	Region of interest
NM	Neuroactive molecules and metabolites
HILIC	hydrophilic liquid interaction chromatography
ESI-MS	electro-spray ionization mass spectrometry

Ach	Acetylcholine
Lac	Lactate
Pyr	Pyruvate
Gln	Glutamine
Glu	Glutamate
ANOVA	Analysis of variance
SC	Spatial coherence
RMSE	Root mean square error
FAIR	flow-sensitive alternating inversion recovery
ATP	Adenosine triphosphate
Na/K ATPase	Sodium/potassium Adenosine triphosphatase
NAD^+/NADH	Nicotinamide adenine dinucleotide / Nicotinamide adenine dinucleotide reduced form

2. Summary:

In the drug development of neurological disorders and in the early diagnostic of such diseases fMRI can become a powerful tool due to its non-invasiveness. However the systematic use of this method needs a deeper understanding of the nature of the measured BOLD signal. The BOLD signal is not a direct measure of neuronal activation but relies on a cascade of metabolic and vascular responses generated by the energy demands of activated cells. We perform pharmacological manipulations to target single steps in this cascade and study the underlying mechanisms of neurovascular coupling. To correctly interpret drug induced BOLD fMRI changes we need corroborating evidence: In parallel to the BOLD fMRI studies we use electrophysiological measurements to define the underlying neuronal activity and neurochemical analysis to define the neurotransmitters or metabolites responsible for changes in the BOLD and electrophysiological signal. The correlation of these different signals and the drug induced changes thereof give further insights into the underlying mechanisms of neurovascular coupling and the generation of the BOLD signal. In our preliminary studies we set the technical prerequisites for a combined and parallel use of fMRI, EEG and systemic neurochemistry for drug screening and diagnostics in the future. We studied the impact of lidocaine on the electrophysiological signal, BOLD signal and EEG. This manipulation dissociates the BOLD and the EEG signals due to a different impact of neuronal synchrony on those signals. Simultaneous EEG-fMRI is becoming more and more a standard technique in clinics and therefore can have important implications in early diagnostics; our results will help to elucidate the relation and possible dissociations of simultaneous EEG-fMRI data. In addition, we examined the relation of different neurotransmitters and metabolites trough blood brain barrier. To study these relations we used microdialysis in brain and blood followed by neurochemical analyses. In the future these findings will help us to extrapolate brain concentrations of relevant compounds from non-invasively measured blood concentrations. This approach can be applied to study blood brain barrier penetrability parameters of drugs or if neurochemical changes in neurodegenerative diseases are reflected in the blood. Furthermore we can trace even subtle changes of plasma lactate concentrations with an increase of the BOLD signal. This finding indicates that the metabolite lactate plays an important role in the neurovascular coupling cascade: The physiologic formation of lactate during neuronal activation is one of the

mechanisms causing the vasodilatation which is responsible for the BOLD effect. On the other hand during neurodegenerative diseases like Alzheimer's this mechanisms are disrupted. Therefore our lactate challenge might be of diagnostic use having a different impact in healthy subjects versus Alzheimer patients.

3. Zusammenfassung:

Durch seine nicht Invasivität hat fMRI das Potential in Zukunft eine sehr wichtige Rolle in der Entwicklung von Medikamenten gegen neurologische Pathologien und in der Früherkennung derselben zu spielen. Zur systematischen Anwendung dieser Methode braucht man allerdings ein klareres Verständnis des gemessenen BOLD Signals und seiner Grundlagen. Dieses Signal entsteht durch eine Kaskade von metabolischen und vaskulären Abläufen, die die Antwort auf den metabolischen Bedarf aktivierter Neuronen sind. Deshalb kann dieses Signal nicht als direktes Maβ der neuronalen Aktivität gesehen werden. Um die Mechanismen, die das BOLD Signal erzeugen zu erforschen, beeinflussen wir einzelne, spezifische Schritte in der Kaskade der neurovaskulären Kopplung mit entsprechenden Medikamenten. Um diese durch Medikamente hervorgerufenen Effekte auf die neurovaskuläre Kopplung besser zu verstehen brauchen wir zusätzliche, ergänzende Informationen: Deshalb messen wir neben dem BOLD Signal auch noch die neuronale Aktivität mit Elektrophysiologie und definieren mit neurochemischen Analysen welche Neurotransmitter oder Metaboliten für die BOLD und elektrophysiologischen Effekte verantwortlich sind. Die Korrelation dieser verschiedenen Signale und die durch pharmakologische Manipulationen induzierten Veränderungen dieser Korrelationen helfen uns die Grundlagen der neurovaskulären Kopplung und die Entstehung des BOLD Signals besser zu verstehen. Mit unseren Experimenten versuchen wir die technischen Voraussetzungen zu erarbeiten um die gleichzeitige Anwendung von fMRI, EEG und systemischer Neurochemie in der Entwicklung vom Medikamenten und der klinischen Diagnostik zu etablieren. Wir haben den Einfluss von Lidokain auf das elektrophysiologische Signal, das BOLD Signal und EEG analysiert. Die lokale Injektion von Lidokain in V1 verursacht die Verstärkung des EEG Signals durch Zunahme der neuronalen Synchronität bei gleichzeitger Abschwächung der lokalen individuellen Aktivität der Neuronen und des BOLD Signals. Dieses Ergebnis unterstreicht die Wichtigkeit der neuronalen Synchronität in der Bildung des EEG Signals. Andererseits könnte der fehlende verstärkende Einfluss der neuronale Synchronität auf das BOLD Signal die Dissoziation zwischen EEG und BOLD Signal erklären. Unsere Beobachtungen sind sehr wichtig in der Interpretation von gleichzeitig gemessenen EEG-fMRI Daten. In einem anderen Experiment haben wir das Verhältnis verschiedener Neurotransmitter und Metaboliten in Hirn und Blut erforscht. Wir entnahmen dafür Proben der extrazellulären Hirnflüssigkeit und des

Blutplasmas mit Mikrodialyse und führten neurochemische Analysen durch. In Zukunft werden diese Ergebnisse uns helfen durch die Analyse der Konzentration einer Substanz im Blut Rückschlüsse auf deren Konzentration im Hirn zu ziehen. Diese Herangehensweise könnte dazu benutzt werden die Permeabilität der Blut-Hirn Schranke für Medikamente zu testen oder ob neurochemische Veränderungen in neurodegenerativen Krankheiten im Blut feststellbar sind. Ausserdem haben wir bestätigt, dass auch kleinste Konzentrationsveränderungen eines Metaboliten wie Laktat mit dem BOLD Singal messbar sind. Dieses Resultat bestätigt die Theorie dass Laktat eine wichtige Rolle in der neurovaskulären Kopplung spielt: Aktivierte Neuronen produzieren Laktat und dieser Metabolit erweitert die Gefäße. Des Weiteren ist eine Gefäßerweiterung als Antwort auf neuronale Aktivität einer der Faktoren die dem BOLD Effekt zu Grunde liegen. Diese Mechanismen sind in neurodegenerativen Pathologien dereguliert. Deshalb können wir annehmen, dass Laktat unterschiedlichen Einfluss auf das BOLD Signal von gesunden Subjekten und Alzheimer Patienten hat. Unser Laktat fMRI Protokoll könnte darum auch in der Früherkennung von Alzheimer benutzt werden.

4. List of Publications:

Accepted:

1. Veronika von Pföstl, Juan Li, Daniel Zaldivar, Jozien Goense, Xiaozhe Zhang, Nadine Serr, Nikos K. Logothetis and Alexander Rauch. „Effects of lactate on V1 of non-human primates investigated by pharmaco-MRI and neurochemical analysis.” Neuroimage 61(1): 98-105.

2. Juan Li, Veronika von Pföstl, Daniel Zaldivar, Xiaozhe Zhang, Nikos K. Logothetis and Alexander Rauch. „Measuring multiple NMs in blood and brain of the rhesus monkey by microdialysis and capillary HILIC-MS.” Anal Bioanal Chem 402(8): 2545-54.

Under review:

3. Simon Musall, Veronika von Pföstl, Alexander Rauch, Nikos K. Logothetis and Kevin Whittingstall. "Effects of neural synchrony on surface EEG." Submitted to Cerebral Cortex

5. Contributions to the publications and manuscripts

(Darstellung des Eigenanteils bei Gemeinschaftsarbeiten nach § 9 (2))

Study 1 Veronika von Pföstl, Juan Li, et al. Effects of lactate on V1 of non-human primates investigated by pharmaco-MRI and neurochemical analysis. Neuroimage 61(1): 98-105.

Veronika von Pföstl's contribution for study 1

Experiment design, manuscript writing and extensive literature search.

fMRI: development of the pharmaco MRI protocol: we perform a control scan to determine visually modulated voxels and then the injection scan. This allows us to monitor the drug induced effect on visually modulated voxels without the need of an a priori determined pharmacokinetic function as a regressor to find relevant voxels. Veronika von Pföstl programmed an online read out routine for the fMRI data which allowed us to observe the drug induced changes on the BOLD signal during the fMRI scan. Based on this algorithm we could adapt the injection to the needs of the subject during the experiment if necessary. Preparation of the fMRI setup, positioning the transmit - receive coils on the monkeys head and positioning of the monkey in the fMRI scanner. Design and continuous optimization of a chair and head holding system which allows us to position monkeys without invasive, surgical implantation of a head holder.

Electrophysiology and microdialysis sampling: experimental protocol, preparation of the custom made electrophysiology setup for recordings in anesthetized non-human primates: preparation of the equipment and software, setup of the recording and stimulation devices; positioning of the monkey on the neurophysiology table (positioning of the head according to stereotactic coordinates to precisely position probes and electrodes); surgical procedures (trepanation hole in the skull, placing sampling probes and electrodes); plasma sampling preparation: insertion of the catheter and positioning of the microdialysis probe in the catheter.

Anesthesia: Generally we used an anesthesia protocol which is fully compatible with the procedures in anesthesia of small children. Hence it requires extensive experience and skills to warrant the optimal outcome of the experiment and the safety of the animal. Preparation of the equipment (different in fMRI and electrophysiology experiments) and drugs, preparation of the monkey for the anesthesia, induction of the anesthesia, insertion of the catheter for the infusion of the anesthetics, intubation of the monkey and supervision of the anesthesia (human standards): operating the ventilator and adaptation of the anesthetics and the muscle relaxant to maintain optimal anesthesia levels for the monkey.

Drug injection: contributed to the design of the custom made pumps (one for local the other for systemic injections) which were operated by custom written software; fabrication of the injectors for local and systemic application; maintenance and operation of the pumps, determination of the injected dosage and preparation of the injected drug.

Data analysis based on custom written MATLAB software by Veronika von Pföstl: fMRI, microdialysis and electrophysiology data

Juan Li's contribution to study 1

Neurochemical analysis

For a detailed description see the points LC-MS and microdialysis sampling in study 2.

Helping and assisting the Manuscript writing, especially for neurochemical analysis parts and corresponding, extensive reference search.

Data analysis for neurochemical analysis parts

Assisting: drug preparation, drug injection, monkey preparation, probe insertion

Study 2 Juan Li, Veronika von Pföstl, et al. Measuring multiple NMs in blood and brain of the rhesus monkey by microdialysis and capillary HILIC-MS. Anal Bioanal Chem 402(8): 2545-54.

Juan Li's contribution to study 2

Experiment design and manuscript writing and corresponding, extensive literature search.

LC-MS: Juan operated the LC-MS system and developed the LC-MS methods and protocols by her own. Before the MS experiment, Juan did the calibration of the MS system, to make sure that the MS reaches the best specificity and selectivity. Juan optimized the MS for each analyte, including parameters such as ICC smart target and accumulation time, capillary, end plate offset, skimmer, cap exit, oct dc, oct RF, lens and trap driver. The optimized MS/MS parameters include isolation mass and width, fragmentation cutoff and ampli. Juan packed the LC column (HILIC column) in our lab and optimized the LC parameters with different mobile phases, including pH value, buffer concentration and the gradient of elution. Afterwards, Juan did the validation test of the developed LC-MS method. Juan prepared all the solution for the LC-MS experiment, such as stock solution, calibration solution, internal standards solution, calibration curves, and mobile phase. Juan did the daily, weekly and monthly maintenance for LC-MS system, which include the filling of nitrogen, cleaning the spray chamber, spray shield, capillary cap, and capillary, replacing the nebulizer needle, changing rough pump oil. Juan operated the LC-MS Chemstation for the LC-MS sequence, data analysis and quant analysis.

Microdialysis: The microdialysis sampling was used to collect the brain and blood samples. Before the in vivo microdialysis sampling, the in vitro test was conducted by Juan. Different probe membranes were tested, such as the membrane material (PAES, PES cuprophane and cellulose), diameter and flow rate. The probe with best recovery, stability and reproducibility was used for the further in vivo experiments. Juan prepared the microdialysis samples before and after the sampling, as well as the perfusion solution (a-CSF solution).

Assisting: monkey preparation, probe insertion

Data analysis with SPSS software

Veronika von Pföstl's contribution to study 2

For a detailed description see the points Electrophysiology and microdialysis sampling, and Anesthesia in study 1.

Helping and assisting the Manuscript writing, especially for anesthesia and animal preparation.

Data analysis

Study 3 Simon Musall, Veronika von Pföstl, et al. "Effects of neural synchrony on surface EEG." Under review in Cerebral Cortex

Veronika von Pföstl's contribution to study 3

Design of the injection protocol and help with the experimental protocol.

Preparation of the custom made electrophysiology setup for recordings in awake non-human primates

Injection: See the point Drug injection in study 1. Insertion of the injector to V1 and assisting in the insertion of the electrodes.

Data acquisition

Assisting to the analysis, literature search and manuscript writing

6. Introduction

Functional magnetic resonance imaging (fMRI) is one of the most frequently used neuroimaging techniques for basic and clinical brain research in humans, and is used surprisingly less often for clinical diagnostics (Jezzard and Buxton 2006). The effects of a pharmacological manipulation on the functional activation of the brain can be examined with fMRI (Borsook et al. 2006), therefore a systematic application of this method in drug development and diagnostics can be envisioned. The time course of drug induced changes can be assayed non-invasively and relatively quick with pharmaco fMRI (phMRI) in laboratory animals and also in humans. With phMRI the different sensitivity to a pharmacological challenge in health and the early stage of a neurodegenerative disease could be exploited for diagnostics. However this potential till now is not fully exploited because of the difficulty to interpret the measured blood oxygenation level dependent (BOLD) signal and its underlying neuronal and neurochemical correlates. The BOLD signal is not a direct measure of neuronal activation but it relies on metabolic and vascular responses generated by the energy demands of activated cells. This signal reflects changes in cerebral blood flow (CBF), cerebral blood volume (CBV) and the metabolic rate of oxygen ($CMRO_2$) in response to neural activation (neurovascular coupling). Various metabolites and neurotransmitters play a crucial role in the cascade of physiological events that links neural activity the generation of the BOLD signal. Neurodegenerative disorders and pharmacological manipulations can potentially interact with any of the steps of neurovascular coupling which makes the interpretation of the BOLD signal difficult. Therefore before fMRI can be used for diagnostics further studies disentangling the underlying mechanisms of BOLD under physiological conditions need to be preformed. Any of the steps in the neurovascular coupling cascade can be targeted with a specific pharmacological manipulation; this procedure generates a characteristic BOLD response which is potentially drug specific. This approach delivers hints about the importance of single steps in this cascade, the mechanisms of the neurovascular coupling cascade in general and thus a better understanding of the generation of the BOLD signal. However to really pinpoint the mechanism by which this pharmacological manipulation induces changes to the BOLD signal further corroborating evidence is needed (Iannetti and Wise 2007). We combine fMRI with neurochemistry and electrophysiology to provide this corroborating evidence; that allows us to compensate for the shortcomings of the individual

methods. By using neurochemical analysis we can test how the pharmacologically altered neurochemical setting in the brain is reflected in the BOLD signal and see if one or more neurotransmitter or metabolites cause changes in this signal. In addition by using electrophysiology we can study the impact of manipulating one step in the neurovascular coupling cascade on the BOLD signal and neuronal activity.
With our approach we want to validate the concomitant use of both invasive (local electrophysiology, injections and microdialysis sampling) and non-invasive techniques (fMRI, EEG, systemic injections and microdialysis) in non-human primates. The correlations of neuronal activity, neurochemical changes and the BOLD signal help us to get a clear picture of the underlying effects of the BOLD signal and its possible implications for clinical diagnostics. Once we understand the relations and correlations between invasive and non-invasive techniques we can focus on setting up an experimental protocol using non-invasive methods alone. If this protocol is established we can translate it to clinics and test for its diagnostic potential in humans. In the following paragraphs I describe three projects which follow that outlined rationale and are important steps in the simultaneous application of phMRI, plasma sampling and EEG in clinical diagnostics.

In a first test of this concept we observed the effect of systemic lactate injections on the BOLD signal and how that relates to plasmatic lactate levels. This experiment confirms the hypothesis (Magistretti and Pellerin 1996) that lactate plays an important role in neurovascular coupling and contributes to the generation of the BOLD signal. Furthermore this protocol might be of use in the early diagnosis of Alzheimer's disease (AD). There are indications that cerebral metabolism and neurovascular coupling are disrupted in AD and that these alterations worsen during the progression of the disease (Mentis et al. 1998; Redjems-Bennani et al. 1998; Reiman et al. 2001; Iadecola 2004; Reiman et al. 2004; 2005). Furthermore it is known that patients at an advanced stage of the disease - in contrast to healthy subjects (Reiman et al. 1989; Mintun et al. 2004) - do not show any cerebral blood flow changes after a lactate challenge (Kalman et al. 2005). It is likely that the brain suffering from this neurodegenerative disorder adapts to the altered metabolism and consequently the sensitivity to a lactate challenge decreases during the progression of AD. Our experimental protocol would be a rapid and non-invasive tool to validate this hypothesis. The application of lactate might be a biomarker for an early diagnosis of AD:

This protocol helps to differentiate between healthy subjects who present an effect and patients at an early stage of AD who are insensitive to our low dose infusion.
In our second project we studied neurochemical levels in brain and in the blood and determined the relation of these substances across blood brain barrier. This approach might have a future application in the early diagnosis of AD. In this pathology it would be important to know if alterations in the balance of different neurotransmitters (Craig et al. 2011) and the cerebral metabolism (Redjems-Bennani et al. 1998) are reflected in the blood system. Once this is established one could screen non-invasively for potential biomarkers for neurodegenerative diseases in the blood system. These biomarkers could be concentration changes of single substances, the change of metabolic ratios like lactate/pyruvate or also the change of the neurochemical environment (several different neurotransmitters).
In the third project we use non-invasive fMRI, EEG and invasive electrophysiology together to see how these signals relate to each other and the effect of a pharmacological manipulation with lidocaine on these signals. This approach gives us further insight into the relation of BOLD and EEG and if those signals are produced by the same neuronal generators. This is an important step in the direction of a routine use of simultaneous EEG-fMRI in drug screening and clinical diagnostics of AD for example. Markers for AD have been found in both the EEG and the fMRI signal separately (Bookheimer et al. 2000; Drago et al. 2011). Since EEG and BOLD fMRI signal complement each other using both methods simultaneously we can exploit the high spatial resolution of fMRI and the specificity to neuronal activity and high temporal resolution of EEG (Rosenkranz and Lemieux 2010).

6.1. Neurochemistry:

The extracellular brain fluid (EBF) contains an entire range of neurotransmitters, neuromodulators and different metabolites involved in neural transmission. Their changes in time reflect changes in neuronal activity, homeostasis or in general brain function in health and disease (Zhang et al. 2007; Zhang et al. 2008). A pharmacological manipulation changes this neurochemical setting in the brain: the injected drug can trigger metabolic reactions and the release of neurotransmitters. We qualitatively and quantitatively monitor the changes of multiple neurochemicals with microdialysis sampling of the extracellular brain fluid (EBF) and HILIC-

MS. Since the blood brain barrier prevents free diffusion of polar solutes into and out of the CNS, blood and brain concentrations do not relate to each other in a linear way (Begley 2004). Therefore simultaneously to the EBF we sample blood plasma and determine the concentrations of neurotransmitters and metabolites in the blood. With this approach we can establish the relation between blood and brain concentration of neuroactive compounds which can then be used to extrapolate from non-invasively acquired blood measurements to brain concentrations. With this experimental setup we are able to study blood brain penetrability parameters of neurotransmitters, neuromodulators, metabolites and drugs.

6.2 Electrophysiology:

In a first approach our group applied the anesthetic lidocaine locally to V1 during an fMRI experiment combined with electrophysiological recordings (Rauch et al. 2008). Lidocaine blocks neuronal firing in the cortical area where it is applied; this is reflected in the electrophysiological signal where both multi unit activity (MUA) and the local field potential (LFP) are reduced. Also in the BOLD signal the stimulus-induced modulation is reduced during drug application. Furthermore we can dissociate LFP and MUA pharmacologically and analyze the impact of this dissociation to the BOLD signal (Rauch et al. 2008). The activation of 5-HT 1A receptor causes hyperpolarization in efferent neurons raising the threshold for the spiking output. Because of this gatekeeper function during a pharmacological manipulation with a 5-HT 1A agonist (BP 554) MUA is reduced. On the other hand, LFP remain largely intact because thalamic and corticocortical inputs continue to stream to the network and keep generating local synaptic activity. Also the BOLD activity remains intact suggesting that the efferents of a neuronal network pose relatively little metabolic burden compared with the overall presynaptic and postsynaptic processing of incoming afferents. These results are in line with the finding that BOLD activation in the region of interest reflects the incoming input and the local processing (local field potential, LFP) more than the spiking activity (multiunit activity, MUA) (Logothetis et al. 2001).

My third project is a continuation of the BOLD/electrophysiology study with a local lidocaine injection. We wanted to test the impact of this injection on the EEG signal and compare that effect to the already described BOLD effect. The understanding of this relation is important since

simultaneous EEG-fMRI is more and more used for basic neuroscience and clinical research. It has long been assumed that the surface EEG signal depends on both the amplitude and spatial synchronization of underlying neural activity; though the impact of their respective contribution is still not clear. In a first approach to study this relation we used a local lidocaine injection to V1 using the same injection protocol as in our earlier study (Rauch et al. 2008) while measuring LFPs, MUA and the EEG signal. We decrease neuronal activity with lidocaine, at the same time also the BOLD signal decreases (Rauch et al. 2008). In contrast to the decrease in neuronal activity we observed an increase in neuronal synchrony during lidocaine injection. We set out to measure what happens to the EEG if we dissociate neuronal power and synchrony. We found that during lidocaine application the EEG amplitude increases, most likely because of an increase in neuronal synchrony. On the other hand we already described a lidocaine induced decrease in the BOLD signal. This finding is important for the interpretation of simultaneous EEG-fMRI data since it indicates that a dissociation of EEG and fMRI data could be explained by the different impact of neuronal synchronization on those signals.

6.3 Pharmaco MRI

With pharmaco MRI we can measure drug induced changes in the brain using the BOLD signal. This method offers the possibility to do fast and non-invasive pharmacodynamic assays, furthermore it could be used to establish brain-penetrability parameters or dose-response relations (Leslie and James 2000). Moreover pharmaco MRI might have diagnostic use: for example in the different sensitivity of the BOLD signal to a pharmacological challenge in health and the early stage of a disease. Alzheimer patients for example show abnormalities in the regulation of cerebral metabolism and potentially neurovascular coupling (Iadecola 2004). Before one can investigate how these abnormalities affect the blood oxygenation level-dependent (BOLD) signal we should focus on the question of how physiological events like the formation of lactate contribute to the BOLD signal. Lactate is produced during neuronal activation (Prichard et al. 1991; Hu and Wilson 1997), furthermore this metabolite has a vasodilatative effect (Reiman et al. 1989). Altogether these facts suggest a pivotal role of lactate in neurovascular coupling (Mangia et al. 2009). We set out to study fMRI responses in the non-human primate brain following moderate increases of systemic lactate concentration. To mimic

the physiological formation of lactate we used direct systemic application and measured BOLD contrast in the early visual cortex of anesthetized macaques, while monitoring blood concentration using microdialysis (venous catheter). In addition, we monitored lactate induced changes in cerebral blood flow and its effect on neuronal activity to study underlying mechanisms of the lactate effect. This experiment is a good example for the translational potential of our approach: Part of the study still relies on invasive methods to detect underlying mechanisms but the gross part is non-invasive and directly applicable in humans after minor adaptations.
In order to perform these experiments we had to meet certain requirements: we had to establish a non biased method to select relevant voxels and ensure a precise and continuous drug application; these two points will be explained in the next subchapters.

6.3.1 Voxel selection:

Since the BOLD signal is a relative signal, it has to be referenced to a regressor in order to find relevant voxels and see an effect. There are several regressors that can be used as a reference to the BOLD signal; for example a regressor reflecting stimulus induced changes or task induced modulation of the brain activity (Sheline et al. 2001; Goekoop et al. 2004; Gerdelat-Mas et al. 2005; Loubinoux et al. 2005). In addition, in many pharmaco MRI studies the drugs plasma concentration or a model of it is used as a regressor for voxel selection (Stein et al. 1998; Gozzi et al. 2006). Also an a priori selection of regions of interest (ROI) for a certain drug can be used (Schwarz et al. 2004; Ceolin et al. 2007) and the average signal of this area can be observed over time to find drug induced changes. We use phMRI to extract pharmacodynamics directly from the BOLD signal data without using a regressor based approach during the actual drug application phase to warrant an unbiased view on the induced BOLD dynamic by the drug. To do so we need to select relevant voxels without jeopardizing our selection by biasing towards a certain pharmacodynamic based regressor. For our experiments we use an unbiased method to select relevant voxels: We select a ROI covering primary visual cortex (V1). This is the best studied area in the cortex (Hubel and Wiesel 1977) and the distribution and densities of different receptors in V1 is well known (Rakic et al. 1988; Lidow et al. 1989; Eickhoff et al. 2008). We determine visual stimulus-modulated voxels in a short scan before the actual injection scan by

calculating the correlation to a boxcar model of the stimulus paradigm convolved to the haemodynamic response function. The voxels selected by this paradigm are then monitored during the injection and their timecourse used for further analysis and the extraction of pharmacodynamic variables. Hence the selection is based on the criteria of visually induced modulation before the actual drug application and is independent of any a priori assumption regarding the evolving pharmacodynamic effect.

6.3.2 Pump and injection:

For both systemic and local injections we use custom-made, pressure-operated pumps. During drug application flow and applied volume are monitored with high-precision flow meters (Sensirion, Switzerland). The careful monitoring assures that the right amount of drug is infused during a certain time window. The pressure operated pump enables a careful drug application in the sense that the infusion is slow with no sudden changes in application pressure or volume. This is important for the local application since applying too much volume too fast would disrupt the microenvironment potentially changing neuronal activity or even damaging the neurons. For local injections a custom-made injector was build consisting of a triple-barrel glass tube which contained three sharpened injection lines which entered cortex. For the systemic injection we use a glass capillary directly connected to the infusion line for Jonosteril electrolyte solution and the anesthetics. Thereby we can apply low volumes of a concentrated solution of the drug to a continuous infusion of electrolyte solution (10 ml/kg/h). The electrolyte solution dilutes the applied drug and ensures that any pH changes stay within a small range. Our pressure operated pump prevents a too fast application of a large volume of drug which could disrupt the haemodynamics (blood pressure) causing a change in the BOLD signal. For the systemic injections we programmed Matlab functions (The MathWorks, Natick, MA, USA) to provide an online readout of the infusion parameters and also the BOLD effect, in this way we can dynamically adapt the dosage according to the needs of the subject.

7. Aim of the study

In the drug development for neurological disorders and in the early diagnostic of such diseases fMRI can become a powerful tool due to its non-invasiveness. It offers a proper temporal resolution combined with a high spatial resolution which allows us to investigate region specific pharmacodynamics or changes of metabolism and neuronal activity induced by neurodegenerative disorders. Hence we set out to investigate about the technical prerequisites which would enable us to envision such diagnostic and developmental use for pharmaco fMRI. The systematic implementation of fMRI in diagnostics and drug screening needs representative studies to better understand the underlying mechanisms of the blood oxygenation level dependent (BOLD) signal. The BOLD signal is not a direct measure of neuronal activity but relies on metabolic and vascular responses generated by the energy demands of active neurons. Neural activity is coupled to the generation of the MRI signal trough a cascade of physiological events where various metabolites or neurotransmitters play a role. Neurodegenerative disorders and drugs can interact and modify different steps in this cascade, affect the BOLD signal and render its interpretation even more difficult. For diagnostics we need to be able to interpret the fMRI findings correctly and pinpoint the mechanisms by which the pathology or drugs change the BOLD signal. Therefore we use specific pharmacological manipulations which target individual sites in the neurovascular coupling cascade which elucidates the underlying mechanisms of the neurovascular coupling and the generation of the BOLD signal. To substantiate these findings on the BOLD signal, corroborating evidence is needed to better interpret the pharmacologically induced effects (Iannetti and Wise 2007). We decided to combine different methods in parallel to compensate for the shortcomings of the single methods alone: phMRI offers spatial resolution over the whole brain, electrophysiology measures the neuronal activity offering a good temporal resolution and neurochemistry offers the qualitative and quantitative determination of relevant neurotransmitters and metabolites. The correlation of these signals to each other helps to better understand the underlying mechanisms of the BOLD signal: With neurochemistry we find the substance mainly responsible for the observed changes in the electrophysiology and the BOLD. With electrophysiology we determine neuronal effects underlying the BOLD effect and how they are related to neurochemical changes. Part of these methods are invasive like local electrophysiology, injections and microdialysis sampling, others are non-invasive like EEG, systemic injections and microdialysis. In the starting phase of our

project invasive and non-invasive methods will be used in parallel but later our findings will be exploited for diagnostics in humans only using the non-invasive part of our approach, blood sampling and fMRI combined with systemic injections. By using both invasive and non-invasive methods in parallel we can determine the relation of these signals to each other under different pharmacological regimes. For example the use of fMRI and EEG together with electrophysiology will allow us to better understand underlying mechanisms of both signals, dissociations between these signals and their potential causes. In addition, the neurochemical analysis of neuroactive substances (neurotransmitters, neuromodulators and metabolites) in the blood and the brain in parallel will allow us to establish their relation across the blood brain barrier (Li et al. 2011). Once these relations are known we can extrapolate to the cortical concentration by measuring the blood concentration alone, non-invasively. In the study ”Effects of lactate on the early visual cortex of non-human primates, investigated by pharmaco-MRI and neurochemical analysis” we mainly relied on this non-invasive approach (von Pföstl et al. 2012). The results show that our chosen approach is indeed successful; we were able to track a slow infusion of lactate using fMRI which correlated well with the changes in plasma lactate levels. Since interindividual differences are also expected in humans it is of relevance that even in a heterogeneous group of different non-human primates this protocol delivered reliable data. In a further step this protocol could be applied to humans after minor adaptations to test for its diagnostic potential in early stages of Alzheimer’s disease where lactate plays an important role.

8. Results and Discussion

8.1 Study 2: "Measuring multiple NMs in blood and brain of the rhesus monkey by microdialysis and capillary HILIC-MS"

We applied capillary HILIC-ESI/MS together with simultaneous blood and brain microdialysis sampling to measure the concentrations of five neuroactive substances from two anesthetized male non-human primates. The microdialysis probe in the brain was placed into the primary visual cortex (V1) through a small incision in the dura. The probe for blood sampling was placed into a superficial leg vein using an intravenous catheter. We determined the concentrations of acetylcholine, lactate, pyruvate, glutamine, and glutamate in dialysates from primary visual cortex and blood. The values we monitored in the brain were Ach 4.0±1.4 nM; Lac 220.4±90.9 μM; Pyr 21.3±8.3 μM; Gln 50.4±21.9 μM; Glu 1.1±0.2 μM and in the blood Ach 10.3±4.4 nM; Lac 511.3±78.7 μM; Pyr 91.5±37.6 μM; Gln 176.4±45.3 μM; Glu 26.7±5.3 μM.

Table 1 Concentrations of acetylcholine, lactate, pyruvate, glutamine, and glutamate in the dialysates of brain and blood

Compounds	Ach (nM)	Lac (μM)	Pyr (μM)	Gln (μM)	Glu (μM)
Brain	4.0 ± 1.4	220.4 ± 90.9	21.3 ± 8.3	50.4 ± 21.9	1.1 ± 0.2
Blood	10.3 ± 4.4	511.3 ± 78.7	91.5 ± 37.6	176.4 ± 45.3	26.7 ± 5.3

Values are given as mean ± standard error of the mean (S.E.M.); n=4.

To further understand the distribution differences of neuroactive substances across the blood brain barrier, respectively, between the brain and the blood, we examined and compared the lactate/pyruvate and glutamine/glutamate ratios between the brain and blood dialysates. These ratios reflect metabolic processes in the brain and their imbalance might indicate a pathology. The results showed that the concentration ratio of lactate/pyruvate and glutamine/glutamate was significantly different between the brain and the blood. The mean lactate/pyruvate ratio in the brain was 14.5, but only reached 9.0 in the blood system. The mean ratio of glutamine/glutamate in the brain was 53.4, significantly higher than the blood value of 7.9. One-way ANOVA analysis confirmed the statistical significance of these findings ($p<0.05$).

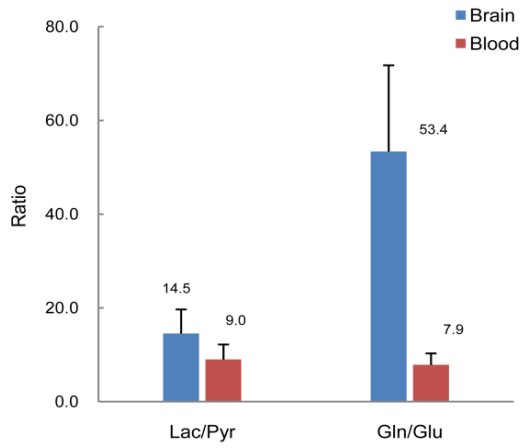

Figure 1 Comparison of lactate/pyruvate (Lac/Pyr) and glutamine/glutamate (Gln/Glu) in primary visual cortex and the blood system of rhesus monkey. Ratios of Lac/Pyr and Gln/Glu in monkey primary visual cortex were significantly higher than the blood system ($p<0.05$).

By using microdialysis and HILIC-MS we can determine the concentration of neuroactive compounds in brain and blood simultaneously. We have successfully demonstrated that our method can reliably quantify acetylcholine, lactate, pyruvate, glutamine and glutamate. Additionally we found that the concentration ratio of lactate/pyruvate and glutamine/glutamate was significantly different between the brain and the blood, reflecting the active transports and different metabolic processes between the blood and the nervous system respectively across the BBB. Quantified coupling parameters between the blood and the nervous system of neurotransmitters and metabolites are of outmost importance due to the possibility to extrapolate from non-invasively acquired blood measurements to brain concentrations. With this experimental setup we are able to study blood brain permeability of neurotransmitters, neuromodulators, metabolites and drugs. On one side we can study if neurometabolic imbalances due to pathologies are reflected in the blood system, on the other hand if a systemically administered drug passes BBB. The determination of the permeability of the blood brain barrier is a very important early step in drug development (Begley 2004) since the scarce permeability to the brain is the main reason to discard neuroactive drugs from clinical use. In addition, in pathologic conditions like Alzheimer's disease the balance of different neurotransmitters (Craig et al. 2011) and the cerebral metabolism (Redjems-Bennani et al. 1998) are disrupted. For the purpose of early diagnosis it would be important to know if these alterations are reflected in the blood system and screen for potential biomarkers for neurodegenerative diseases in the blood system. Although our findings are still preliminary for diagnosis, we consider the simultaneous

monitoring of blood and brain concentrations of important compounds a necessary step in the direction to get a clear understanding of their chemical relation across the BBB. On the basis of this data, extrapolations from the blood concentrations to brain concentrations of pathologically relevant neurochemicals might be envisioned. To further investigate the correlation of these NMs between the brain and the blood systems, we will use the developed analytical method to test the dynamic change of these neurochemicals across the BBB by pharmacologically simulating dysfunctional states of the brain.

8.2 Study 3: “Effects of neural synchrony on surface EEG”

We try to find experimental confirmation that the amplitude of a surface EEG measure is not only dependent on the magnitude of individual current dipole, but also on the degree of their temporal synchronization across space. This is due to the superposition principle, which suggests that the net sum of temporally coherent dipole sources is larger than that of their individual source magnitudes. We measure how the LFP amplitude and synchronization over space affect the surface EEG. We observe that trial-by-trial fluctuations in EEG power are not only reflected changes in neural activity but also the degree of temporal synchrony between LFP electrode pairs (spatial coherence - SC). In figure 2A we show the correlation between trial-by-trial fluctuations in LFP (ΔLFP), SC (ΔSC) and EEG (ΔEEG) in the drug-free baseline condition. The relationship between ΔSC and the difference in magnitude of ΔEEG and ΔLFP ($\Delta_{EEG-LFP}$) is of particular interest. The upper left quadrant of Figure 2A reflects trials where ΔLFP is negatively and ΔSC positively modulated. In these trials, also the average ΔEEG was significantly positively modulated. When ΔLFP was positive but ΔSC negative (bottom right quadrant) the average ΔEEG was also more negative. Accordingly, we found a high positive correlation between $\Delta_{EEG-LFP}$ and ΔSC (Figure 2B). We used both ΔSC and ΔLFP as regressors in a general linear model (GLM) to modulate ΔEEG. This is illustrated in Figure 2C for a subset of trial-by-trial measures of ΔEEG (red), ΔSC (black) and ΔLFP (blue) as well as modeled ΔEEG (dashed red line). The difference between ΔEEG and ΔLFP varies considerably across trials, indicating that ΔLFP alone cannot fully explain ΔEEG. When combining ΔLFP and ΔSC, the modeled ΔEEG (dashed red line) better resembles the measured ΔEEG values. To quantify this effect, we computed two additional metrics: First, we calculated the F-statistic by comparing the full GLM containing both ΔLFP and ΔSC as regressors, against a null model consisting of only the ΔLFP regressor (Figure 2D). For all frequency bands but the alpha range, the F-statistic was significant ($p<0.01$), confirming that ΔSC explains a component of the ΔEEG that cannot be explained by ΔLFP. Secondly, we computed the root mean square error (RMSE) between the measured and modeled ΔEEG (Figure 2E). In all frequency bands, the addition of ΔSC decreased the RMSE. A similar effect was seen when performing the same analysis on data obtained during the fixation period prior to visual stimulation (i.e., no visual stimulus), thus confirming that our results are largely invariant to external stimulation. Due to the link between EEG gamma power and MUA

(Whittingstall 2009), we additionally investigated to what extent EEG-LFP dissociations are related to changes in firing rates and MUA synchrony. We found a positive correlation between $\Delta_{EEG\text{-}LFP}$ and MUA synchrony while correlations between $\Delta_{EEG\text{-}LFP}$ and firing rates were slightly negative. For both cases, relations were strongest in the high-gamma range. This suggests that changes in neural firing and synchrony have an opposing impact on high-frequency EEG-LFP dissociations.

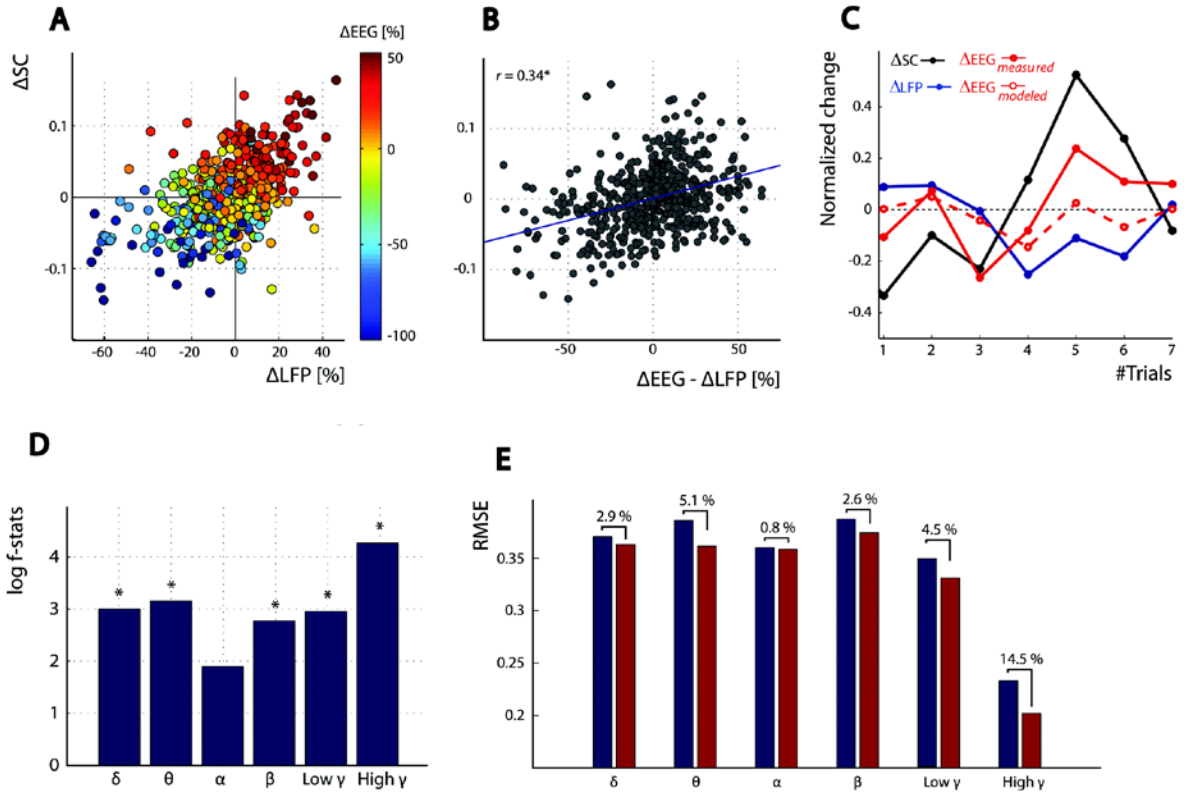

Figure 2. *EEG-LFP dissociations are explained by SC.* (A) Scatter plot of trial-by-trial modulation in the high-gamma range (60-100Hz) for LFP (ΔLFP), EEG (ΔEEG) and SC (ΔSC) across all non-human primates. ΔLFP and ΔEEG represent the percent change from the trial-average, while ΔSC is computed as difference (see methods). Statistical analysis shows that ΔSC is significantly higher in trials where ΔEEG is greater than ΔLFP (see results). (B) Scatter plot of trial-by-trial differences in ΔEEG and ΔLFP (ΔEEG - ΔLFP) versus ΔSC. $\Delta_{EEG\text{-}LFP}$ is positively correlated to ΔSC ($p<0.05$), indicating a relation between SC and the dissociation of EEG and LFP power. (C) An example trace of trial-by-trial fluctuations of LFP (blue), SC (black) and EEG (red). Dashed red line with open circles is the modeled EEG ($EEG_{modeled}$) using LFP and SC as regressors in a GLM. For visual purposes only, all measures were normalized to their maximum change ('Normalized Change'). (D) F-statistics obtained when comparing F-values of the full GLM to a reduced GLM (using ΔLFP as a single regressor) for all frequency bands. Stars indicate that adding ΔSC as a regressor in the GLM explained a significant amount of ΔEEG variance ($p < 0.01$) which could not be explained by ΔLFP alone (see methods). (E) When only using LFP to model the EEG (reduced model, blue bars), the mean root-mean squared error (RMSE) was consistently higher than when including ΔSC as an additional regressor (full model, red bars).

Amplitude dissociations between EEG and LFP are directly related to changes in neural synchrony. In some cases, we observed trials where the LFP was negatively modulated while both EEG and SC were positively modulated, suggesting that the contribution of SC is strong enough to 'amplify' neural signals. However, because only few trials exhibited clear EEG-LFP dissociations, we sought to reproduce this effect in a more robust manner, using localized pharmacological manipulation. We injected lidocaine locally in V1 to dissociate EEG amplitude and LFP power.

Lidocaine has been shown to reduce LFP (Bollimunta et al. 2011) and MUA (Logothetis et al. 2002; Bollimunta et al. 2008), though paradoxically increase the surface EEG (Sheinberg and Logothetis 2001), thus creating a strong dissociation between EEG and LFP power. Given our previous findings, we hypothesized that a lidocaine-induced dissociation between EEG and LFP can be explained by a concomitant change in SC. Indeed, we found that LFP activity during lidocaine application was not only attenuated but also more synchronized. As expected, the LFP exhibited a significant broadband decrease in power (Figure 3A). On the other hand, EEG power was increasing, particularly in the high-frequency range. These LFP and EEG findings are in line with previous lidocaine studies in non-human primates and humans (Detsch et al. 1997; Rauch et al. 2008). Aside from changes in amplitude, we found that SC significantly increased with lidocaine (Figure 3B). Statistical analysis (two-sided paired t-test) revealed that lidocaine-triggered changes in LFP and SC were significant across all frequency bands ($p<0.01$, Figure 3C), while increases in the EEG were only statistically significant in the high gamma range ($p<0.01$, Figure 3C). None of these effects were observed during control injections of ACSF. Again we modulated ΔEEG by inserting ΔSC and ΔLFP as regressors in a general linear model (GLM) and calculated F-statistics and the RMSE. F-statistics (Figure 3D) were significant for all but the theta and the alpha band, while values in the high-frequency range were higher compared to the control condition. The increased importance of ΔSC can also be seen with RMSE (Figure 3E), showing a reduction of 26% in unexplained variability with the addition of ΔSC in the high-gamma range. In summary, trial-by-trial analysis of data obtained during baseline as well as the drug condition shows that a significant portion of EEG-LFP dissociations can be explained by changes in neural synchrony.

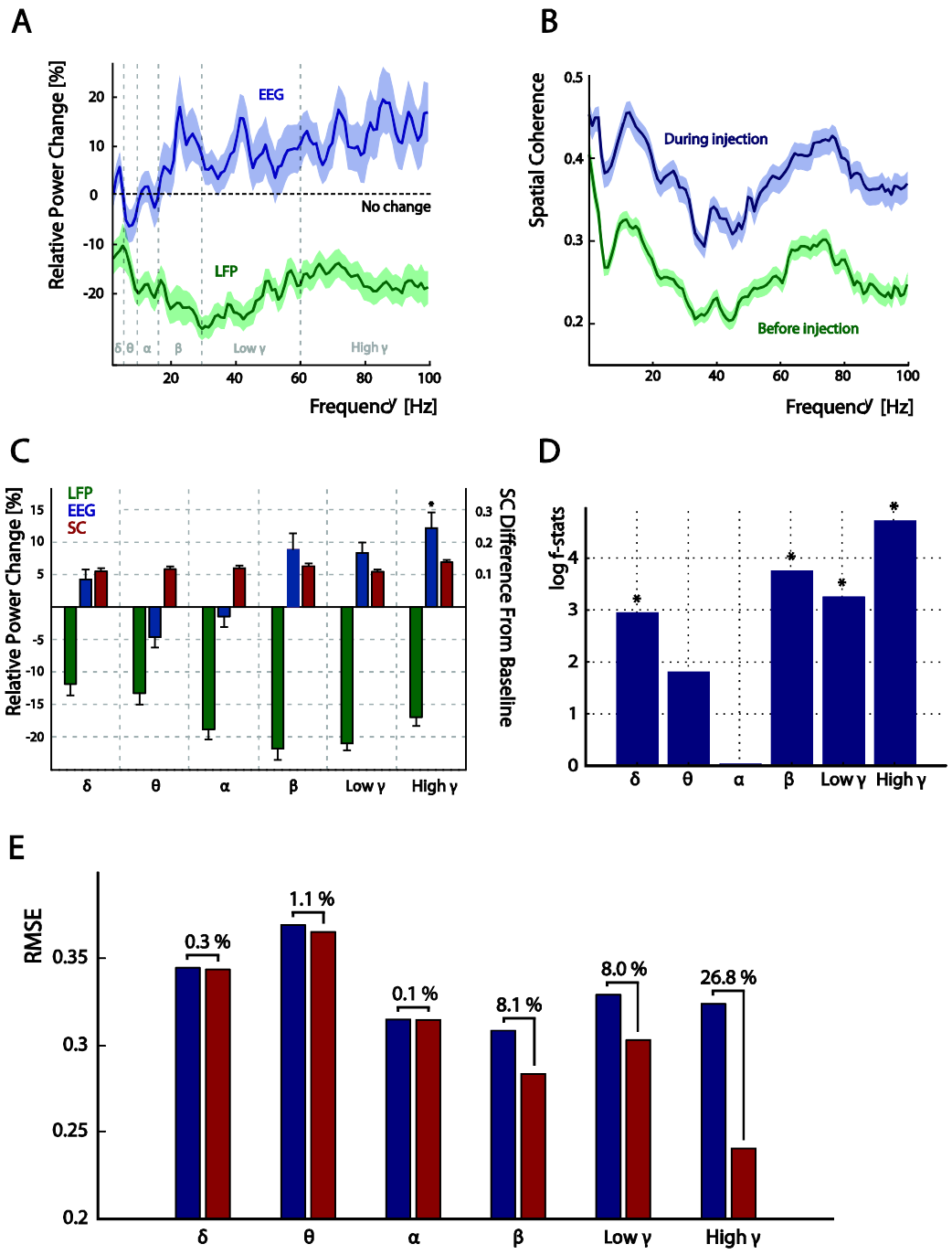

Figure 3. *Effects of lidocaine on EEG, LFP and Spatial Coherence (SC).* (A) Average lidocaine-induced changes in EEG and LFP. Results are displayed as percent change from baseline condition. (B) SC spectra before (green) and after (blue) lidocaine application (C) Lidocaine induced changes (as in A and B), for all classical EEG frequency bands. Stars indicate a statistically significant change ($p<0.01$) of EEG power. Changes in LFP and SC were significant for all frequency bands. (D) F-statistics for the addition of ΔSC into the GLM analysis in the drug condition (as in Figure 2D). (E) RMSE values for all frequency bands using ΔLFP (blue bars) or a combination of ΔLFP and ΔSC to model ΔEEG (red bars) Addition of ΔSC into the GLM strongly reduced RMSE, especially in the high-gamma range (see also Figure 2E).

The findings presented here demonstrate how neural synchrony 'amplifies' the contribution of localized neural activity into the EEG, thus explaining the amplitude differences often observed between intracranial and surface measurements of neural activity. This offers direct experimental evidence for the long hypothesized dependence of EEG amplitude on the synchrony of neuronal sources rather than simply the strength of their activation.

Our results are in line with the modeling study of epileptic activity by Cosandier-Rimele et al. (2008), who showed that when the magnitude of neural activity is held constant, increases in the degree of synchronous activity result in increasing scalp EEG. In addition, we found that if synchrony is sufficiently high, increases in EEG can also coincide with decreases in LFP activity.

We observed that the effect of SC on EEG was similar across stimulus type (movie, fixation) and pharmacological condition (baseline, drug). Our results are thus not solely shaped by the visual stimulus or type of pharmacological manipulation, and might reflect a more general phenomenon of cortical processing. It is therefore important to include the role of neural synchrony in the interpretation of EEG signals obtained in basic and clinical research. Concerning the latter, several studies have shown how various types of anesthetics reduce localized measures of neural activity (MUA, LFP) (Antkowiak and Helfrich-Forster 1998; Hentschke et al. 2005; Greenberg et al. 2008), though paradoxically increase surface EEG activity in humans (Maksimow et al. 2006; Murphy et al. 2011). Interestingly, it has also been shown that these types of anesthesia have the effect of synchronizing neural activity (Antkowiak 2002; Greenberg et al. 2008; Kreuzer et al. 2010; Murphy et al. 2011). Kreuzer et al. (2010) recorded LFPs from the somatosensory cortex of rats chronically implanted with multielectrode arrays and compared activity patterns in the awake state with those at increasing concentrations of isoflurane, enflurane and halothane. In line with our studies, they found that cortical LFP signals were more synchronous in the presence of anesthetics. Although we cannot directly compare our local lidocaine applications with these studies, they nonetheless suggest that cortical synchrony may be a key factor in explaining 'paradoxical' EEG amplitude changes observed under anesthesia (Antkowiak 2002).

The lidocaine-induced increase in neural synchrony raises the question about its origin. One possibility is that lidocaine simply diminishes background neural activity, which could increase the signal-to-noise ratio (SNR) of stimulus evoked-transients and result in spuriously high inter-

electrode synchrony. However, we found a similar increase in SC during the fixation period, indicating that the increase in synchrony is unrelated to stimulus-selective projection neurons but rather reflects unselective mass activity. Since lidocaine more strongly affects neurons with high firing rates (Fozzard et al. 2005), it may particularly suppress fast-spiking interneurons (Tanaka and Yamasaki 1966), thus leading to a loss of controlled neuromodulation. Given that active decorrelation has been shown to be a fundamental property of intracortical processing (Cohen and Maunsell 2009; Wiechert et al. 2010), lidocaine infusion may disrupt this process, resulting in the observed overly-correlated network activity.

Lastly, our findings have an important implication for basic EEG studies, particularly those combining EEG with other imaging modalities such as fMRI. We have previously shown that the local application of lidocaine significantly decreases the amplitude of the BOLD signal (Rauch et al. 2008), while we here demonstrate that it triggers an increase in surface EEG amplitude. This highlights the impact of neural synchrony as an important mechanism behind any potential dissociation between EEG and fMRI measurements (Nunez and Silberstein 2000; Meltzer et al. 2009; Yesilyurt et al. 2010). A likely cause of this observation is that synchronization among a large population of neurons is less metabolically demanding (Buzsaki and Draguhn 2004; Torrealdea et al. 2006), thus explaining why increases in EEG may appear concurrently with a reduction of the BOLD signal. Should this be the case, dissociations between EEG and BOLD may prove extremely informative in serving as a non-invasive marker for separating the effects of synaptic input (fMRI) vs. global synchronization (EEG), and potentially open a new avenue for identifying distinct neural codes used in behavioral tasks.

8.3 Study 1: "Effects of lactate on V1 of non-human primates investigated by pharmaco-MRI and neurochemical analysis"

We measured the BOLD response after a pharmacological challenge by lactate, which we applied systemically and monitored the induced plasma lactate levels in anesthetized non-human primates. Our study results demonstrate that lactate induces a reliably detectable BOLD response, with even low lactate doses producing plasma concentrations comparable to those brought about by moderate muscular exercise (Freund et al. 1990). We observed reliable lactate-induced BOLD responses, which could be confirmed at population and individual level

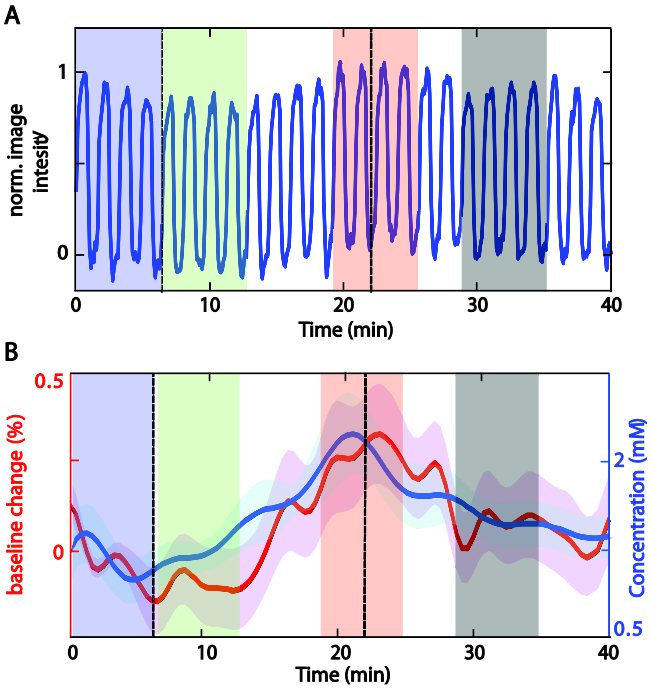

Figure 4 (A) Mean time course over 30 functional magnetic resonance imaging (fMRI) sessions; the lactate infusion started after the fourth stimulus repetition (6.4 min) and lasted for a mean duration of 18 min (black dashed lines). Shading indicates the time windows used for statistical analysis: blue, before injection (0 – 6.4 min); green, during injection (6.5 – 12.8 min); red, shortly after injection (19.2 – 25.6 min); and gray, recovery phase (27.2 – 33.6 min). (B) The mean plasma lactate concentration over 8 experiments (blue) and the mean baseline change over 30 fMRI experiments (blood oxygen level-dependent signal, red); lactate injection started after 6.4 min and lasted for a mean duration of 18 min.

by their strong correlation with systemic lactate concentrations (coefficients of correlation: 0.60 for J08, 0.52 for C06, 0.69 for K07, 0.85 for J07 and 0.87 for the average data). Even in this rather heterogeneous group of test subjects, we could reliably detect lactate-induced changes in the BOLD signal (an important finding because the differences in physiological respectively metabolic conditions did not interfere with our measurements). In every test subject, lactate induced a positive baseline shift in the BOLD signal, although the amplitude varied from 16% of the stimulus induced modulation in the weakest responder to 39% in the strongest responder (Figure 5). The onset of the BOLD baseline increases began between 7.6 min (onset effect, early responder) and 19.8 min (onset effect, late responder), with a mean onset of 16.9 ± 7.5 min. The

actual BOLD response lasted for a period of 5.6 to 27.6 min (short versus long pharmacokinetics), with a mean duration of 11.0 ± 8.5 min. Differences in the lactate-induced BOLD response are also reflected in the actual plasma lactate levels. We extracted the

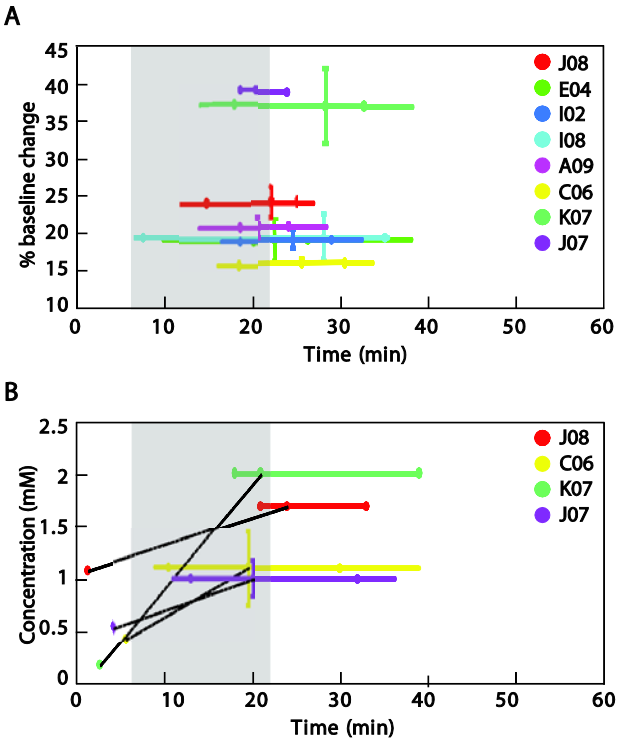

Figure 5 Inter-individual differences in blood oxygen level-dependent functional magnetic resonance imaging (BOLD-fMRI) (A) and plasma lactate concentration (B). For both datasets, we determined four variables that defined the effect: the maximal change, the start of the change (when baseline or concentration crossed the threshold of *P* = 0.05), the time of the maximal effect, and the end of the effect (the final point above the threshold). These variables were averaged for each subject and plotted here. Panel A depicts the percentage BOLD baseline change and respective standard deviation for each subject; the percentage value is referenced to the stimulus-induced modulation before the injection (100%). Panel B depicts plasma lactate concentration before injection, and maximal concentration reached after lactate injection. For both panels, timing and standard deviation of the effect are plotted on the X-axis.

individual lactate levels before and after infusion and the timing of the peak concentration. The lactate levels ranged from 0.3 to 2.1 mM before infusion and reached maximum levels between 2.0 and 4.0 mM. The onset of plasma lactate increases began between 10.1 (early responder) and 20.6 min (late responder), with a mean onset of 14.1 ± 4.5 min. Lactate remained elevated for a duration of 12 to 21 min (short versus long pharmacokinetics), with a mean duration of 18.4 ± 7.4 min. Comparable BOLD effects where observed after a slow infusion of pyruvate; baseline increased in average to 98.9 ±63.3% of the stimulus induced modulation. This effect had earlier onset then the lactate effect lasting from 9.2 ± 2.3 min to 27.5 ± 5.9 min with the maximal effect at 17.1± 3.1 min. The observed increase in BOLD baseline after monocarboxylic acid injection could be explained by an increase in CBF or also increased neuronal activity. We only expected subtle CBF increases below the detection threshold of our FAIR method with our low dose challenge. To test if lactate has an effect on neuronal activity we performed electrophysiological recordings in V1. By applying lactate, a potential fuel for activated neurons, we increase LfpH

(24 – 90 Hz) power and modulation at the same time as the BOLD baseline increases. The power increased in average of 23.0 ±1.2% and the modulation of 76.0 ± 20%; this effect lasted from 12.5 ± 1.5 min to 32.0 ±4 .3 min. In the MUA (400-3000 Hz) no significant effect was observed. The pyruvate injection showed a comparable effect in the LfpH band. The power increases in average of 31.0 ± 7.3%; this effect lasted from 8.5 ± 2.1 min to the end of the recording. In two cases we saw also a significant increase in modulation. As with lactate also with pyruvate injections no significant effect was observed in the MUA.

We show here that physiological changes in lactate and pyruvate levels are indeed reflected in the BOLD signal, and describe the technical prerequisites to reliably trace a lactate challenge using BOLD-fMRI. The main part of this study relies on non-invasive BOLD fMRI and plasma sampling. With these methods alone we were able to define lactate induced changes in the BOLD signal. We observe interindividual differences in the onsets and dynamics after lactate application. However, these differences were not substantial enough to jeopardize our use of subtle lactate concentrations and at an individual level we have shown a high degree of consistency between BOLD response and plasma lactate levels. Especially if clinical applications are envisioned in the future, substantial jitter in the BOLD response must be anticipated because of physiological differences between individuals. Above all, lactate metabolism depends critically on the training condition and general physiology of human subjects (Oyono-Enguelle et al. 1990) and this should also hold true for non-human primates that show an overlap with human physiology to a very high degree (Voytko and Tinkler 2004).
These findings are important from two different points of view, on one side they give us insight into the bases of the BOLD signal; on the other hand they can have implications for future clinical research in the early diagnosis of Alzheimer's disease.
Part of the observed BOLD signal change is due to changes in neuronal activity: by applying lactate, a potential fuel for activated neurons, we increase LfpH power and modulation but not the spiking activity. Since LfpH is a reliable driver of the BOLD signal (Logothetis et al. 2001)at least part of the lactate effect on the BOLD signal can be explained by an increase in neuronal activity.
In addition, these results give further indications that lactate could be one of the signaling molecules in neurovascular coupling contributing to the increase in the BOLD signal during

neuronal activation (Mangia et al. 2009). The tight coupling between neuronal activity and the associated local increase in both blood flow and energy metabolism is the basis for functional imaging. This so called neurovascular coupling is mediated by different mechanisms, one of these could depend on lactate, a metabolite of glucose. The production of lactate a vasodilatative substance (Reiman et al. 1989) increases during neuronal activation (Prichard et al. 1991; Hu and Wilson 1997) suggesting a pivotal role of lactate in neurovascular coupling. The formulation of the astrocyte neuron lactate shuttle hypothesis (Magistretti and Pellerin 1999) shed light on the potential importance of lactate in brain metabolism and neurovascular signaling. During neuronal activation glutamate, the main excitatory neurotransmitter in cerebral cortex is released. From the synaptic cleft glutamate is then taken up by astrocytes. The glutamate transporter uses the favorable electrochemical gradient of Na^+ to take up glutamate together with three molecules of Na^+. In the astrocyte this uptake stimulates aerobic glycolysis - the production of lactate from glucose in the presence of oxygen. The two molecules of ATP obtained by this process are used to reestablish the electrochemical gradient (running the Na/K ATPase bringing Na^+ out of the cell again) and to transform glutamate to glutamine. Both glutamine and lactate are released to the extracellular space from where they can be removed by neurons. In the neurons lactate is metabolized trough the tricarboxylic acid cycle to provide energy. The high extracellular lactate levels during neuronal activation cause vasodilatation trough different mechanisms. As mentioned before lactate is metabolized to provide energy, the first step to do that is the transformation of lactate to pyruvate together with the reduction of NAD^+ to NADH. Thereafter the NAD^+ pool has to be restored trough metabolic pathways producing nitric oxide which in turn increases blood flow (Ido et al. 2004). In addition, high extracellular lactate levels prevent the reuptake and inactivation of prostaglandin E2 another vasodilatative molecule (Gordon et al. 2008). We can summarize that lactate a vasodilatative molecule is produced during neuronal activation. The fact that a systemic lactate application causes increases in the BOLD signal is a strong indicator that also the physiological formation of lactate can contribute to the BOLD signal.

8.4 Future applications in clinical diagnostics

Since lactate levels in the cerebrospinal fluid rise during the progression of Alzheimer's disease (Redjems-Bennani et al. 1998), the findings of study 1 might even have implications in the early diagnosis of this disease. Higher lactate levels can be caused by reduced enzymatic activity in AD patients, which is important for neuronal energy metabolism (Gibson et al. 1998) and consequently leads to an increase in oxidative stress in the brain (Zhu et al. 2005; Aon et al. 2010). Such changes reflect abnormalities in the regulation of cerebral metabolism and potentially neurovascular coupling, which in turn could have diverse effects on the fMRI signal (Reiman et al. 2001; Iadecola 2004; Reiman et al. 2004; 2005). Reduced responsiveness of CBF to sensory stimulation is apparently a characteristic of AD, and this reduction correlates with the severity of AD progression (Mentis et al. 1998). In agreement with these findings, Kalman et al. did not observe a single-photon emission computed tomography response after a lactate challenge (2.5 mmol/kg) in AD patients that induced plasma lactate levels of 5.5 ± 1.226 mM (Kalman et al. 2005). We consider the lack of lactate-induced responses in BOLD signal and CBF a potential hallmark that characterizes patients suffering from AD. Therefore, a missing BOLD response to a subtle lactate challenge like the one used for our study might sensitively indicate AD onset. The described temporal dissociation between AD-induced dysregulation and later-appearing clinical symptoms (Reiman et al. 2001; 2004; 2005) suggests the usefulness of a diagnostic procedure that is already sensitive at the earliest possible stage. Our hypothesis of reduced responsiveness to lactate in AD is also in agreement with a recent review highlighting the close resemblance of AD to a vascular disorder in which delayed and weakened responses to increased metabolic demand might be a preclinical feature (Iadecola 2004). This lack of responsiveness to lactate could be explained by "adaptation mechanisms" induced by steadily increasing levels of lactate and pyruvate in the cerebrospinal fluid that occur in the course of AD (Redjems-Bennani et al. 1998). We consider our approach a first step in the direction of potential diagnostics for AD at early stages when clinical symptoms are not yet obvious, which is of importance for individuals at risk of AD (Richard and Amouyel 2001).

Also the other two studies might have potential implications in the early diagnostics of AD:
Study 2: The levels of neurochemicals like Acetylcholine, Lactate, Pyruvate, Glutamate and Glutamine change during the progression of AD. For example, cholinergic neuron dysfunction appears very early in AD (Geula et al. 2008). Even a better measure for metabolic imbalance in AD is the determination of lactate/pyruvate and glutamate/glutamine ratios which reflect important metabolic reactions. The lactate/pyruvate ratio in the human brain is currently considered a specific, sensitive marker that could potentially indicate whether glucose and oxygen supply meet the energy requirements of the brain tissue (Bellander et al. 2004). Such marker, that hint upon the adequacy of energy and metabolite supply are of great importance for the detection of onset of neurodegenerative diseases like Alzheimer's disease (Redjems-Bennani et al. 1998; Iadecola 2004). In addition, it is hypothesized that the glutamate – glutamine cycling is disrupted in AD causing excitotoxic neurodegeneration trough elevated glutamate levels in the synaptic cleft (Walton and Dodd 2007) and a decreased production of glutamine. We could test for an altered glutamate/glutamine ratio in the brain of Alzheimer patients. A further step into the direction of early diagnosis of AD is to determine if these potential changes are reflected in the blood.
Study 3: The reported findings give further insights into the generation of the EEG signal and their relation to the BOLD signal which is important for the use of both methods in clinical diagnostics. As discussed before Alzheimer patients show abnormalities in the regulation of cerebral metabolism and potentially neurovascular coupling, which in turn could have diverse effects on the fMRI signal (Reiman et al. 2001; Iadecola 2004; Reiman et al. 2004; 2005). In addition, Alzheimer patients present distinctive patterns in the EEG signal (Drago et al. 2011). Even a pharmacological manipulation like a lactate infusion generated a distinct pattern in the EEG of AD patients making it possible to characterize severely damaged, moderately affected and not affected areas (Jardanhazy et al. 2008). We measured the effect of a lactate infusion on the electrophysiological signal of healthy non-human primates, this application increases the LFP. For a future application of our infusion protocol to fMRI-EEG studies the EEG effect of a lactate infusion to healthy subjects should be studied. Afterwards clinical application in the early diagnostics of AD might be envisioned.

8.5 Conclusion:

We envision phMRI to become a reliable tool for drug screening and early diagnostics of neurodegenerative disorders but to fully exploit its potential we need a better understanding of the BOLD signal and its underlying mechanisms. To reach this aim we combine phMRI with complementary methods which will provide us with corroborating evidence to elucidate the underlying neuronal, metabolic and vascular activity of the BOLD signal. We validated the simultaneous use of both invasive (electrophysiology and local microdialysis) and non-invasive (EEG and systemic microdialysis) techniques in non-human primates. Once the relation between these signals is known we can proceed with only non invasive methods for diagnostics and drug screening in humans. We determined neurochemical levels in brain and blood and the relation of these substances across the blood brain barrier. This study is an important step on the way to answer the questions if pathologic neurochemical changes are reflected in the blood and also if and to what extend a systemic drug injection passes blood brain barrier. Furthermore using this approach we are able to extrapolate from plasma to brain concentrations of relevant neurochemicals. In addition, we combined non-invasive EEG and invasive electrophysiology to analyze how these signals relate to each other by applying lidocaine locally. The results bring us a step further in understanding the EEG signal and its relation to underlying neuronal activity and the BOLD signal. We deliver one potential explanation of dissociations between EEG and BOLD signal important for the future use of both methods in diagnostics.
Now we can establish an experimental protocol in the non-human primate with both invasive and non invasive methods and then translate it to clinical use in humans relying on only non-invasive data. BOLD fMRI can be combined with EEG and plasma sampling for diagnostic purposes or drug screening. Our first approach to test for the feasibility of this non invasive approach is the combination of phMRI with systemic lactate injection and plasma sampling. We proof that we can detect even a subtle change in plasma lactate concentrations in the BOLD signal. This experimental procedure now validated in non-human primates could be applied in humans after relative minor adaptations, where it might be of use in the early diagnosis of Alzheimer's disease.

9. References:

Antkowiak, B. (2002). "In vitro networks: cortical mechanisms of anaesthetic action." Br J Anaesth **89**(1): 102-11.

Antkowiak, B. and C. Helfrich-Forster (1998). "Effects of small concentrations of volatile anesthetics on action potential firing of neocortical neurons in vitro." Anesthesiology **88**(6): 1592-605.

Aon, M. A., S. Cortassa and B. O'Rourke (2010). "Redox-optimized ROS balance: A unifying hypothesis." Biochim Biophys Acta **1797**(6-7): 865-877.

Begley, D. J. (2004). "Delivery of therapeutic agents to the central nervous system: the problems and the possibilities." Pharmacol Ther **104**(1): 29-45.

Bellander, B. M., E. Cantais, P. Enblad, P. Hutchinson, C. H. Nordström, C. Robertson, J. Sahuquillo, M. Smith, N. Stocchetti and U. Ungerstedt (2004). "Consensus meeting on microdialysis in neurointensive care." Intensive Care Medicine **30**(12): 2166-2169.

Bollimunta, A., Y. Chen, C. E. Schroeder and M. Ding (2008). "Neuronal mechanisms of cortical alpha oscillations in awake-behaving macaques." J Neurosci **28**(40): 9976-88.

Bollimunta, A., J. Mo, C. E. Schroeder and M. Ding (2011). "Neuronal mechanisms and attentional modulation of corticothalamic alpha oscillations." J Neurosci **31**(13): 4935-43.

Bookheimer, S. Y., M. H. Strojwas, M. S. Cohen, A. M. Saunders, M. A. Pericak-Vance, J. C. Mazziotta and G. W. Small (2000). "Patterns of brain activation in people at risk for Alzheimer's disease." N Engl J Med **343**(7): 450-6.

Borsook, D., L. Becerra and R. Hargreaves (2006). "A role for fMRI in optimizing CNS drug development." Nat Rev Drug Discov **5**(5): 411-24.

Buzsaki, G. and A. Draguhn (2004). "Neuronal oscillations in cortical networks." Science **304**(5679): 1926-9.

Ceolin, L., A. J. Schwarz, A. Gozzi, T. Reese and A. Bifone (2007). "Effects of cocaine on blood flow and oxygen metabolism in the rat brain: implications for phMRI." Magn Reson Imaging **25**(6): 795-800.

Cohen, M. R. and J. H. Maunsell (2009). "Attention improves performance primarily by reducing interneuronal correlations." Nat Neurosci **12**(12): 1594-600.

Cosandier-Rimele, D., I. Merlet, J. M. Badier, P. Chauvel and F. Wendling (2008). "The neuronal sources of EEG: modeling of simultaneous scalp and intracerebral recordings in epilepsy." Neuroimage **42**(1): 135-46.

Craig, L. A., N. S. Hong and R. J. McDonald (2011). "Revisiting the cholinergic hypothesis in the development of Alzheimer's disease." Neurosci Biobehav Rev **35**(6): 1397-409.

Detsch, O., U. Erkens, U. Jacofsky, A. Thiel, E. Kochs and G. Hempelmann (1997). "Topographical analysis of the EEG effects of a subconvulsive dose of lidocaine in healthy volunteers." Acta Anaesthesiol Scand **41**(8): 1039-46.

Drago, V., C. Babiloni, D. Bartres-Faz, A. Caroli, B. Bosch, T. Hensch, M. Didic, H. W. Klafki, M. Pievani, J. Jovicich, L. Venturi, P. Spitzer, F. Vecchio, P. Schoenknecht, J. Wiltfang, A. Redolfi, G. Forloni, O. Blin, E. Irving, C. Davis, H. G. Hardemark and G. B. Frisoni (2011). "Disease tracking markers for Alzheimer's disease at the prodromal (MCI) stage." J Alzheimers Dis **26 Suppl 3**: 159-99.

Eickhoff, S. B., C. Rottschy, M. Kujovic, N. Palomero-Gallagher and K. Zilles (2008). "Organizational principles of human visual cortex revealed by receptor mapping." Cereb Cortex **18**(11): 2637-45.

Fozzard, H. A., P. J. Lee and G. M. Lipkind (2005). "Mechanism of local anesthetic drug action on voltage-gated sodium channels." Curr Pharm Des **11**(21): 2671-86.
Freund, H., S. Oyono-Enguelle, A. Heitz, C. Ott, J. Marbach, M. Gartner and A. Pape (1990). "Comparative lactate kinetics after short and prolonged submaximal exercise." Int J Sports Med **11**(4): 284-8.
Gerdelat-Mas, A., I. Loubinoux, D. Tombari, O. Rascol, F. Chollet and M. Simonetta-Moreau (2005). "Chronic administration of selective serotonin reuptake inhibitor (SSRI) paroxetine modulates human motor cortex excitability in healthy subjects." Neuroimage **27**(2): 314-22.
Geula, C., N. Nagykery, A. Nicholas and C. K. Wu (2008). "Cholinergic neuronal and axonal abnormalities are present early in aging and in Alzheimer disease." J Neuropathol Exp Neurol **67**(4): 309-18.
Gibson, G. E., K. F. Sheu and J. P. Blass (1998). "Abnormalities of mitochondrial enzymes in Alzheimer disease." J Neural Transm **105**(8-9): 855-70.
Goekoop, R., S. A. Rombouts, C. Jonker, A. Hibbel, D. L. Knol, L. Truyen, F. Barkhof and P. Scheltens (2004). "Challenging the cholinergic system in mild cognitive impairment: a pharmacological fMRI study." Neuroimage **23**(4): 1450-9.
Gordon, G. R., H. B. Choi, R. L. Rungta, G. C. Ellis-Davies and B. A. MacVicar (2008). "Brain metabolism dictates the polarity of astrocyte control over arterioles." Nature **456**(7223): 745-9.
Gozzi, A., A. Schwarz, T. Reese, S. Bertani, V. Crestan and A. Bifone (2006). "Region-specific effects of nicotine on brain activity: a pharmacological MRI study in the drug-naive rat." Neuropsychopharmacology **31**(8): 1690-703.
Greenberg, D. S., A. R. Houweling and J. N. Kerr (2008). "Population imaging of ongoing neuronal activity in the visual cortex of awake rats." Nat Neurosci **11**(7): 749-51.
Hentschke, H., C. Schwarz and B. Antkowiak (2005). "Neocortex is the major target of sedative concentrations of volatile anaesthetics: strong depression of firing rates and increase of GABAA receptor-mediated inhibition." Eur J Neurosci **21**(1): 93-102.
Hu, Y. and G. S. Wilson (1997). "A temporary local energy pool coupled to neuronal activity: fluctuations of extracellular lactate levels in rat brain monitored with rapid-response enzyme-based sensor." J Neurochem **69**(4): 1484-90.
Hubel, D. H. and T. N. Wiesel (1977). "Ferrier lecture. Functional architecture of macaque monkey visual cortex." Proc R Soc Lond B Biol Sci **198**(1130): 1-59.
Iadecola, C. (2004). "Neurovascular regulation in the normal brain and in Alzheimer's disease." Nat Rev Neurosci **5**(5): 347-60.
Iannetti, G. D. and R. G. Wise (2007). "BOLD functional MRI in disease and pharmacological studies: room for improvement?" Magn Reson Imaging **25**(6): 978-88.
Ido, Y., K. Chang and J. R. Williamson (2004). "NADH augments blood flow in physiologically activated retina and visual cortex." Proc Natl Acad Sci U S A **101**(2): 653-8.
Jardanhazy, A., T. Jardanhazy and J. Kalman (2008). "Sodium lactate differently alters relative EEG power and functional connectivity in Alzheimer's disease patients' brain regions." Eur J Neurol **15**(2): 150-5.
Jezzard, P. and R. B. Buxton (2006). "The clinical potential of functional magnetic resonance imaging." J Magn Reson Imaging **23**(6): 787-93.
Kalman, J., A. Palotas, G. Kis, K. Boda, P. Turi, F. Bari, F. Domoki, I. Doda, M. Argyelan, G. Vincze, T. Sera, L. Csernay, Z. Janka and L. Pavics (2005). "Regional cortical blood flow

changes following sodium lactate infusion in Alzheimer's disease." Eur J Neurosci **21**(6): 1671-8.
Kreuzer, M., H. Hentschke, B. Antkowiak, C. Schwarz, E. F. Kochs and G. Schneider (2010). "Cross-approximate entropy of cortical local field potentials quantifies effects of anesthesia--a pilot study in rats." BMC Neurosci **11**: 122.
Leslie, R. A. and M. F. James (2000). "Pharmacological magnetic resonance imaging: a new application for functional MRI." Trends Pharmacol Sci **21**(8): 314-8.
Li, J., V. von Pfostl, D. Zaldivar, X. Zhang, N. Logothetis and A. Rauch (2011). "Measuring multiple neurochemicals and related metabolites in blood and brain of the rhesus monkey by using dual microdialysis sampling and capillary hydrophilic interaction chromatography-mass spectrometry." Anal Bioanal Chem **402**(8): 2545-54.
Lidow, M. S., P. S. Goldman-Rakic, D. W. Gallager and P. Rakic (1989). "Quantitative autoradiographic mapping of serotonin 5-HT1 and 5-HT2 receptors and uptake sites in the neocortex of the rhesus monkey." J Comp Neurol **280**(1): 27-42.
Logothetis, N., H. Merkle, M. Augath, T. Trinath and K. Ugurbil (2002). "Ultra high-resolution fMRI in monkeys with implanted RF coils." Neuron **35**(2): 227-42.
Logothetis, N. K., J. Pauls, M. Augath, T. Trinath and A. Oeltermann (2001). "Neurophysiological investigation of the basis of the fMRI signal." Nature **412**(6843): 150-7.
Loubinoux, I., D. Tombari, J. Pariente, A. Gerdelat-Mas, X. Franceries, E. Cassol, O. Rascol, J. Pastor and F. Chollet (2005). "Modulation of behavior and cortical motor activity in healthy subjects by a chronic administration of a serotonin enhancer." Neuroimage **27**(2): 299-313.
Magistretti, P. J. and L. Pellerin (1996). "Cellular bases of brain energy metabolism and their relevance to functional brain imaging: evidence for a prominent role of astrocytes." Cereb Cortex **6**(1): 50-61.
Magistretti, P. J. and L. Pellerin (1999). "Cellular mechanisms of brain energy metabolism and their relevance to functional brain imaging." Philos Trans R Soc Lond B Biol Sci **354**(1387): 1155-63.
Maksimow, A., M. Sarkela, J. W. Langsjo, E. Salmi, K. K. Kaisti, A. Yli-Hankala, S. Hinkka-Yli-Salomaki, H. Scheinin and S. K. Jaaskelainen (2006). "Increase in high frequency EEG activity explains the poor performance of EEG spectral entropy monitor during S-ketamine anesthesia." Clin Neurophysiol **117**(8): 1660-8.
Mangia, S., F. Giove, I. Tkac, N. K. Logothetis, P. G. Henry, C. A. Olman, B. Maraviglia, F. Di Salle and K. Ugurbil (2009). "Metabolic and hemodynamic events after changes in neuronal activity: current hypotheses, theoretical predictions and in vivo NMR experimental findings." J Cereb Blood Flow Metab **29**(3): 441-63.
Meltzer, J. A., G. A. Fonzo and R. T. Constable (2009). "Transverse patterning dissociates human EEG theta power and hippocampal BOLD activation." Psychophysiology **46**(1): 153-62.
Mentis, M. J., G. E. Alexander, J. Krasuski, P. Pietrini, M. L. Furey, M. B. Schapiro and S. I. Rapoport (1998). "Increasing required neural response to expose abnormal brain function in mild versus moderate or severe Alzheimer's disease: PET study using parametric visual stimulation." Am J Psychiatry **155**(6): 785-94.

Mintun, M. A., A. G. Vlassenko, M. M. Rundle and M. E. Raichle (2004). "Increased lactate/pyruvate ratio augments blood flow in physiologically activated human brain." Proc Natl Acad Sci U S A **101**(2): 659-64.

Murphy, M., M. A. Bruno, B. A. Riedner, P. Boveroux, Q. Noirhomme, E. C. Landsness, J. F. Brichant, C. Phillips, M. Massimini, S. Laureys, G. Tononi and M. Boly (2011). "Propofol anesthesia and sleep: a high-density EEG study." Sleep **34**(3): 283-91A.

Nunez, P. L. and R. B. Silberstein (2000). "On the relationship of synaptic activity to macroscopic measurements: does co-registration of EEG with fMRI make sense?" Brain Topogr **13**(2): 79-96.

Oyono-Enguelle, S., J. Marbach, A. Heitz, C. Ott, M. Gartner, A. Pape, J. C. Vollmer and H. Freund (1990). "Lactate removal ability and graded exercise in humans." J Appl Physiol **68**(3): 905-11.

Prichard, J., D. Rothman, E. Novotny, O. Petroff, T. Kuwabara, M. Avison, A. Howseman, C. Hanstock and R. Shulman (1991). "Lactate rise detected by 1H NMR in human visual cortex during physiologic stimulation." Proc Natl Acad Sci U S A **88**(13): 5829-31.

Rakic, P., P. S. Goldman-Rakic and D. Gallager (1988). "Quantitative autoradiography of major neurotransmitter receptors in the monkey striate and extrastriate cortex." J Neurosci **8**(10): 3670-90.

Rauch, A., G. Rainer, M. Augath, A. Oeltermann and N. K. Logothetis (2008). "Pharmacological MRI combined with electrophysiology in non-human primates: effects of Lidocaine on primary visual cortex." Neuroimage **40**(2): 590-600.

Rauch, A., G. Rainer and N. K. Logothetis (2008). "The effect of a serotonin-induced dissociation between spiking and perisynaptic activity on BOLD functional MRI." Proc Natl Acad Sci U S A **105**(18): 6759-64.

Redjems-Bennani, N., C. Jeandel, E. Lefebvre, H. Blain, M. Vidailhet and J. L. Gueant (1998). "Abnormal substrate levels that depend upon mitochondrial function in cerebrospinal fluid from Alzheimer patients." Gerontology **44**(5): 300-4.

Reiman, E. M., R. J. Caselli, K. Chen, G. E. Alexander, D. Bandy and J. Frost (2001). "Declining brain activity in cognitively normal apolipoprotein E epsilon 4 heterozygotes: A foundation for using positron emission tomography to efficiently test treatments to prevent Alzheimer's disease." Proc Natl Acad Sci U S A **98**(6): 3334-9.

Reiman, E. M., K. Chen, G. E. Alexander, R. J. Caselli, D. Bandy, D. Osborne, A. M. Saunders and J. Hardy (2004). "Functional brain abnormalities in young adults at genetic risk for late-onset Alzheimer's dementia." Proc Natl Acad Sci U S A **101**(1): 284-9.

Reiman, E. M., K. Chen, G. E. Alexander, R. J. Caselli, D. Bandy, D. Osborne, A. M. Saunders and J. Hardy (2005). "Correlations between apolipoprotein E epsilon4 gene dose and brain-imaging measurements of regional hypometabolism." Proc Natl Acad Sci U S A **102**(23): 8299-302.

Reiman, E. M., M. E. Raichle, E. Robins, M. A. Mintun, M. J. Fusselman, P. T. Fox, J. L. Price and K. A. Hackman (1989). "Neuroanatomical correlates of a lactate-induced anxiety attack." Arch Gen Psychiatry **46**(6): 493-500.

Richard, F. and P. Amouyel (2001). "Genetic susceptibility factors for Alzheimer's disease." Eur J Pharmacol **412**(1): 1-12.

Rosenkranz, K. and L. Lemieux (2010). "Present and future of simultaneous EEG-fMRI." MAGMA **23**(5-6): 309-16.

Schwarz, A. J., A. Zocchi, T. Reese, A. Gozzi, M. Garzotti, G. Varnier, O. Curcuruto, I. Sartori, E. Girlanda, B. Biscaro, V. Crestan, S. Bertani, C. Heidbreder and A. Bifone (2004). "Concurrent pharmacological MRI and in situ microdialysis of cocaine reveal a complex relationship between the central hemodynamic response and local dopamine concentration." Neuroimage **23**(1): 296-304.

Sheinberg, D. L. and N. K. Logothetis (2001). "Noticing familiar objects in real world scenes: the role of temporal cortical neurons in natural vision." J Neurosci **21**(4): 1340-50.

Sheline, Y. I., D. M. Barch, J. M. Donnelly, J. M. Ollinger, A. Z. Snyder and M. A. Mintun (2001). "Increased amygdala response to masked emotional faces in depressed subjects resolves with antidepressant treatment: an fMRI study." Biol Psychiatry **50**(9): 651-8.

Stein, E. A., J. Pankiewicz, H. H. Harsch, J. K. Cho, S. A. Fuller, R. G. Hoffmann, M. Hawkins, S. M. Rao, P. A. Bandettini and A. S. Bloom (1998). "Nicotine-induced limbic cortical activation in the human brain: a functional MRI study." Am J Psychiatry **155**(8): 1009-15.

Tanaka, K. and M. Yamasaki (1966). "Blocking of cortical inhibitory synapses by intravenous lidocaine." Nature **209**(5019): 207-8.

Torrealdea, F. J., A. d'Anjou, M. Grana and C. Sarasola (2006). "Energy aspects of the synchronization of model neurons." Phys Rev E Stat Nonlin Soft Matter Phys **74**(1 Pt 1): 011905.

von Pföstl, V., J. Li, D. Zaldivar, J. Goense, X. Zhang, N. Serr, N. K. Logothetis and A. Rauch (2012). "Effects of lactate on the early visual cortex of non-human primates, investigated by pharmaco-MRI and neurochemical analysis." Neuroimage **61**(1): 98-105.

Voytko, M. L. and G. P. Tinkler (2004). "Cognitive function and its neural mechanisms in nonhuman primate models of aging, Alzheimer disease, and menopause." Front Biosci **9**: 1899-914.

Walton, H. S. and P. R. Dodd (2007). "Glutamate-glutamine cycling in Alzheimer's disease." Neurochem Int **50**(7-8): 1052-66.

Wiechert, M. T., B. Judkewitz, H. Riecke and R. W. Friedrich (2010). "Mechanisms of pattern decorrelation by recurrent neuronal circuits." Nat Neurosci **13**(8): 1003-10.

Yesilyurt, B., K. Whittingstall, K. Ugurbil, N. K. Logothetis and K. Uludag (2010). "Relationship of the BOLD signal with VEP for ultrashort duration visual stimuli (0.1 to 5 ms) in humans." J Cereb Blood Flow Metab **30**(2): 449-58.

Zhang, X., A. Rauch, H. Lee, H. Xiao, G. Rainer and N. K. Logothetis (2007). "Capillary hydrophilic interaction chromatography/mass spectrometry for simultaneous determination of multiple neurotransmitters in primate cerebral cortex." Rapid Commun Mass Spectrom **21**(22): 3621-8.

Zhang, X., A. Rauch, H. Xiao, G. Rainer and N. K. Logothetis (2008). "Mass spectrometry-based neurochemical analysis: perspectives for primate research." Expert Rev Proteomics **5**(5): 641-52.

Zhu, X., H. G. Lee, G. Casadesus, J. Avila, K. Drew, G. Perry and M. A. Smith (2005). "Oxidative imbalance in Alzheimer's disease." Mol Neurobiol **31**(1-3): 205-17.

Appendix

Publications

Study 1

NeuroImage 61 (2012) 98–105

Contents lists available at SciVerse ScienceDirect

NeuroImage

journal homepage: www.elsevier.com/locate/ynimg

Effects of lactate on the early visual cortex of non-human primates, investigated by pharmaco-MRI and neurochemical analysis

Veronika von Pföstl [a,1], Juan Li [a,1], Daniel Zaldivar [a,b], Jozien Goense [a], Xiaozhe Zhang [c], Nadine Serr [a], Nikos K. Logothetis [a,d], Alexander Rauch [a,*]

[a] Max Planck Institute for Biological Cybernetics, Spemannstrasse 38, D-72076 Tuebingen, Germany
[b] International Max Planck Research School for Neural and Behavioral Science; Österbergstrasse 3 D-72074 Tübingen-Germany
[c] Department of Medicine, University of Fribourg, Chemin de Musee 5, Fribourg, CH-1700, Switzerland
[d] Division of Imaging Science and Biomedical Engineering, University of Manchester, Manchester M13 9PT, United Kingdom

ARTICLE INFO

Article history:
Accepted 29 February 2012
Available online 8 March 2012

Keywords:
Alzheimer disease
BOLD-fMRI
Diagnostics
Lactate
Metabolism

ABSTRACT

In contrast to the limited use of functional magnetic resonance imaging (fMRI) in clinical diagnostics, it is currently a mainstay of neuroimaging in clinical and basic brain research. However, its non-invasive use in combination with its high temporal and spatial resolution would make fMRI a perfect diagnostic tool. We are interested in whether a pharmacological challenge imposed on the brain can be reliably traced by the blood oxygen level-dependent (BOLD) signal and possibly further exploited for diagnostics. We have chosen a systemic challenge with lactate and pyruvate to test whether the physiological formation of these monocarboxylic acids contributes to the BOLD signal and can be detected using fMRI. This information is also of interest because lactate levels in the cerebrospinal fluid rise concomitantly with reduced vascular responsiveness of the brain during the progression of Alzheimer disease (AD). We studied the BOLD response after a low-dose lactate challenge and monitored the induced plasma lactate levels in anesthetized non-human primates. We observed reliable lactate-induced BOLD responses, which could be confirmed at population and individual level by their strong correlation with systemic lactate concentrations. Comparable BOLD effects where observed after a slow infusion of pyruvate. We show here that physiological changes in lactate and pyruvate levels are indeed reflected in the BOLD signal, and describe the technical prerequisites to reliably trace a lactate challenge using BOLD-fMRI.

1. Introduction

Functional magnetic resonance imaging (fMRI) is one of the most frequently used neuroimaging techniques for basic and clinical brain research in humans, and is used surprisingly less often for clinical diagnostics (Jezzard and Buxton, 2006). The systematic implementation of fMRI in diagnostics would evidently require extensive preliminary investigations of the degree to which fMRI may be sensitive to changes in the concentrations of various metabolites or neurotransmitters that are often induced by neurodegenerative disorders. For example, lactate exhibits a prominent role in brain metabolism (Fox and Raichle, 1986; Pellerin and Magistretti, 2004). Transient neuronal activation can apparently trigger glycolysis, resulting in elevated lactate levels (Prichard et al., 1991; Hu and Wilson, 1997). Lactate and pyruvate can then be funneled into the tricarboxylic acid cycle to provide neurons with energy (Pellerin and Magistretti, 2004). The apparent use of the glycolytic pathway was demonstrated by an increase in cerebral blood flow (CBF), and the metabolic rate of glucose which was accompanied by only a slight increase in the metabolic rate of oxygen (Fox and Raichle, 1986; Fox et al., 1988). The coupling of the CBF response to the NADH/NAD+ ratio which is in near equilibrium with the lactate/pyruvate ratio was then shown by Mintun et al. (2004; Vlassenko et al., 2006). Given the importance of lactate in the context of physiological brain metabolism, changes in lactate levels are to be expected under pathological circumstances. For example, elevated lactate levels in the cerebrospinal fluid of patients suffering from Alzheimer disease (AD) have already been observed (Redjems-Bennani et al., 1998). Such changes reflect abnormalities in the regulation of cerebral metabolism and potentially neurovascular coupling, which in turn could have diverse effects on the fMRI signal (Reiman et al., 2001; Iadecola, 2004; Reiman et al., 2004, 2005). However, before one can investigate how these abnormalities affect the blood oxygen level-dependent (BOLD) signal, we should focus on the question of how the physiological formation of lactate contributes to the BOLD signal.

We set out to study fMRI responses in the monkey brain after moderate increases of systemic lactate concentration. To do so, we used direct systemic application to mimic the physiological formation of lactate and measured BOLD contrast in the early visual cortex of

* Corresponding author. Fax: +49 7071 601 658.
E-mail address: arauch@tuebingen.mpg.de (A. Rauch).
[1] Equal contribution.

1053-8119/$ – see front matter © 2012 Elsevier Inc. All rights reserved.
doi:10.1016/j.neuroimage.2012.02.082

anesthetized macaques, while using microdialysis (venous catheter) to monitor blood lactate concentration. To best simulate the physiological formation of lactate in the brain, we increased plasma lactate levels moderately and continuously over the course of minutes, with overall increments in blood lactate concentration corresponding to light physical exercise (Freund et al., 1990). We present evidence that such moderate changes in blood lactate concentration are indeed detectable using BOLD fMRI, and are accompanied by moderate increases in neuronal activity. This finding suggests that, at least in principle, changes in lactate levels due to physiological, age-related, or pathological metabolic adaptations, such as those reported in neurodegenerative disorders, can be assessed using noninvasive BOLD-fMRI methodology.

2. Materials and methods

For this study, we used ten anesthetized rhesus monkeys (*Macaca mulatta*, 7 male and 3 female, age range 4 to 11 years, weighing 4.6 to 12.5 kg). The experimental procedures were approved by the local authorities (Regierungspraesidium) and are in agreement with guidelines of the European Community for the care of laboratory animals. Procedures have previously been described in detail (Logothetis et al., 1999). All vital parameters were monitored during anesthesia. After sedation of the animals using ketamine (15 mg/kg), anesthesia was initiated with fentanyl (31 μg/kg), thiopental (5 mg/kg), and succinylcholine chloride (3 mg/kg), and then the animals were intubated and ventilated. A Servo Ventilator 900C (Siemens, Germany) was used for ventilation, with respiration parameters adjusted to each animal's age and weight. Anesthesia was maintained using remifentanil (0.2–1 μg/kg/min) and mivacurium chloride (4–7 mg/kg/h). An iso-osmotic solution (Jonosteril, Fresenius Kabi, Germany) was infused at a rate of 10 ml/kg/h. During the entire experiment, each animal's body temperature was maintained between 38.5 °C and 39.5 °C, and SpO_2 was maintained above 95%.

Every test subject received the same amount of lactate per minute adjusted to its individual body weight (0.04 mmol/kg/min) to ensure the comparability of any lactate-induced effects. The individual dose was adjusted by adapting lactate concentration and the infusion flow rate to each individual test subject. The lactate concentrations used ranged from 0.15 M to 0.6 M (pH, 7.2–7.35) and the flow rates ranged from 0.8 ml/min to 2.5 ml/min, resulting in an infusion time of 12 min to 20 min. Lactate solution was applied to the continuous infusion of Jonosteril electrolyte solution (10 ml/kg/h) to dilute lactate to the above-mentioned concentrations. This application protocol also ensured that any pH changes stayed within a small range. We explicitly did not use a bolus injection because we wanted to mimic a physiological lactate increase comparable to lactate increases during moderate physical exercise (Freund et al., 1990). We applied the same volume of phosphate-buffered saline in five experimental sessions for control experiments (131.5 mM sodium chloride, 10 mM disodium hydrogen phosphate, 2.5 mM monosodium phosphate; pH = 7.2). Furthermore, we applied 0.04 mmol/kg/min of pyruvate in eight experimental sessions. Lactate was applied using a custom-made, pressure-operated pump that used high-precision flow meters to control flow and volume (Sensirion, Switzerland), in combination with Matlab functions to provide an online readout (The MathWorks, Natick, MA, USA). All chemicals were purchased from Sigma-Aldrich (Schnelldorf, Germany).

MR images were acquired using a vertical 4.7 T Bruker BioSpec scanner with an inner bore diameter of 40 cm and a 7 T Bruker BioSpec scanner with an inner bore diameter of 60 cm (Bruker BioSpin, Ettlingen, Germany). We performed three experiments at 4.7 T (lactate), 40 experiments at 7 T (27 lactate, five saline, eight pyruvate) and five cerebral blood flow (CBF) experiments at 7 T (lactate). At 4.7 T, we used a custom-built phased array (Goense et al., 2010) in combination with a linear transmit-coil and eight-shot gradient echo planar imaging (EPI) with a field of view (FOV) = 64 × 48 mm, matrix = 128 × 96, 7 slices (slice thickness = 1 mm), echo time/repetition time (TE/TR) = 20/500 ms, and flip angle (FA) = 40°. At 7 T, we used a custom-made quadrature volume coil (Augath et al., in preparation) and an eight-shot gradient echo EPI, FOV = 96 × 96 mm, matrix = 128 × 128, 13 slices (slice thickness = 2 mm), TE/TR = 20/750, and FA = 47.6°. To further improve efficiency at 7 T, we also used a single-shot gradient EPI, with FOV = 72 × 72 mm, matrix = 96 × 96, 11 slices (slice thickness = 2 mm), TE/TR = 20/3000, and FA = 90°. For the six functional CBF measurements at 7 T, we used a volume coil to transmit in combination with a custom-built, 4-channel phased array (Goense et al., 2010). Perfusion imaging was performed using flow-sensitive alternating inversion recovery (FAIR; Kim, 1995) for arterial spin labeling, with alternating slab-selective and non-selective inversion pulses (13–15 ms hyperbolic secant pulse). Inversion time was 1300 ms, slab 6 mm, FOV = 64 × 48 mm, resolution = 1 × 1 mm, slice thickness = 3 mm, receiver BW = 150 kHz, a shortest possible TE = 6 to 7 ms, TR = 3000 ms, and FA = 90°.

Visual stimuli were presented using a fiber optic system (Avotec, Silent Vision, USA). To adjust the plane of focus, contact lenses (hard PMMA lenses, Wöhlk, Kiel, Germany) were inserted to the monkey's eyes. The stimulus was presented in a block design that showed a full field rotating polar checkerboard for 48 s (ON period), followed by an isoluminant blank screen for the same duration (OFF period). The direction of rotation was reversed every 8 s to avoid adaptation.

We used low-flow microdialysis for systemic lactate sampling in 8 experiments. Lactate concentrations were analyzed using hydrophilic liquid interaction chromatography coupled to electro-spray ionization mass spectrometry (Li et al., 2011). We sampled from a superficial large leg vein using a microdialysis catheter CMA 64, 20-mm PAES membrane, 0.6 mm o.d., 20 kDa cut-off (CMA Microdialysis AB, Sweden). We allowed the semi-permeable membrane to stabilize for 1 h, then sampling was initiated with a flow rate of 2 μl/min. We used a refrigerated fraction collector CMA 740 (CMA Microdialysis AB, Sweden) in which the samples were stored at 6 °C. The temporal resolution of the sampling process was 3 min. After the experiment, the samples were diluted with a solution of 80% acetonitrile containing 0.1% formic acid, and then centrifuged for 3 min (4000 rpm at 4 °C). 3-^{13}C-Lactate (^{13}C-Lac) was used as internal standard for lactate. The mass spectrometer was operated in multiple-reaction monitoring (MRM) mode for quantitative analysis. Lactate and ^{13}C-Lac were monitored based on transfers of m/z 89 → 89, and m/z 90 → 90, respectively. The detection limit of lactate was 0.9 pmol (for a 6-μl in vivo sample).

We applied lactate and pyruvate to two monkeys in nine electrophysiology experiments. These two monkeys had miniaturized chambers implanted over V1 and were used for invasive recordings. We used NeuroNexus probes (NeuroNexus Technologies, Ann Arbor, USA) of 150 μm thickness and 3 mm long shank with 16 electrode sites with 50 μm site spacing and 413 μm^2 electrode sites. The impedance of the electrodes was in the range of 700 kΩ. The preamplifiers for the electrophysiological recordings were custom-made. The signals were amplified and filtered into a band of 1–8 kHz (Alpha-Omega Engineering, Nazareth, Israel) and then digitized at 20.833 kHz with 16-bit resolution (National Instruments, Austin, TX), ensuring enough resolution for both local field and spiking activities. The analog-to-digital converter was linked directly to a PC running a real-time QNX operating system, where the signal was stored.

2.1. Data analysis

Our region of interest (ROI) consisted of the early visual cortex (V1 and V2). A short scan (12 min) preceding the injection scan

was used to identify voxels within the ROI that showed reliable visually-induced modulation. We used a boxcar convolved with a hemodynamic response function (gamma variate function) as a regressor to detect visually-induced modulation. The correlation coefficient of every voxel with this regressor was calculated. Voxels demonstrating robust visually-induced modulation ($P<0.02$) were considered for further analysis. The voxels identified by the short preceding scan were then monitored during the long (40 min) injection scan and studied for lactate-induced effects. This approach allowed us to investigate lactate-induced effects without making any a priori assumptions regarding the potentially induced BOLD response. The same approach was used for the CBF measurements, for which voxels were selected according their visually-induced modulation during the short scan preceding the injection scan. The time course of CBF changes was obtained with linear surround subtraction (Wong et al., 1997). We acquired BOLD fMRI data in 35 sessions during lactate injections. Five of these scans were discarded: two because of a defect in the infusion pump, two because of artifacts caused by a shift in the monkey's position, and one because of a lack of visually-induced modulation. Additionally, one of the six functional CBF measurements was discarded because of a positioning artifact. The remaining 30 BOLD fMRI and five CBF voxel time courses were linearly detrended and then normalized. The single traces were normalized so that the mean amplitude of the stimulus-induced modulation before lactate injection corresponded to one. Every trace was tested for lactate-induced changes in the visually-induced modulation and the baseline. Visually-induced modulation was calculated by subtracting the OFF periods from the ON periods in the averaged voxel time course of our ROI. The baseline shifts in the BOLD signal were analyzed by calculating the mean values of the ON and OFF periods. The threshold for changes in modulation and baseline was set at $P>0.05$. This threshold had to be crossed for at least 6.4 min (the duration of the pre-injection period). We determined four variables that defined the effect: the maximal percentage change, the start of the change (when modulation or baseline crossed the threshold), the time of the maximal effect, and the end of the effect (the last point above the threshold). For statistical analysis, a time window of 6.4 min around the maximum change was selected (range, 19.2–25.6 min) and the modulation and respective baseline during this window was compared with the pre-injection period (range, 0–6.4 min) with a two-tailed t-test (alpha = 0.05). Additionally, two other time windows before (range, 6.5–12.8 min) and after (range, 28.9−35.3 min) the maximum change were defined for further comparison. The plasma lactate levels were also compared using two-tailed t-tests (alpha = 0.05) during these different time windows. The time windows were adapted to match even numbers of scanned volumes, which explains the odd time stamps of the selected windows. Analysis was performed using custom written code based on Matlab.

To analyze the electrophysiological data, we used a one-second window to calculate the power spectral density of two bands: 24–90 Hz LfpH (high local field potential) and 800–3000 Hz multiunit activity MUA (multiunit activity, Rauch et al., 2008). We did not consider layer-specific effects, and averaged the obtained PSD trace over all 16 channels. Next, we calculated changes in modulation and baseline. Visually-induced modulation was calculated by subtracting the OFF periods from the ON periods in the averaged PSD trace. The baseline shifts were analyzed by calculating the mean values of the ON and OFF periods. From these traces, we extracted the maximal percentage change, the start of the change (when modulation or baseline crossed the threshold), the time of the maximal effect, and the end of the effect (the final point above the threshold). In addition, we performed two-tailed t-tests using the same time windows as were used for the BOLD analysis in the single experiments (averaged over 16 channels), as well as in the average of the six experiments.

3. Results

We applied lactate systemically in eight monkeys, with a total of 30 fMRI scans. We used systemic lactate concentrations comparable to those produced by moderate physical exercise (Freund et al., 1990). The concentrations were adapted such that all monkeys received an identical amount of lactate per minute according to individual body weight (see Methods).

Fig. 1 depicts the effects on the BOLD signal after a lactate infusion, and the corresponding plasma lactate concentrations for a single experiment (J08, an 8-year-old, 10.5-kg, male monkey). Fig. 1A–C show the distribution of the visually-activated voxels in the early visual cortex (V1 and V2), while Fig. 1D shows the averaged BOLD time course across the depicted voxels (gray) and the time course of the plasma lactate levels (green). We depict the distribution of the selected voxels for the three central slices in V1 and V2 with an in-plane resolution of 0.75×0.75 mm and 2-mm inter-slice distance; the depicted voxels are color-coded according to their correlation with the visual stimulation paradigm. Lactate application started after the fourth ON–OFF period (6.4 min) and lasted 14 min (gray shading). First, a reliable, visually-induced modulation was observed throughout the entire experimental period, and was not significantly affected by lactate. Second, we induced a positive baseline shift in the BOLD response after the systemic application of lactate. The positive shift in the BOLD response was tightly correlated with the monitored increase of plasma lactate, which reached its peak at 24 min of total scan time. Plasma lactate levels reached 3.4 mM (which is comparable to serum lactate levels observed during moderate physical exercise; Freund et al., 1990), starting from levels slightly above 2 mM before infusion.

To test for the consistency of the observed effects on BOLD response and plasma lactate levels, we performed a group analysis of all 30 experiments. Our population of test animals consisted of 1 female and 7 male monkeys (J08, E04, I02, I08, A09, C06, K07, J07) with an age range from 4 to 11 years, weighing between 4.6 and 12.5 kg, provided with identical housing and comparable food supply. In Fig. 2A, the averaged time courses of the BOLD response across all 30 experiments are depicted with the onset of systemic lactate application after the fourth ON–OFF period. The time windows were selected to match even numbers of acquired volumes and are of identical size. During the pre-infusion period (blue) we observed a reliable, visually-induced modulation of $2.8\pm1.1\%$. As in the single experiment depicted in Fig. 1, we observed a positive baseline shift in BOLD signal that peaked within a time window of 19.2 to 25.6 min (red). The positive baseline shift resulted in an increase of $0.6\pm0.2\%$ of the mean BOLD signal compared with pre-infusion (blue), which corresponds to $22.1\pm7.4\%$ of the visually-induced modulation ($2.8\pm1.1\%$ of the signal). This baseline shift was significant in 26 of the 30 experiments ($P<0.05$); no reliable effect was observed in the remaining four experiments. The lactate-induced BOLD response lasted up to 27.8 min of the total scan time, and then recovered so that no changes were detectable in the time window from 28.9 to 35.3 min (gray). In the time window just after the start of lactate application (from 6.5 to 12.8 min of total scan time; green), no apparent changes in BOLD response were observed, and plasma lactate remained at pre-infusion levels. This finding is most likely due to our slow infusion protocol and the capacity of erythrocytes to buffer lactate to a certain degree, mitigating sudden increases (Smith et al., 1997).

In Fig. 2B, we compared the mean plasma lactate levels across eight experiments (blue trace) with the mean baseline shift over all 30 experiments (red trace). Four male monkeys (J08, C06, K07, J07; age range 6 to 9 years; weight range 5 to 11.5 kg) were used to monitor plasma lactate levels. The induced effects were compared for the identical time window as is depicted in Fig. 2A. We observed significant plasma lactate increases in all eight experiments ($P<0.05$). In

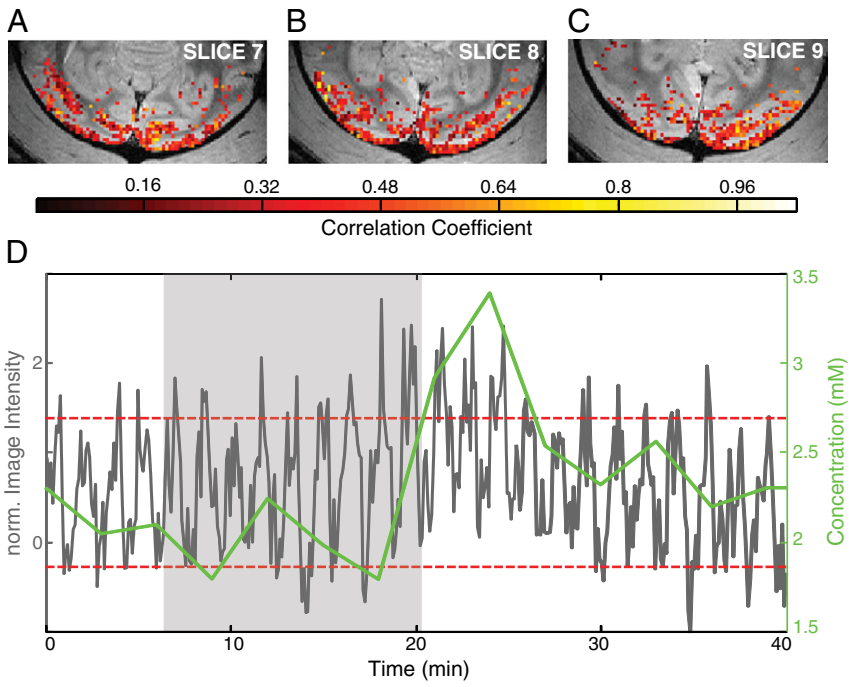

Fig. 1. Example experiment functional magnetic resonance imaging (fMRI) and systemic lactate application: Panels A–C depict the distribution of voxels that are significantly correlated with the stimulus (eight-shot GE-EPI overlaid on an anatomical scan (FLASH), acquired at 7 T, slices 7 through 9, 0.75 × 0.75 mm resolution, and 2-mm inter-slice distance). The correlation coefficient with the regressor is color-coded. The gray trace in panel D depicts the mean time course of the above voxels during the scan with lactate infusion. The infusion began after the fourth stimulus repetition and lasted for 14 min (gray shading). The red dashed lines delineate the amplitude of stimulus-induced modulation during the pre-injection period. Image intensity has been normalized so that the modulation of the pre-injection period corresponds to one. The green trace shows the plasma lactate levels of the same monkey in a separate experiment using the same infusion protocol as was used for the fMRI experiment.

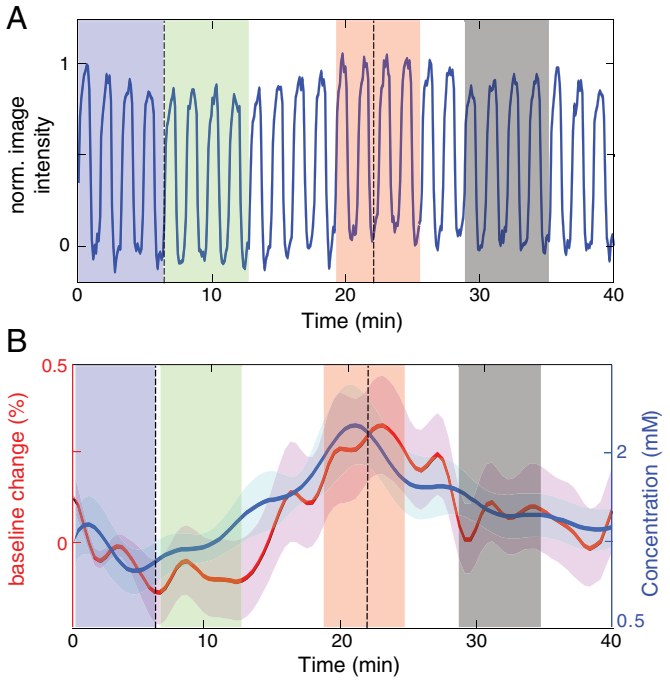

Fig. 2. (A) Mean time course over 30 functional magnetic resonance imaging (fMRI) sessions; the lactate infusion started after the fourth stimulus repetition (6.4 min) and lasted for a mean duration of 18 min (black dashed lines). Shading indicates the time windows used for statistical analysis: blue, before injection (0–6.4 min); green, during injection (6.5–12.8 min); red, shortly after injection (19.2–25.6 min); and gray, recovery phase (27.2–33.6 min). (B) The mean plasma lactate concentration over 8 experiments (blue) and the mean baseline change over 30 fMRI experiments (blood oxygen level-dependent signal, red); lactate injection started after 6.4 min and lasted for a mean duration of 18 min.

the red time window (19.2 to 25.6 min), plasma lactate levels reached a mean maximum of 2.5 ± 0.9 mM, starting from a mean baseline concentration of 1.1 ± 0.5 mM (blue time window, 6.5 to 12.8 min). Maximum plasma lactate was reached at 22.9 ± 4.8 min of total scan time. Compared with lactate levels, BOLD response reached its maximum after 23.4 ± 8 min of total scan time, which we consider a very reliable match considering the different temporal resolutions of the fMRI and the sampling method. Reliability is also indicated by the high correlation between the plasma lactate time course and the BOLD response at an individual level (coefficients of correlation: 0.60 for J08, 0.52 for C06, 0.69 for K07, and 0.85 for J07).

To estimate the distribution of the observed effects on BOLD response within the studied population, we extracted the timing and the peak of the lactate-induced baseline shift, and compared them to each other in a scatter plot (Fig. 3A). The amplitude of the BOLD response was extracted as a percentage of the overall visually-induced modulation (see above). In every test subject, lactate induced a positive baseline shift in the BOLD signal, although the amplitude varied from 16% in the weakest responder to 39% in the strongest responder. The onset of the BOLD baseline increases began between 7.6 min (onset effect, early responder) and 19.8 min (onset effect, late responder), with a mean onset of 16.9 ± 7.5 min. The actual BOLD response lasted for a period of 5.6 to 27.6 min (short versus long pharmacokinetics), with a mean duration of 11.0 ± 8.5 min. Differences in the lactate-induced BOLD response are also reflected in the actual plasma lactate levels (Fig. 3B). We extracted the individual lactate levels before and after infusion and the timing of the peak concentration. The lactate levels ranged from 0.3 to 2.1 mM before infusion and reached maximum levels between 2.0 and 4.0 mM. The onset of plasma lactate increases began between 10.1 (early responder) and 20.6 min (late responder), with a mean onset of 14.1 ± 4.5 min. Lactate remained elevated for a duration of 12 to 21 min (short versus

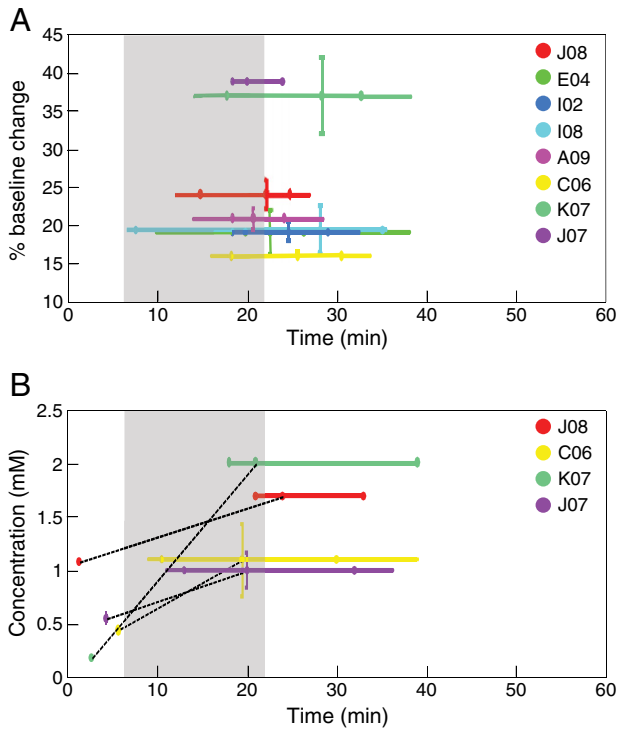

Fig. 3. Inter-individual differences in blood oxygen level-dependent functional magnetic resonance imaging (BOLD-fMRI) (A) and plasma lactate concentration (B). For both datasets, we determined four variables that defined the effect: the maximal change, the start of the change (when baseline or concentration crossed the threshold of $P=0.05$), the time of the maximal effect, and the end of the effect (the final point above the threshold). These variables were averaged for each subject and plotted here. Panel A depicts the percentage BOLD baseline change and respective standard deviation for each subject; the percentage value is referenced to the stimulus-induced modulation before the injection (100%). Panel B depicts plasma lactate concentration before injection, and maximal concentration reached after lactate injection. For both panels, timing and standard deviation of the effect are plotted on the X-axis.

long pharmacokinetics), with a mean duration of 18.4 ± 7.4 min. Lactate infusion is indicated by gray shading, and onset timings are provided in relation to total scan time (Fig. 3A, B). Taken together, and also taking into account the variability within the studied population and irrespective of differences in temporal resolution between the methods used, the BOLD response and the actual plasma lactate levels correlated to a high degree. The variability observed in the timing and amplitude of the lactate-induced effects reflects known differences in lactate turnover that depend on the training level and metabolic state of the test subject (Oyono-Enguelle et al., 1990).

We were also interested in whether we could observe reliable vascular effects induced by lactate application, because it has already been shown that lactate has distinct vasodilatory effects (Reiman et al., 1989). However, these vascular effects were triggered by relatively high doses of lactate. Therefore, we only expected subtle changes in CBF using our infusion protocol, which is comparable to a protocol used by Ido et al. that produced CBF changes only in the range of 4% (Ido et al., 2004). Fig. 4 depicts the mean of five CBF measurements after lactate infusion. We observed reliable visually-induced modulation in the CBF recordings in the range of 19 ± 7% (Zappe et al., 2008), but did not detect any significant baseline shifts comparable to the changes in the BOLD recordings.

To investigate the neuronal activity underlying the BOLD effect, we performed six electrophysiological recordings in two monkeys. During the lactate infusion, we observed an effect in the LfpH band (24–90 Hz, Fig. 5). Both baseline and stimulus-induced modulation increased significantly in five of six experiments. Lactate infusion induced a mean baseline increase of 23.0 ± 1.2% and a mean

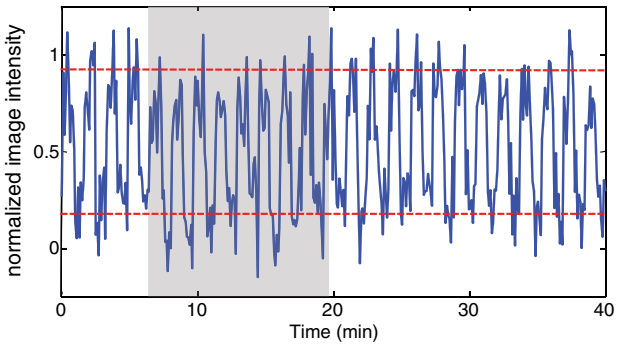

Fig. 4. Mean time course of regional cerebral blood flow (CBF) measurements during lactate infusion (N = 5). The red dashed lines delineate the amplitude of stimulus-induced modulation during the pre-injection period. Gray shading symbolizes the time of lactate application (13.5 min). Image intensity has been normalized so that the modulation of the pre-injection period corresponds to one.

modulation increase of 76.0 ± 20%; this effect lasted from 12.5 ± 1.5 min to 32.0 ± 4.3 min. No significant effect was observed in the MUA (400–3000 Hz). We also tested the effect of pyruvate on the BOLD signal and electrophysiology, because of the dependence of lactate and pyruvate mediated by lactate dehydrogenase (Williamson et al., 1967). Here we report the electrophysiology results, the BOLD effect is described later. The three pyruvate injections exhibited a comparable effect in the LfpH band (Fig. 6) with a mean baseline increase of 31.0 ± 7.3%. This effect lasted from 8.5 ± 2.1 min to the end of the recording. In two cases, we also observed a significant increase in modulation. Also the pyruvate injections did not show a significant effect in the MUA.

As control experiments, we infused buffered saline solution to ensure that lactate-induced BOLD responses were primarily caused by lactate itself. We also wanted to test whether the applied volumes (although relatively small) triggered any cardiovascular responses

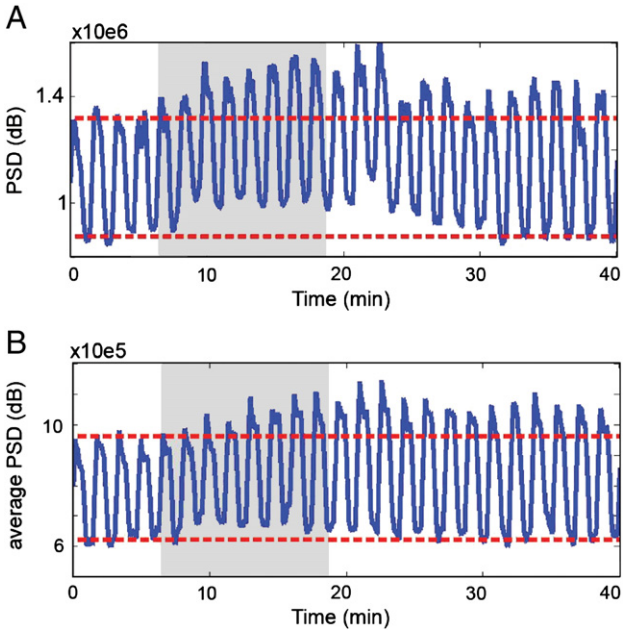

Fig. 5. The power spectrum density of the LfpH band (24–90 Hz). Lactate injection started at 6.4 min and lasted for 12 min (gray shading). The average over the 16 channels in one representative experiment (A), and the average over all six experiments (B) are shown. The red dashed lines depict the amplitude of stimulus-induced modulation during the pre-injection period.

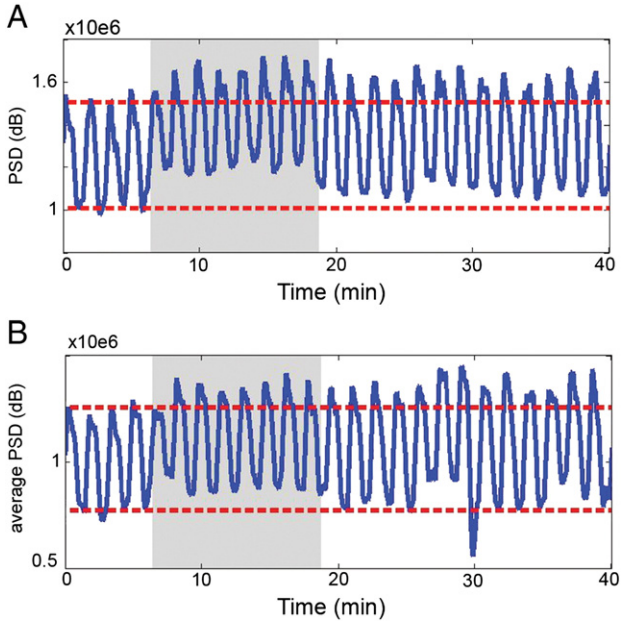

Fig. 6. The power spectrum density of the LfpH band (24–90 Hz). Pyruvate injection started at 6.4 min and lasted for 12 min (gray shading). The average over the 16 channels in one representative experiment (A), and the average over all six experiments (B) are shown. The red dashed lines depict the amplitude of stimulus-induced modulation during the pre-injection period.

that interfered with the BOLD signal. We used buffered saline (pH = 7.2) for five applications in three monkeys (Fig. 8). No significant changes were observed in the BOLD signal after saline infusion using the same protocol as was used for lactate infusion ($P > 0.05$). During pyruvate injection (Fig. 7), we observed a mean baseline increase of $0.9 \pm 0.5\%$, which corresponds to $98.9 \pm 63.3\%$ of the

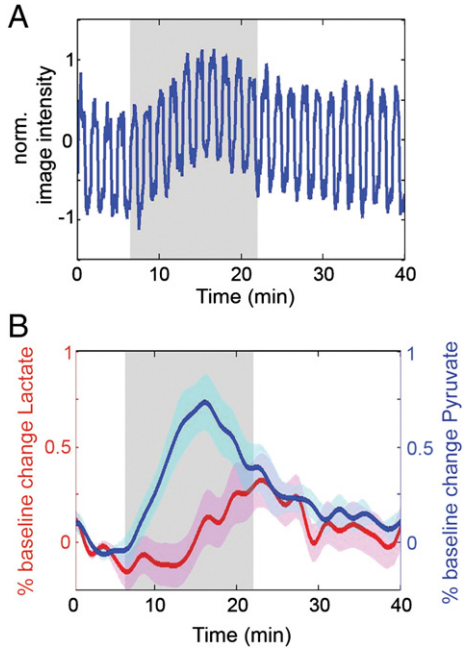

Fig. 7. (A) Mean time course over eight functional magnetic resonance imaging (fMRI) sessions. The pyruvate infusion started after the fourth stimulus repetition (6.4 min) and lasted for a mean duration of 18 min (gray shading). (B) The mean baseline change over 30 fMRI experiments with lactate injection (red), and the mean baseline change over eight fMRI experiments with pyruvate injection (blue).

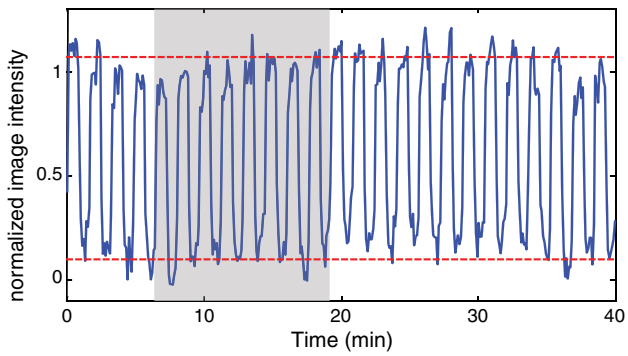

Fig. 8. Control experiment: The mean time course of five experiments with phosphate-buffered saline injection. Saline infusion began after the fourth stimulus repetition and lasted for 12 min (gray shading).

stimulus-induced modulation. This effect exhibited earlier onset than the lactate effect, lasting from 9.2 ± 2.3 min to 27.5 ± 5.9 min, with the maximal effect at 17.1 ± 3.1 min.

4. Discussion

Our study results demonstrate that lactate induces a reliably detectable BOLD response, with even low lactate doses producing plasma concentrations comparable to those brought about by moderate muscular exercise (Freund et al., 1990). We measured the BOLD response after a pharmacological challenge by lactate, which we induced by systemic application in eight anesthetized monkeys. We primarily observed an increase in the BOLD baseline in visually stimulated early visual cortex, with little effect on the visually-induced modulation. The BOLD baseline change correlated directly with the increase in systemic lactate levels. Moreover, even in this rather heterogeneous group of test subjects, we could reliably detect lactate-induced changes in the BOLD signal (this is an important finding because the differences in physiological respectively metabolic conditions did not interfere with our measurements). Especially if clinical applications are envisioned in the future, substantial jitter in the BOLD response must be anticipated precisely because of the above-mentioned physiological differences between individuals. Above all, lactate metabolism depends critically on the training condition and general physiology of human subjects (Oyono-Enguelle et al., 1990), and this should also hold true for non-human primates that show an overlap with human physiology to a very high degree (Voytko and Tinkler, 2004). Indeed, such metabolic differences are reflected in the different onsets and dynamics observed after lactate application. However, they were not substantial enough to jeopardize our use of subtle lactate concentrations, and at an individual level we have shown a high degree of consistency between BOLD response and plasma lactate levels.

The observed increase in the BOLD response after lactate application most likely originates from a combination of neuronal and vascular effects. Therefore, we also performed electrophysiological recordings in two monkeys after lactate application, and observed an increase of neuronal activity in the LfpH band. From previous studies conducted in our lab, we had already shown that LfpH neuronal activity is a reliable driver of the BOLD signal (Logothetis et al., 2001; Rauch et al., 2008). Although lactate-induced increases in neuronal activity have been described in rat hippocampus, the reason for these increases is yet not fully understood (Bergold et al., 2009). Furthermore, lactate is known to increase CBF by inducing the production of nitric oxide and other vasodilatory molecules (Ido et al., 2004; Gordon et al., 2008). However these CBF changes apparently depend to a certain degree on lactate dose and application modality (bolus vs. slow infusion). For example, a bolus injection that increases systemic lactate to 9.8 ± 2.4 mM has induced a

change in CBF in the range of 38–53% in human visual cortex (Mintun et al., 2004). This finding contrasts with the results of a subtle and continuous application of lactate (2 mmol/kg) in rats (reaching plasma concentrations of 3.5 ± 0.4 mM), which did not yield CBF changes greater than 4% (Ido et al., 2004). We verified the CBF changes induced by lactate application (low-dose and continuous infusion) using FAIR recordings, which did not demonstrate reliable CBF changes. We must consider two possible reasons for the lack of CBF changes. The first reason is most likely the very low changes in CBF induced by our lactate application protocol, which would agree with the findings in rats described by Ido et al. (2004). The second reason is related to the detection threshold of the FAIR recordings, which is just within the range of the expected CBF changes (namely, approximately 5%). Consequently, the detection threshold was better for the BOLD response (namely, 0.5%) than for the FAIR recordings. Therefore the lactate challenge described herein (flow 0.04 mmol/kg/min) most likely does not trigger changes in CBF appreciably greater than 5%. It follows that although we are reliably able to observe lactate-induced BOLD responses, a CBF increase in the range of 5% cannot be excluded, but is not detectable to a statistically significant extent in the same animals. It has been hypothesized that the increase of CBF observed in the work of Mintun et al. (2004) depends on NADH/NAD+ ratio which is in near equilibrium with the lactate/pyruvate ratio. Elevated NADH and lactate levels partially trigger the CBF increase, which in turn can be counterbalanced by increasing the levels of pyruvate and NAD+, respectively (Vlassenko et al., 2006). However, our systemic application of pyruvate (using a dosage identical to the dosage of lactate) did exhibit effects in BOLD and neuronal responses comparable to lactate. Apparently, in this low physiological range, lactate and pyruvate may serve as equivalent substrates to induce the BOLD and neuronal effects that we have observed. The faster BOLD response to pyruvate might be explained by pyruvate's direct access to the tricarboxylic acid cycle, while lactate must still be transformed into pyruvate.

The main focus of this study was to test the lower detection boundaries of lactate-induced BOLD responses to investigate the impact of the physiological formation of lactate on the BOLD signal. If the physiological formation of lactate has an impact on the BOLD signal (which we mimic using our slow infusion protocol), then a potential diagnostic application could be developed. For example, the changes in lactate metabolism in neurodegenerative disorders like AD are gradual and develop over a long period of time. Therefore, the lack of BOLD responsiveness to a lactate challenge within the physiological range of lactate formation might be a potential hallmark of AD. The reduced responsiveness of CBF to sensory stimulation has already been described in AD patients; this reduced CBF responsiveness also correlated with the severity of AD progression (Mentis et al., 1998). In agreement with these findings, Kalman et al. did not observe a single-photon emission computed tomography response after a lactate challenge (2.5 mmol/kg) in AD patients induced plasma lactate levels of 5.5 ± 1.226 mM (Kalman et al., 2005). Reduced responsiveness to physiological lactate formation in AD is in agreement with a recent review highlighting the close resemblance of AD to a vascular disorder in which delayed and weakened responses to increased metabolic demand might be a preclinical feature (Iadecola, 2004).

Taken together, we demonstrate that physiological lactate formation can contribute to the BOLD signal, and therefore can be reliably traced by fMRI. This finding might be exploited for neurodegenerative disorders like AD in which lactate metabolism is disturbed (Redjems-Bennani et al., 1998). Patients at risk of (Richard and Amouyel, 2001) or in the early stages of AD might potentially exhibit a change of the BOLD signal in response to physiological lactate formation. Future clinical studies are needed to demonstrate whether our approach can deliver such diagnostics.

Acknowledgments

This work was supported by the Max Planck Society. Juan Li and Alexander Rauch were supported by the BMBF Grant Nr. 01EV0701. We thank Hellmut Merkle for designing and manufacturing the RF coils; Yvette Bohraus, Mark Augath, and Thomas Steudel for operating the scanners; and Deniz Ipek and Mirko Lindig for supervising the anesthesia.

References

Bergold, P.J., Pinkhasova, V., Syed, M., Kao, H.Y., Jozwicka, A., Zhao, N., Coplan, J.D., Dow-Edwards, D., Fenton, A.A., 2009. Production of panic-like symptoms by lactate is associated with increased neural firing and oxidation of brain redox in the rat hippocampus. Neurosci. Lett. 453 (3), 219–224.

Fox, P.T., Raichle, M.E., 1986. Focal physiological uncoupling of cerebral blood flow and oxidative metabolism during somatosensory stimulation in human subjects. Proc. Natl. Acad. Sci. U.S.A. 83 (4), 1140–1144.

Fox, P.T., Raichle, M.E., Mintun, M.A., Dence, C., 1988. Nonoxidative glucose consumption during focal physiologic neural activity. Science 241 (4864), 462–464.

Freund, H., Oyono-Enguelle, S., Heitz, A., Ott, C., Marbach, J., Gartner, M., Pape, A., 1990. Comparative lactate kinetics after short and prolonged submaximal exercise. Int. J. Sports Med. 11 (4), 284–288.

Goense, J., Logothetis, N.K., Merkle, H., 2010. Flexible, phase-matched, linear receive arrays for high-field MRI in monkeys. Magn. Reson. Imaging 28 (8), 1183–1191.

Gordon, G.R., Choi, H.B., Rungta, R.L., Ellis-Davies, G.C., MacVicar, B.A., 2008. Brain metabolism dictates the polarity of astrocyte control over arterioles. Nature 456 (7223), 745–749.

Hu, Y., Wilson, G.S., 1997. A temporary local energy pool coupled to neuronal activity: fluctuations of extracellular lactate levels in rat brain monitored with rapid-response enzyme-based sensor. J. Neurochem. 69 (4), 1484–1490.

Iadecola, C., 2004. Neurovascular regulation in the normal brain and in Alzheimer's disease. Nat. Rev. Neurosci. 5 (5), 347–360.

Ido, Y., Chang, K., Williamson, J.R., 2004. NADH augments blood flow in physiologically activated retina and visual cortex. Proc. Natl. Acad. Sci. U.S.A. 101 (2), 653–658.

Jezzard, P., Buxton, R.B., 2006. The clinical potential of functional magnetic resonance imaging. J. Magn. Reson. Imaging 23 (6), 787–793.

Kalman, J., Palotas, A., Kis, G., Boda, K., Turi, P., Bari, F., Domoki, F., Doda, I., Argyelan, M., Vincze, G., Sera, T., Csernay, L., Janka, Z., Pavics, L., 2005. Regional cortical blood flow changes following sodium lactate infusion in Alzheimer's disease. Eur. J. Neurosci. 21 (6), 1671–1678.

Kim, S.G., 1995. Quantification of relative cerebral blood flow change by flow-sensitive alternating inversion recovery (FAIR) technique: application to functional mapping. Magn. Reson. Med. 34 (3), 293–301.

Li, J., von Pfostl, V., Zaldivar, D., Zhang, X., Logothetis, N., Rauch, A., 2011. Measuring multiple neurochemicals and related metabolites in blood and brain of the rhesus monkey by using dual microdialysis sampling and capillary hydrophilic interaction chromatography-mass spectrometry. Anal. Bioanal. Chem. 402 (8), 2545–2554.

Logothetis, N.K., Guggenberger, H., Peled, S., Pauls, J., 1999. Functional imaging of the monkey brain. Nat. Neurosci. 2 (6), 555–562.

Logothetis, N.K., Pauls, J., Augath, M., Trinath, T., Oeltermann, A., 2001. Neurophysiological investigation of the basis of the fMRI signal. Nature 412 (6843), 150–157.

Mentis, M.J., Alexander, G.E., Krasuski, J., Pietrini, P., Furey, M.L., Schapiro, M.B., Rapoport, S.I., 1998. Increasing required neural response to expose abnormal brain function in mild versus moderate or severe Alzheimer's disease: PET study using parametric visual stimulation. Am. J. Psychiatry 155 (6), 785–794.

Mintun, M.A., Vlassenko, A.G., Rundle, M.M., Raichle, M.E., 2004. Increased lactate/pyruvate ratio augments blood flow in physiologically activated human brain. Proc. Natl. Acad. Sci. U.S.A. 101 (2), 659–664.

Oyono-Enguelle, S., Marbach, J., Heitz, A., Ott, C., Gartner, M., Pape, A., Vollmer, J.C., Freund, H., 1990. Lactate removal ability and graded exercise in humans. J. Appl. Physiol. 68 (3), 905–911.

Pellerin, L., Magistretti, P.J., 2004. Neuroenergetics: calling upon astrocytes to satisfy hungry neurons. Neuroscientist 10 (1), 53–62.

Prichard, J., Rothman, D., Novotny, E., Petroff, O., Kuwabara, T., Avison, M., Howseman, A., Hanstock, C., Shulman, R., 1991. Lactate rise detected by 1H NMR in human visual cortex during physiologic stimulation. Proc. Natl. Acad. Sci. U.S.A. 88 (13), 5829–5831.

Rauch, A., Rainer, G., Logothetis, N.K., 2008. The effect of a serotonin-induced dissociation between spiking and perisynaptic activity on BOLD functional MRI. Proc. Natl. Acad. Sci. U.S.A. 105 (18), 6759–6764.

Redjems-Bennani, N., Jeandel, C., Lefebvre, E., Blain, H., Vidailhet, M., Gueant, J.L., 1998. Abnormal substrate levels that depend upon mitochondrial function in cerebrospinal fluid from Alzheimer patients. Gerontology 44 (5), 300–304.

Reiman, E.M., Caselli, R.J., Chen, K., Alexander, G.E., Bandy, D., Frost, J., 2001. Declining brain activity in cognitively normal apolipoprotein E epsilon 4 heterozygotes: a foundation for using positron emission tomography to efficiently test treatments to prevent Alzheimer's disease. Proc. Natl. Acad. Sci. U.S.A. 98 (6), 3334–3339.

Reiman, E.M., Chen, K., Alexander, G.E., Caselli, R.J., Bandy, D., Osborne, D., Saunders, A.M., Hardy, J., 2004. Functional brain abnormalities in young adults at genetic risk for late-onset Alzheimer's dementia. Proc. Natl. Acad. Sci. U.S.A. 101 (1), 284–289.

Reiman, E.M., Chen, K., Alexander, G.E., Caselli, R.J., Bandy, D., Osborne, D., Saunders, A.M., Hardy, J., 2005. Correlations between apolipoprotein E epsilon4 gene dose

and brain-imaging measurements of regional hypometabolism. Proc. Natl. Acad. Sci. U.S.A. 102 (23), 8299–8302.
Reiman, E.M., Raichle, M.E., Robins, E., Mintun, M.A., Fusselman, M.J., Fox, P.T., Price, J.L., Hackman, K.A., 1989. Neuroanatomical correlates of a lactate-induced anxiety attack. Arch. Gen. Psychiatry 46 (6), 493–500.
Richard, F., Amouyel, P., 2001. Genetic susceptibility factors for Alzheimer's disease. Eur. J. Pharmacol. 412 (1), 1–12.
Smith, E.W., Skelton, M.S., Kremer, D.E., Pascoe, D.D., Gladden, L.B., 1997. Lactate distribution in the blood during progressive exercise. Med. Sci. Sports Exerc. 29 (5), 654–660.
Vlassenko, A.G., Rundle, M.M., Raichle, M.E., Mintun, M.A., 2006. Regulation of blood flow in activated human brain by cytosolic NADH/NAD+ ratio. Proc. Natl. Acad. Sci. U.S.A. 103 (6), 1964–1969.
Voytko, M.L., Tinkler, G.P., 2004. Cognitive function and its neural mechanisms in non-human primate models of aging, Alzheimer disease, and menopause. Front. Biosci. 9, 1899–1914.
Williamson, D.H., Lund, P., Krebs, H.A., 1967. The redox state of free nicotinamide-adenine dinucleotide in the cytoplasm and mitochondria of rat liver. Biochem. J. 103 (2), 514–527.
Wong, E.C., Buxton, R.B., Frank, L.R., 1997. Implementation of quantitative perfusion imaging techniques for functional brain mapping using pulsed arterial spin labeling. NMR Biomed. 10 (4–5), 237–249.
Zappe, A.C., Pfeuffer, J., Merkle, H., Logothetis, N.K., Goense, J.B., 2008. The effect of labeling parameters on perfusion-based fMRI in nonhuman primates. J. Cereb. Blood Flow Metab. 28 (3), 640–652.

Study 2

Anal Bioanal Chem
DOI 10.1007/s00216-011-5427-z

ORIGINAL PAPER

Measuring multiple neurochemicals and related metabolites in blood and brain of the rhesus monkey by using dual microdialysis sampling and capillary hydrophilic interaction chromatography–mass spectrometry

Juan Li · Veronika von Pföstl · Daniel Zaldivar · Xiaozhe Zhang · Nikos Logothetis · Alexander Rauch

Received: 7 June 2011 / Revised: 25 August 2011 / Accepted: 17 September 2011

Abstract In vivo measurement of multiple functionally related neurochemicals and metabolites (NMs) is highly interesting but remains challenging in the field of basic neuroscience and clinical research. We present here an analytical method for determining five functionally and metabolically related polar substances, including acetylcholine (quaternary ammonium), lactate and pyruvate (organic acids), as well as glutamine and glutamate (amino acids). These NMs are acquired from samples of the brain and the blood of non-human primates in parallel by dual microdialysis, and subsequently analyzed by a direct capillary hydrophilic interaction chromatography (HILIC)–mass spectrometry (MS) based method. To obtain high sensitivity in electrospray ionization (ESI)–MS, lactate and pyruvate were detected in negative ionization mode whereas the other NMs were detected in positive ionization mode during each HILIC-MS run. The method was validated for linearity, the limits of detection and quantification, precision, accuracy, stability and matrix effect. The detection limit of acetylcholine, lactate, pyruvate, glutamine, and glutamate was 150 pM, 3 μM, 2 μM, 5 nM, and 50 nM, respectively. This allowed us to quantitatively and simultaneously measure the concentrations of all the substances from the acquired dialysates. The concentration ratios of both lactate/pyruvate and glutamine/glutamate were found to be higher in the brain compared to blood ($p<0.05$). The reliable and simultaneous quantification of these five NMs from brain and blood samples allows us to investigate their relative distribution in the brain and blood, and most importantly paves the way for future non-invasive studies of the functional and metabolic relation of these substances to each other.

Keywords Neurochemicals · HILIC-MS · Microdialysis · Rhesus monkey · Brain · Blood

Juan Li and Veronika von Pföstl contributed equally to this paper.

Published in the special issue *Analytical Sciences in Switzerland* with guest editors P. Dittrich, D. Günther, G. Hopfgartner, and R. Zenobi.

J. Li · V. von Pföstl · D. Zaldivar · N. Logothetis · A. Rauch (✉)
Max Planck Institute for Biological Cybernetics,
Spemannstrasse 38,
72076 Tübingen, Germany
e-mail: arauch@tuebingen.mpg.de

X. Zhang (✉)
Department of Medicine, University of Fribourg,
Chemin de Musee 5,
Fribourg 1700, Switzerland
e-mail: xiaozhe.zhang@unifr.ch

N. Logothetis
Division of Imaging Science and Biomedical Engineering,
University of Manchester,
Manchester M13 9PT, UK

D. Zaldivar
Graduate School of Neural and Behavioural Science/International Max Planck Research School, University Tübingen,
72074 Tübingen, Germany

Introduction

The physiological function of neurons and the correct information processing within the brain depend critically on neuroactive molecules and metabolites (NMs). These NMs consisting of neurotransmitters like glutamate or neuromodulators like acetylcholine can be detected by appropriate techniques in the extracellular fluid of the brain. The concentrations of these NMs are tightly controlled and

Published online: 29 September 2011

stable within narrow boundaries. Many disorders of the central nervous system (CNS) such as Parkinson's disease [1], Alzheimer's disease [2], and schizophrenia [3], are correlated with or even caused by changes in the concentrations of such substances. NMs can be sampled from the extracellular brain fluid (EBF) which allows us to investigate their dynamic reflecting changes in neuronal activity. The EBF forms a complex, dynamic environment embedding all neural elements and serves as medium for the cell-to-cell communication and metabolite transport. Many of these NMs also exist in the blood system, but their concentrations are commonly different from those in the brain because of the differential permeability of the blood brain barrier (BBB) and of differences in absorption mechanisms, synthesis, and metabolism. Simultaneous and quantitative monitoring of these NMs from the brain and the blood system will therefore allow us to assess their relation between the brain and the blood system.

In the present study, we focused on a selection of NMs functionally and metabolically related and developed a direct and sensitive analytical method to monitor acetylcholine, lactate, pyruvate, glutamine, and glutamate in parallel from the brain and the blood. All these five substances are derivates from glucose and the citrate cycles [4, 5]. Additionally, acetylcholine is able to modulate glutamatergic release and can interact with the brain energy metabolism [6–8]. To do so, we used microdialysis to collect samples from EBF and blood of anesthetized non-human-primates in parallel. This will allow us to investigate changes in their relation caused by functional and metabolic challenges or by pathologies in the future. However, their chemical and physical properties are different which makes it difficult to separate and detect these NMs together. To the best of our knowledge, there is currently no report describing the simultaneous determination of all five aforementioned substances by a single analysis. Indeed, so far, most analytical methods developed were only focusing on the determination of one or two of such targeted substances. For example, electrochemical detection (ECD) is commonly used to monitor these compounds [9–11], but an additional enzyme reactor is needed to generate electrochemically detectable hydrogen peroxide for acetylcholine detection [12], so it is difficult to monitor all these substances in a single analytical run using ECD as detector. Compared to the classical ECD, mass spectrometry (MS) is able to detect diverse NMs with high sensitivity and selectivity. Recent analytical advances have been made by using MS detection coupled with ion-pair reversed-phase liquid chromatography (RPLC) or ion exchange chromatography (IEC) as separation tools. For instance, acetylcholine has been analyzed by strong cation exchange (SCX)-MS [13] or ion-pair RPLC-MS [14, 15]. Pyruvate was analyzed by weak anion exchange (WAX)-MS [16], while lactate and pyruvate together were detected by RPLC-ESI/MS (electro spray ionization, ESI), but a time-consuming derivatization process with 3-nitrophenyl-hydrazine was needed [17]. Glutamine and glutamate were determined by ion-pair RPLC-MS using an ion-pairing regent which might cause ESI suppression [18].

In contrast to ion-pair RPLC or IEC-based analytical approaches, hydrophilic interaction liquid chromatography (HILIC)–MS is an alternative technique that allows separating and determining multiple polar analytes irrespective of being a base or an organic acid [19, 20]. It already has proved its merits in determining peptides, proteins and small polar molecular compounds in complex matrices [21–24]. Recent reports demonstrated that HILIC-MS is well suited to determine polar neurotransmitters in EBF offering high sensitivity combined with time-saving procedures for sample preparation [23, 25].

In this study, we report the successful combination of capillary HILIC-ESI/MS with dual microdialysis sampling for simultaneous measurement of five NMs together in brain and blood dialysates of non-human primates. First, our approach allows us to compare the relation of these NMs to each other under different physiological and pathological states of the brain. Second, the simultaneous sampling from the brain and the blood can be used to extrapolate from blood measurements to brain concentrations of these NMs. Relation changes of these NMs detectable in the blood can serve as easy accessible biomarkers reflecting physiological or pathological states of the brain [26].

Experimental

Chemicals

HPLC-MS grade acetonitrile, formic acid, and ammonium formate were purchased from Sigma-Aldrich (Munich, Germany). [3-^{13}C] lactate (as aqueous solution, 20% *w*/*w* in H_2O) (^{13}C-lactate), glutamine-L-2, 3, 3, 4, 4-d_5 (glutamine-d_5), and glutamic acid-L-2, 3, 3, 4, 4-d_5 (glutamate-d_5) were purchased from Cambridge Isotope Laboratories (Andover, USA). Acetylcholine-*N*,*N*,*N*-trimethyl-d_9 chloride (acetylcholine-d_9) was bought from Medical Isotopes, Inc (Pelham, USA). Acetylcholine chloride, sodium lactate (lactate), sodium pyruvate, glutamine, glutamate, [1-^{13}C] sodium pyruvate (^{13}C-pyruvate), and the chemicals for preparing frits were all obtained from Sigma-Aldrich. Pure water was produced by a TKA superpure water system (Niederelbert, Germany). Artificial cerebral spinal fluid (a-CSF) for standard solutions consisted of 148 mM NaCl, 3.00 mM KCl, 0.80 mM $MgCl_2$, and 1.40 mM $CaCl_2$, pH 7.3.

Fabrication of capillary columns

The preparation of capillary columns was adopted and modified from Zhang et al. [23]. To prevent the packing material from spilling out of the column a frit was formed at one end by in situ free radical polymerization modified from Viklund et al. [27]. Compared to the frit formed by sintered reaction, our frit can easily withstand long exposure to high pressure (>3,000 psi) and minimize extra-column band broadening. After the reaction, unreacted material and other soluble compounds were removed from the pores by washing with ethanol followed by purging with helium for 15 min. The column was packed with acetone slurry (1.5 mL) containing 50 mg of 5 μm polyhydroxyethyl aspartamide particles (PolyLC, USA) with the help of a helium pressure cell with a stirring bar to maintain particle suspension running under a pressure of 100 bars for 30 min. The packed column was cut to 15 cm for use.

Preparation of calibration standards and internal standards

To increase the reproducibility of the quantitative analysis of acetylcholine, lactate, pyruvate, glutamine, and glutamate, acetylcholine-d_9, ^{13}C-lactate, ^{13}C-pyruvate, glutamine-d_5, and glutamate-d_5 were used as their respective internal standards (IS). Stock solutions of the analytes were prepared in 30% acetonitrile containing 0.1% formic acid and stored at 5 °C. To characterize the analytical performance of capillary HILIC-MS methods for the quantitative measurement of the analytes, the stock solution was serially diluted using a solution containing a-CSF/solution A (90% acetonitrile, 0.1% formic acid; 1:4, *v*/*v*). The calibration solutions of acetylcholine ranged from 0.5–250 nM and consisted of three levels (low, medium, and high) of quality control (QC) samples with 2.5, 25, and 125 nM. For lactate and pyruvate, the calibration solutions ranged from 10–5,000 μM, and QC samples were 50, 500, and 2500 μM. For glutamine, the calibration solutions ranged from 0.5–250 μM, and QC samples were 2.5, 25, and 125 μM. For glutamate the calibration solutions ranged from 0.25–125 μM, and QC samples were 1.25, 12.5, and 62.5 μM. Two IS stock solutions were prepared in water containing 0.1% formic acid: one (IS_1) is used for the calibration curve preparation and the blood microdialysate samples analysis, which contains 500 nM acetylcholine-d_9, 10 mM ^{13}C-lactate, 10 mM ^{13}C-pyruvate, 500 μM glutamine-d_5, and 250 μM glutamate-d_5; the other one (IS_2) is used for the monkey brain microdialysate samples analysis containing 300 nM acetylcholine-d_9, 6 mM ^{13}C-lactate, 6 mM ^{13}C-pyruvate, 300 μM glutamine-d_5, and 150 μM glutamate-d_5. These internal standards were diluted ten times (IS_1) and six times (IS_2) on the day of the assay using a-CSF/solution A (90% acetonitrile, 0.1% formic acid; 1:4, *v*/*v*). The calibration curve was constructed based on the response ratio of the peak area ($P_{analyte}/P_{IS}$) versus the nominal standard concentrations by a least-squares regression using a weighting factor of 1/concentration^2.

Microdialysis sampling

Two male rhesus monkeys (*Macaca mulatta*) were used with an age of 5 years weighing between 6 and 7 kg. The experimental procedures were approved by the local authorities (in German: "Regierungspraesidium Tuebingen") and were in agreement with guidelines of the European Community (EUVD 86/609/EEC) for the care and use of laboratory animals. During the experiment, the monkeys were anesthetized with full monitoring of all vital parameters. Before the experiment, the monkeys were sedated with ketamine (15 mg/kg). Anesthesia was induced with fentanyl (31 μg/kg), thiopental (5 mg/kg), and succinyl chloride (3 mg/kg). Afterwards, the monkeys were intubated and ventilated with a Servo Ventilator 900 C (Siemens, Germany). The maintenance of anesthesia was attained with remifentanyl (0.2–1 μg/kg/min) and mivacurium chloride (4–7 mg/kg/h). A crystalloid solution (Ionosteril, Fresenius Kabi, Germany) with 2.5% glucose was infused at a rate of 10 ml/kg/h. During the experiment, body temperature was kept between 38.5 and 39.5 °C, SpO_2 above 95% and end tidal CO_2 at 35 mmHg.

The monkeys had a miniaturized PEEK chamber over the primary visual cortex that gave access to the brain. The probe was inserted through a small incision in the dura. The probe for blood sampling was placed into a superficial leg vein using an intravenous catheter.

For brain sampling, microdialysis probes CMA 12 with 2 mm PAES membrane of 0.5 mm outer diameter (o.d.) and a 20 kDa cut-off (CMA Microdialysis AB, Sweden) were used. The probe was flushed with a-CSF solution at a flow rate of 2 μL/min for 15 min, and then conditioned at a flow rate of 600 nL/min for 2 h before insertion into the cortex of the monkey. For the blood sampling, a microdialysis catheter CMA 64, 20 mm PAES membrane, 0.6 mm o.d., 20 kDa cut-off (CMA Microdialysis AB, Sweden) was flushed with saline containing fragmin 25 IU/mL (Pfizer Pharma GmbH, Germany) at a flow rate of 2 μL/min for 2 h before insertion. The collections of microdialysis samples were started 2 h after the insertion of the probes for blood sampling as well as for brain sampling.

The dialysates were collected in parallel by two refrigerated fraction collectors CMA 740 (CMA Microdialysis AB, Sweden) at 6 °C for 1 h. The samples were collected at an interval of 3 min for both brain and blood sampling. We collected simultaneously five brain and five

blood samples each time. The sampling experiments were repeated two times from each animal. Before sampling, the IS solution was added to the glass inserts used for sample collection and then put into the refrigerated fraction collectors. After the experiment, the brain microdialysate samples were concentrated by a vacuum concentrator (Eppendorf, Germany) under room temperature for 5 min and reconstituted by solution B (60% acetonitrile, 0.1% formic acid) for further analysis. The blood microdialysate samples were directly diluted by solution C (80% acetonitrile, 0.1% formic acid) and then analyzed.

In vitro recovery of CMA 12 probes has been tested in our lab, and it was 50.2–66.8% for all analytes with a reliable stability not exceeding 3.6% standard errors. The measured in vitro recovery of CMA 64 probes for all analytes was 42.5–49.3% with good reliable stability not exceeding 4.3% standard errors.

Capillary liquid chromatography and mass spectrometry

An Agilent capillary HPLC 1100 system coupled to a XCT plus ion-trap mass spectrometer (Agilent, Waldbronn, Germany) was used for analysis. Mobile phase A was an aqueous solution containing 50 mM ammonium formate and 1.0% formic acid (pH 2.87), and mobile phase B was acetonitrile. The analysis was performed using a gradient profile: 0.0–10.0 min, 85% B to 45% B, then 45% B was kept for 5 min. The column was reconditioned using an 85% solution of B for 10 min before further injection. The flow rate was 3.5 μL/min, and a sample of 0.3 μL was injected in the column each time.

MS analysis was performed by switching between positive and negative ion mode. Ion-trap tandem mass spectrometry (MS/MS) experiments were applied to isolate and fragment the precursor ions. The mass spectrometer was operated in MRM mode (multiple-reaction-monitoring) for the quantitative analysis. Five scans were averaged for each spectrum with the scan range of m/z 50–2,000. MS scans were split into three segments considering the different MS behaviors of five compounds. In the first segment (0.0–3.5 min) acetylcholine and acetylcholine-d_9 were monitored under a positive mode with the capillary voltage of 3,500 V, while lactate, ^{13}C-lactate, pyruvate and ^{13}C-pyruvate were monitored under a negative mode in the second segment (3.5–8.6 min) with the capillary voltage of 2,541 V, and glutamine, glutamine-d_5, glutamate, and glutamate-d_5 were monitored under a positive mode in the third segment (8.6–15.0 min) with capillary voltage of 3200 V. The MS parameters of five analytes and their corresponding internal standards are listed in Table 1. Lactate and pyruvate did not generate significant and stable product ions, so we could not use the product ions for lactate and pyruvate in MRM conditions. We used ion fragmentation amplitude of 0.5 V and ion fragmentation cut-off of 58 which reduced the background noise keeping the lactate and pyruvate unaffected. This procedure could compensate for the lack of specificity which is achieved by monitoring the transfer from the precursor ion to the product ion. The MS settings such as capillary exit, skimmer and lens voltages were optimized and tuned by the data acquisition software during infusion of a standard solution for each compound.

Results and discussion

HILIC-MS analytical method development

Highest intensities for all the analytes were achieved when both the positive and the negative ionization mode of the mass spectrometer were used in the ESI experiments. Previous studies showed that chemicals can have different ESI/MS responses because of their different physical and chemical properties [28]. In our case, lactate and pyruvate, which are organic acids, had much higher intensities in negative ionization mode than in positive ionization mode. The other analytes, acetylcholine, glutamine and glutamate generated responses with high intensity only in positive ionization mode. For our experiments, we thus used positive ionization mode for detecting acetylcholine, glutamine, and glutamate, while negative ionization mode for lactate and pyruvate. In the analytical experiments, we selected HILIC as the method to separate the five polar analytes. Our initial tests showed that HILIC was able to separate them simultaneously (data not shown). The elution order was acetylcholine, lactate, pyruvate, glutamine, and glutamate. Because both positive and negative ionization mode were used for ESI/MS detection, the efficient separation of lactate and pyruvate from the other analytes has to be achieved to ensure that each analyte reliably matches the time window of the appointed ionization mode.

To achieve optimal separation and intensity of the five analytes on the HILIC-MS, we examined the influence of pH value, water content and buffer concentration of the mobile phase on the retention behavior and MS signal of each analyte. Figure 1a shows that the pH value had clearly stronger effects on lactate and glutamate compared to the other three analytes when we varied the pH of mobile phase A from 2.7–4.2 by adjusting formic acid proportions from 0.05–1.50%. In particular, the elution order of lactate and pyruvate reversed when pH value ranged from 3.9–2.7. This may be because lactate is ionized at higher pH values compared to its pK_a of 3.85. Figure 1d indicates that the MS intensity of the five analytes was also affected by the pH value. Their intensities were on average higher at lower pH value; 1.0% formic acid (pH 2.9) was finally used for

Table 1 MS parameters for five analytes and their internal standards

Compounds	MRM transition	Width	Frag. cut-off (*m*/*z*)	Frag. amplitude (V)	ICC smart target (*m*/*z*)	ICC accumulation time (ms)
Ach	146→87	1.0	62	1.38	200,000	200
Ach-d_9	155→87	1.0	62	1.38	200,000	200
Lac	89→89	1.0	58	0.50	200,000	100
^{13}C-Lac	90→90	1.0	58	0.50	200,000	100
Pyr	87→87	1.0	58	0.50	200,000	100
^{13}C-Pyr	88→88	1.0	58	0.50	200,000	100
Gln	147→130	1.0	69	1.20	50,000	200
Gln-d_5	152→135	1.0	69	1.20	50,000	200
Glu	148→130	1.0	60	0.98	50,000	200
Glu-d_5	153→135	1.0	60	0.98	50,000	200

the following optimization warranting efficient separation combined with high intensity.

The water content had strong influence on the chromatographic behaviors and MS signal intensities of all five analytes. When the water content was decreased to 30% or lower, lactate and pyruvate could be very well separated from their neighboring peaks of acetylcholine and glutamine in the chromatogram (Fig. 1b). Figure 1e illustrates that the reduced water content (from 60–30%) could enhance the MS intensity, which is the benefit of the increased electrospray ionization efficiency in a high organic phase. On the other hand, a MS signal decline was observed when the water content ranged from 30% to 20%. This might result from the low solubility of the polar compounds in the high organic phase mobile.

During the method development, we found that the salt content in the buffer solution had a great impact on the peak shapes and MS signal of the analytes (Fig. 1f), but less effect on retention time (Fig. 1c). Sharp peak shapes and high reproducible retention times were obtained for all

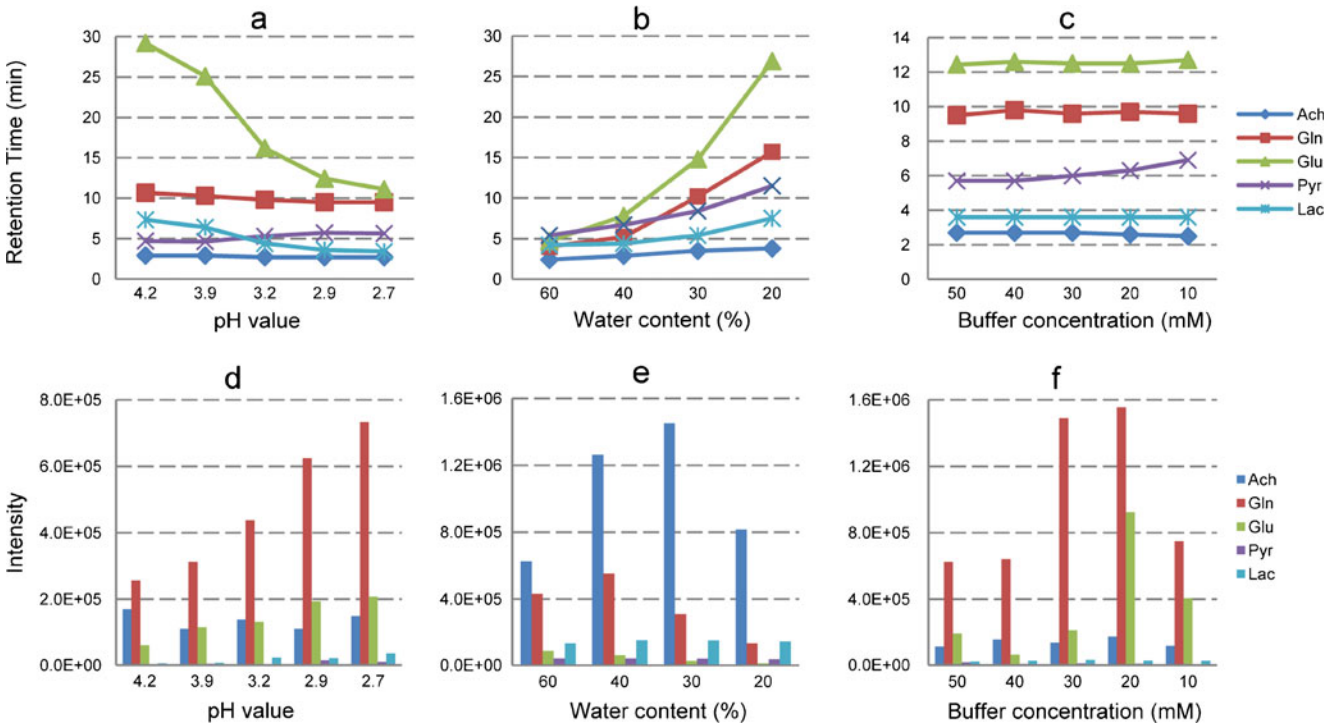

Fig. 1 Influences of mobile phase on retention behavior and MS signal of the five analytes. **a** Effects of pH value on the retention time. **b** Effects of water content on the retention time. The aqueous phase containing 50 mM ammonium formate and 1.0% formic acid. **c** Effects of buffer concentration on the retention time. Mobile phase A containing 1.0% formic acid. **d** Effects of pH value on MS signal. **e** Effects of water content on MS signal. **f** Effects of buffer concentration on MS signal. An isocratic elution of mobile phase A: mobile phase B (15:75, *v*/*v*) was used to test the influence of pH value and buffer concentration. *Acetylcholine (*Ach*), Lactate (*Lac*), Pyruvate (*Pyr*), Glutamine (*Gln*), Glutamate (*Glu*)

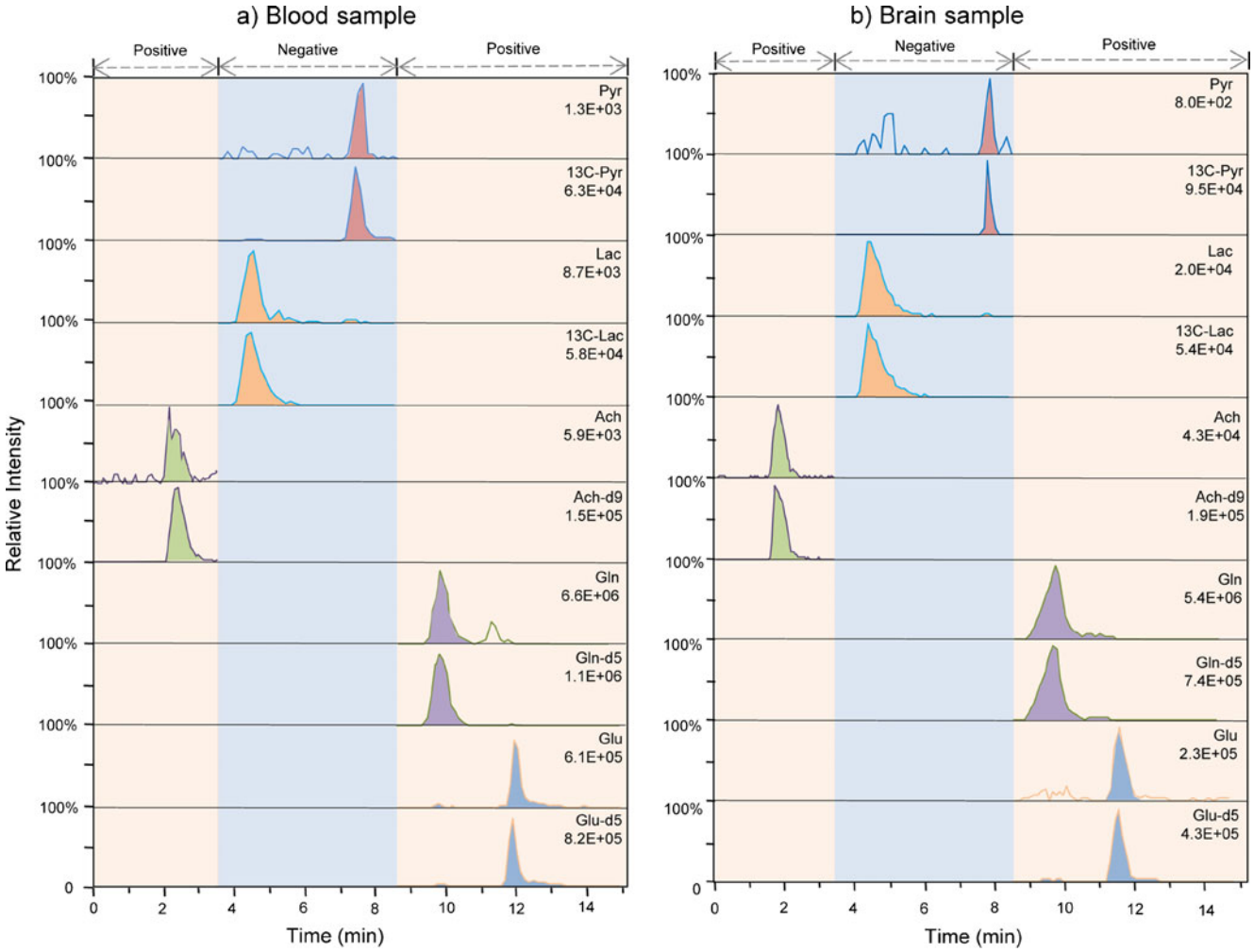

Fig. 2 Representative HILIC-ESI/MS chromatograms of five NMs under the optimized conditions **a** blood sample **b** brain sample. Both positive and negative ion mode was adopted for the detection of five analytes during each run

analytes when the ammonium formate concentration was increased from 10–50 mM. Therefore, a higher concentration of buffer solution was used for the elution, although ion suppression could be observed at this level.

Taken together, the aqueous phase consisted of a buffer solution containing 50 mM ammonium formate and 1.0% formic acid using a gradient profile that started at 85% acetonitrile for separation of the targeted analytes. This optimized separation method ensured that each analyte was matching the appointed time window of the chosen ionization mode without any interferences. The typical HILIC-ESI/MS chromatograms containing the five NMs

Table 2 Validation results of the HILIC-ESI/MS method for the analysis of the five neurochemical analytes

Compounds	LOD	LOQ	Linear range	r^2	Accuracy (%)	Precision [a]	
						Intra-day RSD%, n=5	Inter-day RSD%, n=3
ACh	150 pM	450 pM	0.5–250 nM	0.9989	82.6–109.0	11.6	12.8
Lac	3 μM	10 μM	10–5000 μM	0.9990	86.0–106.8	9.6	15.2
Pyr	2 μM	6 μM	10–5000 μM	0.9989	85.6–117.4	10.5	14.3
Gln	5 nM	15 nM	0.5–250 μM	0.9990	81.5–117.8	10.3	13.3
Glu	50 nM	150 nM	0.25–125 μM	0.9988	86.0–106.9	14.6	15.0

[a] Intra-day and Inter-day precisions were analyzed by one-way ANOVA analysis.

Table 3 Concentrations of acetylcholine, lactate, pyruvate, glutamine, and glutamate in the dialysates of brain and blood

Compounds	Ach (nM)	Lac (μM)	Pyr (μM)	Gln (μM)	Glu (μM)
Brain	4.0±1.4	220.4±90.9	21.3±8.3	50.4±21.9	1.1±0.2
Blood	10.3±4.4	511.3±78.7	91.5±37.6	176.4±45.3	26.7±5.3

Anesthetized monkeys, resting status. Values are given as mean±standard error of the mean (S.E.M.); n=4.

(acetylcholine, lactate, pyruvate, glutamine, and glutamate) are shown in Fig. 2.

Analytical performance of the capillary HILIC-ESI/MS method

The capillary HILIC-ESI/MS method was validated for the quantitative measurements of acetylcholine, lactate, pyruvate, glutamine, and glutamate concentrations from in vivo dialysates. We characterized a series of parameters like the limits of detection (LODs), limits of quantification (LOQs), linearity, selectivity, accuracy, precision and stability by analyzing different levels of standard mixtures of the target NMs while using optimized MRM transitions and positive/negative ionization modes. The validated results of the analytical performance are listed in Table 2. The LODs of lactate and pyruvate in negative mode were 3 and 2 μM, respectively, whereas the LODs of acetylcholine, glutamine, and glutamate in positive mode were 150 pM, 5 nM, and 50 nM, respectively. Although the LODs of lactate and pyruvate were much higher than those of the other three analytes (acetylcholine, glutamine, and glutamate) we still can measure them, because their basal concentrations in the brain as well in the blood are much higher than the other three. The matched MS/MS pattern between the endogenous NMs and their standards allowed confirming the high selectivity of the HILIC-MS method. Additionally, the retention time of the endogenous NMs always matched well with those of internal standards under different gradient elution conditions, which also proved the high selectivity of the method. The accuracy, precision and stability have been tested by replicate analysis (five determinations per concentration) of three different levels of QCs (see the section "Preparation of calibration standards and internal standards"). It is shown in Table 2 that the results of the accuracy, intra- and inter-day precisions were all in good agreement with the requirements of biological analysis [29, 30]. The stability test results indicated that the stock solution was stable for 1 month at −20 °C with the RSD< 12.5%, and the QCs were stable for about 2 weeks in the autosampler at 4 °C with the RSD<15.1%. Additionally, the freeze (−20 °C) and thaw stability has also been tested for these analytes. After two freeze-thaw cycles, the QCs were analyzed on the third cycle, and the results showed a good stability with the RSD<13.1%.

In addition, we adopted the post-extraction spike method proposed by Matuszewski et al. [31] to evaluate the matrix effect of the acquired in vivo samples in our study. To reliably determine the endogenous concentration of the five analytes we analyzed them according our developed method and then checked the same brain and blood samples by spiking with appropriate standard solutions. The spiked concentration of acetylcholine, lactate, pyruvate, glutamine, and glutamate was 8 nM, 150 μM, 10 μM, 40 μM, and 1 μM respectively for the brain samples, while 20 nM, 400 μM, 60 μM, 300 μM, and 30 μM for the blood samples. The total concentrations of the five analytes in the spiked samples and the endogenous concentrations in the non-spiked samples were then determined and used to calculate the recovery of each analyte. We used the following formula for calculating the recovery: (measured value−endogenous value)/added value×100. The obtained recoveries for the five analytes fell in the range of 93–112%.

Concentrations of acetylcholine, lactate, pyruvate, glutamine, and glutamate in the brain and blood microdialysates

We applied capillary HILIC-ESI/MS method together with simultaneous blood and brain microdialysis sampling to measure the concentrations of five NMs from two anesthe-

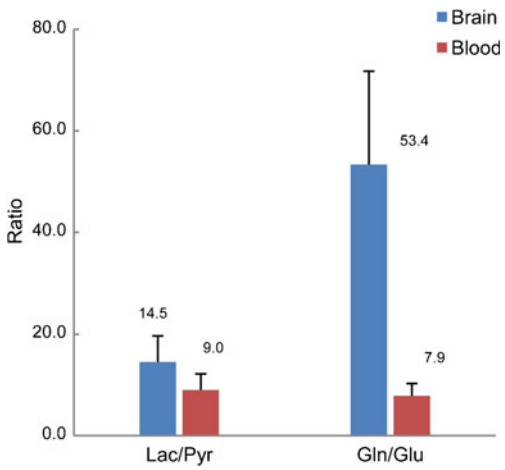

Fig. 3 Comparison of lactate/pyruvate (*Lac/Pyr*) and glutamine/glutamate (*Gln/Glu*) in primary visual cortex and the blood system of rhesus monkey. Ratios of Lac/Pyr and Gln/Glu in monkey primary visual cortex were significantly higher than the blood system (p<0.05)

tized male rhesus monkeys. The microdialysis probe in the brain was placed into the primary visual cortex (V1). The concentrations of acetylcholine, lactate, pyruvate, glutamine, and glutamate in dialysates from primary visual cortex and blood are shown in Table 3. The values we monitored were in good agreement with the Human Metabolome Database Version 2.5 (www.hmdb.ca), and the values reported in the literature [18, 23, 32–39].

Comparison of lactate/pyruvate and glutamine/glutamate ratios in the brain and the blood

To further understand the distribution differences of NMs across the BBB, respectively, between the brain and the blood, we examined and compared the lactate/pyruvate and glutamine/glutamate ratios between the brain and blood dialysates. The results showed that the concentration ratio of lactate/pyruvate and glutamine/glutamate was significantly different between the brain and the blood. The values of lactate/pyruvate and glutamine/glutamate were calculated and are shown in Fig. 3. The mean lactate/pyruvate ratio in the brain was 14.5, but only reached 9.0 in the blood system. The mean ratio of glutamine/glutamate in the brain was 53.4, significantly higher than the blood value of 7.9. One-way ANOVA analysis confirmed the statistical significance of these findings ($p<0.05$).

The lactate/pyruvate ratio in the human brain is currently considered a specific, sensitive marker that could potentially indicate whether glucose and oxygen supply meet the energy requirements of the brain tissue [40]. Such marker, that hint upon the adequacy of energy and metabolite supply are of great importance for the detection of onset of neurodegenerative diseases [41]. In the human brain, a lactate/pyruvate ratio above 40 indicates an “energy crisis” [42]. Additionally it was shown that lactate can increase the cerebral blood flow which correlates with an increase of the lactate/pyruvate ratio in the plasma [36]. A decreased interstitial glutamine/glutamate ratio has been observed in acute and chronic brain damage such as traumatic brain injury [43], hypoxia [44], and epilepsy [45]. Although such findings are still preliminary for diagnosis, we consider the simultaneous monitoring of blood and brain concentrations of important NMs a necessary step in this direction to get a clear understanding of their chemical relation across the BBB. On the basis of this data, extrapolations from the blood concentrations to brain concentrations of pathologically relevant NMs might be envisioned.

Conclusion

We developed a capillary HILIC-ESI/MS method for the simultaneous determination of multiple chemicals including acetylcholine, lactate, pyruvate, glutamine and glutamate from the brain (EBF) and blood system of anesthetized non-human primates. To achieve highest intensity of these NMs, positive and negative ionization modes were used for MS detection. The optimized chromatographic separation allowed us to switch between the two detection modes and to simultaneously measure these NMs in a single run. A simple and fast sample treatment was carried out after collection by microdialysis without any additional sample purification or derivatization. We have successfully demonstrated that our method can reliably quantify these NMs in dialysates collected from the blood and the primary visual cortex of non-human primates. Additionally we found that the concentration ratio of lactate/pyruvate and glutamine/glutamate was significantly different between the brain and the blood, reflecting the active transports and different metabolic processes between the blood and the nervous system respectively across the BBB. Quantified coupling parameters between the blood and the nervous system of NMs are of outmost importance due to their possible use in the diagnosis of pathological processes in the brain. To further investigate the correlation of these NMs between the brain and the blood systems, we will use the developed analytical method to test the dynamic change of these NMs across the BBB by pharmacologically simulating dysfunctional states of the brain.

Acknowledgments This work was supported by the Max Planck Society and BMBF Grant, Nr. 01EV0701. We thank Nadine Serr and Ulrike Passlack-Memaj for assistance in chemical preparations. We thank Mark Augath for assistance with the monkey anesthesia.

References

1. Calabresi P, Centonze D, Gubellini P, Marfia GA, Pisani A, Sancesario G, Bernardi G (2000) Synaptic transmission in the striatum: from plasticity to neurodegeneration. Prog Neurobiol 61:231–265
2. D’Aniello A, Lee JM, Petrucelli L, Di Fiore MM (1998) Regional decreases of free D-aspartate levels in Alzheimer’s disease. Neurosci Lett 250:131–134
3. Carlsson M, Carlsson A (1990) Interactions between glutamatergic and monoaminergic systems within the basal ganglia—implications for schizophrenia and Parkinson’s disease. Trends Neurosci 13:272–276
4. Gibson GE, Peterson C, Sansone J (1981) Neurotransmitter and carbohydrate metabolism during aging and mild hypoxia. Neurobiol Aging 2:165–172
5. Hertz L, Peng L, Dienel GA (2006) Energy metabolism in astrocytes: high rate of oxidative metabolism and spatiotemporal dependence on glycolysis/glycogenolysis. J Cereb Blood Flow Metab 27:219–249
6. Briand LA, Gritton H, Howe WM, Young DA, Sarter M (2007) Modulators in concert for cognition: modulator interactions in the prefrontal cortex. Prog Neurobiol 83:69–91
7. Andersson K, Arner P (1995) Cholinoceptor-mediated effects on glycerol output from human adipose tissue using in situ microdialysis. Br J Pharmacol 115:1155–1162

8. Yang TT, Chang CK, Tsao CW, Hsu YM, Hsu CT, Cheng JT (2009) Activation of muscarinic M-3 receptor may decrease glucose uptake and lipolysis in adipose tissue of rats. Neurosci Lett 451:57–59
9. Tsai TR, Cham TM, Chen KC, Chen CF, Tsai TH (1996) Determination of acetylcholine by on-line microdialysis coupled with pre-and post-microbore column enzyme reactors with electrochemical detection. J Chromatogr B Biomed Sci Appl 678:151–155
10. Yao T, Yano T, Nanjyo Y, Nishino H (2003) Simultaneous determination of glucose and L-lactate in rat brain by an electrochemical in vivo flow-injection system with an on-line microdialysis sampling. Anal Sci 19:61–65
11. Monge-Acuña AA, Fornaguera-Trias J (2009) A high performance liquid chromatography method with electrochemical detection of gamma-aminobutyric acid, glutamate and glutamine in rat brain homogenates. J Neurosci Methods 183:176–181
12. Huang T, Yang L, Gitzen J, Kissinger PT, Vreeke M, Heller A (1995) Detection of basal acetylcholine in rat brain microdialysate. J Chromatogr B Biomed Appl 670:323–327
13. Shackman HM, Shou M, Cellar NA, Watson CJ, Kennedy RT (2007) Microdialysis coupled on-line to capillary liquid chromatography with tandem mass spectrometry for monitoring acetylcholine in vivo. J Neurosci Methods 159:86–92
14. Prokai L, Fry ák P, Stevens SM, Nguyen V (2008) Measurement of acetylcholine in rat brain microdialysates by LC–isotope dilution tandem MS. Chromatographia 68:101–105
15. Zhu Y, Wong PSH, Cregor M, Gitzen JF, Coury LA, Kissinger PT (2000) In vivo microdialysis and reverse phase ion pair liquid chromatography/tandem mass spectrometry for the determination and identification of acetylcholine and related compounds in rat brain. Rapid Commun Mass Spectrom 14:1695–1700
16. van Dam J, Eman M, Frank J, Lange H, van Dedem G, Heijnen S (2002) Analysis of glycolytic intermediates in *Saccharomyces cerevisiae* using anion exchange chromatography and electrospray ionization with tandem mass spectrometric detection. Anal Chim Acta 460:209–218
17. Uran S, Landmark KE, Hjellum G, Skotland T (2007) Quantification of ^{13}C pyruvate and ^{13}C lactate in dog blood by reversed-phase liquid chromatography-electrospray ionization mass spectrometry after derivatization with 3-nitrophenylhydrazine. J Pharm Biomed Anal 44:947–954
18. Eckstein JA, Ammerman GM, Reveles JM, Ackermann BL (2008) Analysis of glutamine, glutamate, pyroglutamate, and GABA in cerebrospinal fluid using ion pairing HPLC with positive electrospray LC/MS/MS. J Neurosci Methods 171:190–196
19. Alpert AJ (1990) Hydrophilic-interaction chromatography for the separation of peptides, nucleic acids and other polar compounds. J Chromatogr 499:177–196
20. Zhang X, Rauch A, Xiao H, Rainer G, Logothetis NK (2008) Mass spectrometry-based neurochemical analysis: perspectives for primate research. Expert Rev Proteomics 5:641–652
21. Schlichtherle-Cerny H, Affolter M, Cerny C (2003) Hydrophilic interaction liquid chromatography coupled to electrospray mass spectrometry of small polar compounds in food analysis. Anal Chem 75:2349–2354
22. Fu B, Gao X, Zhang SP, Cai Z, Shen J (2008) Quantification of acetylcholine in microdialysate of subcutaneous tissue by hydrophilic interaction chromatography/tandem mass spectrometry. Rapid Commun Mass Spectrom 22:1497–1502
23. Zhang X, Rauch A, Lee H, Xiao H, Rainer G, Logothetis NK (2007) Capillary hydrophilic interaction chromatography/mass spectrometry for simultaneous determination of multiple neurotransmitters in primate cerebral cortex. Rapid Commun Mass Spectrom 21:3621–3628
24. Preinerstorfer B, Schiesel S, Lämmerhofer M, Lindner W (2009) Metabolic profiling of intracellular metabolites in fermentation broths from [beta]-lactam antibiotics production by liquid chromatography-tandem mass spectrometry methods. J Chromatogr A 1217:312–328
25. Uutela P, Reinila R, Piepponen P, Ketola RA, Kostiainen R (2005) Analysis of acetylcholine and choline in microdialysis samples by liquid chromatography/tandem mass spectrometry. Rapid Commun Mass Spectrom 19:2950–2956
26. Kaddurah-Daouk R, Krishnan KR (2009) Metabolomics: a global biochemical approach to the study of central nervous system diseases. Neuropsychopharmacology 34:173–186
27. Viklund C, Ponten E, Glad B, Irgum K, Horstedt P, Svec F (1997) "Molded" Macroporous Poly(glycidyl methacrylate-co-trimethylolpropane trimethacrylate) Materials with Fine Controlled Porous Properties: Preparation of Monoliths Using Photoinitiated Polymerization. Chem Mater 463–471
28. Cech NB, Enke CG (2001) Practical implications of some recent studies in electrospray ionization fundamentals. Mass Spectrom Rev 20:362–387
29. Shah VP, Midha KK, Dighe S, McGilveray IJ, Skelly JP, Yacobi A, Layloff T, Viswanathan CT, Cook CE, McDowall RD et al (1991) Analytical methods validation: bioavailability, bioequivalence and pharmacokinetic studies Conference report. Eur J Drug Metab Pharmacokinet 16:249–255
30. Food and Drug Administration (2001) Guidance for industry: bioanalytical method validation. US Department of Health and Human Services, FDA, Center for Drug Evaluation and Research. http://www.fda.gov/cder/guidance/index.htm.
31. Matuszewski BK, Constanzer ML, Chavez-Eng CM (2003) Strategies for the assessment of matrix effect in quantitative bioanalytical methods based on HPLC-MS/MS. Anal Chem 75:3019–3030
32. Molina JA, Gomez P, Vargas C, Ortiz S, Perez-Rial S, Uriguen L, Oliva JM, Villanueva C, Manzanares J (2005) Neurotransmitter amino acid in cerebrospinal fluid of patients with dementia with Lewy bodies. J Neural Transm 112:557–563
33. Hawkins RA (2009) The blood–brain barrier and glutamate. Am J Clin Nutr 90:867S–874S
34. Boutelle MG, Fellows LK, Cook C (1992) Enzyme packed bed system for the on-line measurement of glucose, glutamate, and lactate in brain microdialysate. Anal Chem 64:1790–1794
35. Bjerring PN, Hauerberg J, Frederiksen HJ, Jorgensen L, Hansen BA, Tofteng F, Larsen FS (2008) Cerebral glutamine concentration and lactate-pyruvate ratio in patients with acute liver failure. Neurocrit Care 9:3–7
36. Mintun MA, Vlassenko AG, Rundle MM, Raichle ME (2004) Increased lactate/pyruvate ratio augments blood flow in physiologically activated human brain. Proc Natl Acad Sci USA 101:659–664
37. Kawashima K, Oohata H, Fujimoto K, Suzuki T (1987) Plasma concentration of acetylcholine in young women. Neurosci Lett 80:339–342
38. Fujii T, Yamada S, Yamaguchi N, Fujimoto K, Suzuki T, Kawashima K (1995) Species differences in the concentration of acetylcholine, a neurotransmitter, in whole blood and plasma. Neurosci Lett 201:207–210
39. Cynober LA (2002) Plasma amino acid levels with a note on membrane transport: characteristics, regulation, and metabolic significance. Nutrition 18:761–766
40. Bellander BM, Cantais E, Enblad P, Hutchinson P, Nordström CH, Robertson C, Sahuquillo J, Smith M, Stocchetti N, Ungerstedt U (2004) Consensus meeting on microdialysis in neurointensive care. Intensive Care Med 30:2166–2169
41. Iadecola C (2004) Neurovascular regulation in the normal brain and in Alzheimer's disease. Nat Rev Neurosci 5:347–360

42. Samuelsson C, Hillered L, Zetterling M, Enblad P, Hesselager G, Ryttlefors M, Kumlien E, Lewen A, Marklund N, Nilsson P, Salci K, Ronne-Engstrom E (2007) Cerebral glutamine and glutamate levels in relation to compromised energy metabolism: a microdialysis study in subarachnoid hemorrhage patients. J Cereb Blood Flow Metab 27:1309–1317
43. Richards DA, Tolias CM, Sgouros S, Bowery NG (2003) Extracellular glutamine to glutamate ratio may predict outcome in the injured brain: a clinical microdialysis study in children. Pharmacol Res 48:101–109
44. Raman L, Tkac I, Ennis K, Georgieff MK, Gruetter R, Rao R (2005) In vivo effect of chronic hypoxia on the neurochemical profile of the developing rat hippocampus. Brain Res Dev Brain Res 156:202–209
45. Petroff OA, Errante LD, Rothman DL, Kim JH, Spencer DD (2002) Glutamate-glutamine cycling in the epileptic human hippocampus. Epilepsia 43:703–710

Study 3

Effects of neural synchrony on surface EEG

S. F. Musall[1], V. vPföstl[1], A. Rauch[1], N. K. Logothetis[1,2] and K. Whittingstall[1*†]

[1] Max Planck Institute for Biological Cybernetics
Spemannstrasse 38, D-72076 Tübingen, Germany

[2]Division of Imaging Science and Biomedical Engineering, University of Manchester
Manchester M13 9PT, United Kingdom

*To whom correspondence should be addressed
[†] Current address: Department of Diagnostic Radiology, Faculty of Medicine and Health Science, Université de Sherbrooke, 12e Avenue Nord, Sherbrooke, QC, Canada, J1H 5N4

Acknowledgements: We would like to thank Stefano Panzeri for helpful discussions on data analysis and statistics; Joachim Werner and Axel Oeltermann for help in the acquisition of data and Yusuke Murayama, Christoph Kayser, Jozien Goense, Ulrich Schridde and David Omer for comments on an earlier version of the manuscript. This research was supported by the Max Planck Society (SM, VP, NKL and KW) and the Bundesministerium für Bildung und Forschung (01EV0701, AR).

Abstract

It has long-been assumed that the surface EEG signal depends on both the amplitude and spatial synchronization of underlying neural activity, though isolating their respective contribution remains elusive. To address this, we made simultaneous surface EEG measurements along with intracortical recordings of local field potentials (LFPs) in the primary visual cortex of behaving non-human primates. We found that trial-by-trial fluctuations in EEG power were best explained by a linear combination of LFP power and inter-electrode temporal synchrony. This effect was observed in both stimulus and stimulus-free conditions and particularly strong in the gamma range (30-100Hz). Subsequently, we used pharmacological manipulations to show that neural synchrony can produce a positively modulated EEG signal even if the LFP signal is negatively modulated. Taken together, our results demonstrate that neural synchrony alone can modulate EEG signals in the absence of changes in neural activity amplitude. This finding has strong implications for the interpretation of EEG in basic and clinical research, and helps reconcile EEG response discrepancies observed in different modalities (e.g. EEG vs. fMRI) and different spatial scales (e.g. EEG vs. intra-cranial EEG).

Introduction

Electroencephalography (EEG) is one of the most commonly used methods to measure brain activity in humans. However, despite its widespread use, we still lack a clear understanding of how EEG signals are related to the spatio-temporal organization of underlying neuronal activity. The dominant theory is that a surface electrode provides an aggregate measure of the synaptic potentials of cortical neurons in an open-field arrangement, such as the pyramidal cells that are oriented perpendicular to the cortical surface and form current dipoles [1]. In addition, it has been shown that the surface EEG may also be related to the activity of stellate cells in cortical layer 4C which receive sensory input from the thalamus [2,3]. Regardless of its biological origin, it is of particular importance to note that the amplitude of a surface EEG measure is not only dependent on the magnitude of individual current dipoles [4], but also on the degree of their temporal synchronization across space [1,5]. That is, transient increases in neural activity need to be synchronous over a relatively large patch of cortex [1,6] in order to produce a detectable EEG response. This is due to the superposition principle, where the net sum of temporally coherent dipole sources is larger than that of their individual source magnitudes [7]. It is therefore theoretically possible that increases in cortical neural synchrony alone can enhance surface EEG signals without concomitant changes in the amplitude of cortical activity [1,8,9]. However, experimental confirmation of this hypothesis remains elusive, partly due to the difficulty in reliably separating intracortical measures of signal amplitude and spatial synchrony. In this study, we made simultaneous intracortical recordings of local field potentials (LFPs) with simultaneous surface EEG measurements in the primary visual cortex (V1) of two behaving non-human primates (*Macaca mulatta*) during visual stimulation. Our aim was to assess how unique changes in intracortical activity - defined by LFP amplitude and synchronization over space – affect the surface EEG. We found that trial-by-trial fluctuations in EEG power not only reflected changes in neural activity but also the degree of temporal synchrony between LFP electrode pairs (spatial coherence - SC). To further confirm this finding, we used a pharmacological manipulation (local injections of lidocaine) to dissociate EEG and LFP amplitude. Here, we found that contradicting changes in EEG and LFP were explained by SC. Our results show that neural synchrony alone can not only modulate EEG signals in the absence of changes in the

amplitude of localized neural activity but 'amplify' its contribution, even if such activity is attenuated.

Material and Methods

Data Acquisition

Electrophysiological data recorded from two awake, behaving monkeys (*Macaca mulatta)* are included in the present study. All animal experiments were approved by the local authorities (Regierungspräsidium Tübingen) and are in full compliance with the guidelines of the European Community (EUVD 86/609/EEC) for the care and use of laboratory animals. Surface EEG recordings were made using an AG/AgCL ring electrode positioned over the visual cortex. Electrode impedance was kept below 20 kΩ. The EEG ring electrode of interest was placed at the base of a recording chamber made from PEEK (Polyetheretherketone; Ensinger Inc., Nufringen, Germany), which was secured to the skull with custom-made ceramic screws. The EEG ring electrode rested on the skull, and a small craniotomy was made to place electrodes for intracortical recording. In monkey A03, the resected patch was ~2 mm diameter, while in monkey D02 ~5mm of bone were removed. Surgical procedures are described elsewhere together with hardware details of the recording setup [13]. Three tungsten microelectrodes (FHC, Bowdoinham, ME) were lowered through the middle of the EEG ring electrode into the cortex. Electrode tips were typically positioned in the upper or middle cortical layers of V1 and distance between electrodes was 1.8-2.6 mm. The impedance of the electrodes varied from 300-900 kΩ. All signals were amplified and filtered into a band of 2–8000 Hz (Alpha Omega Engineering, Nazareth, Israel) and then digitized at 20.833 kHz with 16-bit resolution (National Instruments, Austin, TX), ensuring enough resolution to record both local field potentials (LFPs) and spiking activity. All signals were referenced to a nearby wire placed between dura and bone. Prior to analysis, we re-referenced both the LFP and EEG to a frontal electrode placed on the scalp by subtracting the signal measured in the frontal electrode from the occipital EEG/LFP recording electrodes. This was done to ensure compatibility with typical visual EEG studies in humans and did not make a significant qualitative difference to the spectral estimates of LFP (see Results section). Trials exhibiting transients above six standard deviations of the mean were excluded from all subsequent analysis, as they were most likely due to movement artifacts (e.g. jaw movements). This was the case for ~28% of all trials.

Visual Stimulation

Visual stimuli were delivered via a computer screen (refresh rate 90Hz) placed at eye level, 190 cm in front of the monkey. Eye movements were continuously monitored with an infrared camera (RealEye, Avotec, Stuart, FL) with eye tracking software (iView, Sensomotoric Instruments GmbH, Teltow, Germany). Each trial began with a small fixation point (dot size: 0.4°) on black background. After 1s of fixation, a 5 s movie segment (full field, 20.13 x 15.19 in visual degree) was presented, followed by 1s of post-stimulus fixation, resulting in trials totaling 7 s of fixation. In trials where fixation was held throughout, the monkey received a juice reward, whereas trials where the monkey broke fixation were immediately aborted. Each behavioral block consisted of 20 successful fixations. The movie was a fast-moving clip (no soundtrack) from a commercially available movie [4]. Tasks (including movie onset/offset times) were controlled by computers running a real-time operating system (QNX, Ottawa, Canada) [14].

Pharmacological Injections

Each experiment (n=16 over the two animals) consisted of neural recordings in 20 successful movie trials in three separate conditions: 'baseline', 'control' and 'drug'. The baseline condition consisted of no cortical injections, while the drug condition consisted of local injections of lidocaine hydrochloride 2% in artificial cerebrospinal fluid (ACSF). Lidocaine is a local anesthetic that mainly acts through sodium channel blockage and thus reduces LFP and multi-unit spiking activity (MUA) [12], though paradoxically increases the surface EEG [10]. It is also fast acting and reversible [15] and therefore ideal for investigating EEG-LFP dissociations in awake and behaving monkeys. Finally, drug-free ACSF was used as a control solution for the control condition.

The 'baseline' condition was recorded immediately before the start of each injection. The 'drug' and 'control' condition was recorded in the last five minutes of the injection (15 minutes after its start). Lidocaine and ACSF injections were performed in each experiment (in randomized order) with a total delay of 75 minutes between injections. In both lidocaine and ACSF solutions, the pH was adjusted with NaOH to 7.25. ACSF was composed of NaCl: 148.19 mM, KCl: 3.0 mM, $CaCl_2$: 1.40 mM, $MgCl_2$: 0.80 mM, Na2HPO4: 0.80 mM, NaH2PO4: 0.20 mM. All chemicals were purchased from Sigma-Aldrich (Schnelldorf, Germany). Lidocaine and ACSF were applied by a custom-made injector, consisting of a triple-barrel glass tube which contained three sharpened injection lines (outer diameter=150µm, inner diameter=20µm) for a better distribution in cortex. The free shaft length of the injections lines was 3.5mm, which gave sufficient stability to penetrate dura and reach the visual cortex at the same depth as the intracortical sharp electrodes. The distance from the injection tips to the electrodes was held constant at ~2 mm. All three lines branched from the same feed line that was driven by a custom-made application device using compressed helium. Flow and volume of applied lidocaine/ACSF were monitored by a high precision flow-meter (Sensirion, Switzerland). Injections were delivered at 0.6µl/minute per line for a total duration of 20 minutes.

Data Analysis

All data analysis procedures were implemented with the Matlab programming language (Mathworks, Natick, MA) in combination with the EEGlab analysis toolbox [16] as described below.

Multiunit Activity Analysis

The MUA band, used for assessing the effect of lidocaine, was extracted between 1000 and 4000 Hz using bidirectional operation of a FFT filter. Differences in MUA power during lidocaine and ACSF injections were used to dissociate pharmacological effects from general changes that occurred because of the injection itself. To compute inter-electrode spike correlations (MUA synchrony), we used a publicly available spike-sorting algorithm for semiautomatic detection of spike times [16]. The algorithm uses an amplitude threshold of four standard deviations of the mean amplitude for spike detection. Only spikes occurring within at least 1.5ms of one another were kept for analysis. No subsequent spike sorting (e.g., PCA) was applied. The spike timings were binned into 10ms windows, and the resulting spike rate was compared to the neighboring electrodes by computing the Pearson correlation coefficient.

Spectral Analysis

EEG and LFP signals were downsampled to 1000 Hz. For power analysis, we computed the power spectral density for each trial using a 512ms window length with 50% overlap. Spatial coherence was obtained using the magnitude squared coherence estimate C_{xy} from the input signals x and y - in our case LFP signals from two neighboring sharp electrodes in cortex - with the spectral density P_{xx}, P_{yy} and the cross power spectral density P_{xy}.

$$C_{xy}(f) = \frac{|P_{xy}(f)|^2}{P_{xx}(f)P_{yy}(f)}$$

In each trial, we computed the average inter-electrode coherence (Spatial Coherence, SC) between the LFP in a single microelectrode and its two neighbors. We also computed the LFP power at each microelectrode site, along with the EEG power from the single surface electrode. In the baseline condition, we divided the LFP and EEG power in each trial by their respective trial average. For SC, we subtracted the trial-average from each single-trial measure and reported it as a difference (rather than a percent change for LFP and EEG). This approach minimizes the biases introduced when using absolute rather than relative coherence values for analysis (supplementary material and Figure S5). In the drug and control condition, we divided the EEG and LFP power in each trial by the average over all trials in the baseline condition. For SC, we subtracted the trial-average SC in the baseline from each trial in the drug and control condition. For each condition, we label these trial-by-trial changes as ΔEEG, ΔLFP and ΔSC. Lastly, these data were pooled across all experiments and monkeys.

Statistical Analysis

Prior to statistical analysis, we performed a Lilliefors test on each data set to ensure it followed a normal distribution. In cases where we performed statistical analysis over all frequency bands (n=6), we applied Bonferroni correction to correct for the multiple comparisons. Thus, all p-values below 0.05/6=0.008 were deemed statistically significant. To evaluate the contribution of SC into the EEG, we first used ΔSC and ΔLFP as regressors in a general linear model (GLM):

$$Y = \beta_1 X_1 + \beta_2 X_2 + \varepsilon$$

Here Y, X_1 and X_2 are the measured ΔEEG, ΔLFP, ΔSC (respectively); β1 and β2 are weights of ΔLFP and ΔSC (respectively); and ε is the error term. This GLM (Full model) was then compared to a reduced GLM with only ΔLFP as a regressor by computing the F-statistic between the two GLMs. This allowed us to investigate whether SC provides significant information on EEG, beyond what could be achieved when using LFP alone. The root mean square (RMSE) for modeled ΔEEG was computed as the following:

$$RMSE = \sqrt{\frac{1}{n}\sum_{i=1}^{n}(\text{EEG(i)} - \text{modeled EEG(i)})^2}$$

Results

We first computed the correlation between trial-by-trial fluctuations in LFP (ΔLFP), SC (ΔSC) and EEG (ΔEEG) in the drug-free baseline condition. As shown in Table 1, both, ΔLFP and ΔSC were significantly correlated to ΔEEG in all frequency bands ($p<0.01$), with the highest correlations in the high-gamma range (60-100Hz). A scatter plot of high-gamma ΔEEG, ΔLFP and ΔSC is shown in Figure 1A. Here, the relationship between ΔSC and the difference in magnitude of ΔEEG and ΔLFP ($\Delta_{EEG-LFP}$) is of particular interest. For example, the upper left quadrant of Figure 1A reflects trials where ΔLFP is negatively and ΔSC positively modulated. In these trials (n=141), the average ΔEEG was significantly positively modulated (+4.75%, two sided t-test, $p<0.01$). However, in the opposite case - when ΔLFP was positive but ΔSC negative (bottom right quadrant) – the average ΔEEG was also more negative (-3.51%, n=98, $p<0.01$). This indicates that a dissociation between ΔLFP and ΔEEG may be explained by ΔSC. Indeed, the average ΔSC was higher in trials where ΔEEG was greater than ΔLFP ($\Delta SC_{\Delta EEG>\Delta LFP}$=+0.02, n=390) compared to trials where ΔEEG was less than ΔLFP ($\Delta SC_{\Delta EEG<\Delta LFP}$=-0.03, n=306, $p<0.01$). Accordingly, we found a high positive correlation between $\Delta_{EEG-LFP}$ and ΔSC (r=0.34, $p<0.01$; Figure 1B).

To quantify the individual contribution of ΔSC to ΔEEG, we used both ΔSC and ΔLFP as regressors in a general linear model (GLM). This is illustrated in Figure 1c for a subset of trial-by-trial measures of ΔEEG (red), ΔSC (black) and ΔLFP (blue) as well as modeled ΔEEG (dashed red line). For visual purposes only, all values are normalized to their maximum value. The difference between ΔEEG and ΔLFP varies considerably across trials, indicating that ΔLFP alone cannot fully explain ΔEEG. For example, in the transition from trial 3 to 4, ΔLFP decreases while ΔEEG and ΔSC increase. However, when combining ΔLFP and ΔSC, the modeled ΔEEG (dashed red line) better resembles the measured ΔEEG values. To quantify this effect, we computed two additional metrics: First, we calculated the F-statistic by comparing the full GLM containing both ΔLFP and ΔSC as regressors, against a null model consisting of only the ΔLFP regressor (Figure 1D). For all frequency bands but the alpha range, the F-statistic was significant ($p<0.01$), confirming that ΔSC explains a component of the ΔEEG that cannot be explained by ΔLFP. Secondly, we computed the root mean square error (RMSE) between the measured and modeled ΔEEG (Figure 1E). In all frequency bands, the addition of ΔSC decreased the RMSE. A similar effect was seen when performing the same analysis on data obtained during the fixation period prior to visual stimulation (i.e., no visual stimulus, Figure S1A-B), thus confirming that our results are largely invariant to external stimulation. Due to the link between EEG gamma power and MUA (Whittingstall 2009), we additionally investigated to what extent EEG-LFP dissociations are related to changes in firing rates and MUA synchrony. We found a positive correlation between $\Delta_{EEG-LFP}$ and MUA synchrony (Figure S2A) while correlations between $\Delta_{EEG-LFP}$ and firing rates were slightly negative (Figure S2B). For both cases, relations were strongest in the high-gamma range. This suggests that changes in neural firing and synchrony have an opposing impact on high-frequency EEG-LFP dissociations.

The above results demonstrate that amplitude dissociations between EEG and LFP are directly related to changes in neural synchrony. In some cases, we observed trials where the LFP was negatively modulated while both EEG and SC were positively modulated (upper left quadrant, Figure 1A), suggesting that the contribution of SC is strong enough to ‘amplify’ neural signals. However, because only few trials exhibited clear EEG-LFP dissociations, we sought to reproduce this effect in a more robust manner, using localized pharmacological manipulation.

We therefore analyzed EEG and LFP recordings during the application of lidocaine (drug condition). Lidocaine has been shown to reduce LFP [17] and MUA [13,17], though paradoxically increase the surface EEG [14], thus creating a strong dissociation between EEG and LFP power. Given our previous findings, we hypothesized that a lidocaine-induced dissociation between EEG and LFP can be explained by a concomitant change in SC. Indeed, we found that LFP activity during lidocaine application was not only attenuated but also more synchronized. An example of simultaneous EEG-LFP recordings in a single trial is shown in Figure 2. Under lidocaine, LFP signals are reduced in amplitude, though more temporally synchronized (Figure 2A-B) while the surface EEG amplitude slightly increases (Figure 2C). Figure 3 shows the average lidocaine-triggered change in EEG/LFP power and SC across all trials. As expected, the LFP exhibited a significant broadband decrease in power (Figure 3A). MUA was also suppressed, though this reduction was moderate with spiking activity resembling that observed during spontaneous neural activity without lidocaine application (Figure S3A). On the other hand, EEG power was increasing, particularly in the high-frequency range. These LFP and EEG findings are in line with previous lidocaine studies in monkeys and humans [10,11]. Aside from changes in amplitude, we found that SC significantly increased with lidocaine (Figure 3B). Statistical analysis (two-sided paired t-test) revealed that lidocaine-triggered changes in LFP and SC were significant across all frequency bands ($p<0.01$, Figure 3C), while increases in the EEG were only statistically significant in the high gamma range ($p<0.01$, Figure 3C). None of these effects were observed during control injections of ACSF (Figure S3).

The above result demonstrates a clear dissociation between LFP and EEG signal power during local application of lidocaine. A possible explanation is that the observed increase in SC reflects enhanced temporal synchrony of neural sources, which - due to the superposition principle - causes the observed increase in EEG. Alternatively, the application of lidocaine may simply enhance the volume-conducted (VC) or 'far-field' component of the LFP, which is common to all penetrating electrodes, and thus cause a spurious increase in SC. Such a scenario could arise from the presence of noise in the frontal reference electrode. To address this, we compared the SC results obtained using a frontal reference electrode (Figure 3C) to that obtained when using a using a local referencing scheme (see methods). In both cases, the results were similar (Figure S4A), indicating that that the choice of electrical reference cannot explain in the lidocaine-triggered increase in SC. In addition, changes in ΔSC and ΔLFP were positively correlated in the drug condition (Figure S4B). If the observed increase in SC would only be due to reduced LFP signal strength one should expect a negative correlation between the two. Finally, we re-analyzed the data on a trial-by-trial basis (similar to drug-free data). A scatter plot of the lidocaine-induced changes in high-gamma EEG (ΔEEG) and LFP (ΔLFP) values across all trials and monkeys (n=678) is shown in Figure 4A. Although trial-by-trial variations in ΔEEG and ΔLFP are highly correlated (r=0.6), their modulation values are markedly different. That is, the fitted curve in Figure 4A (blue line) is different from unity (dashed line), confirming an amplitude offset between ΔEEG and ΔLFP. Here, the ΔLFP zero-crossing (green vertical line) occurs at a ΔEEG value of ~30%. A summary of this result for all frequency bands is shown in Figure 4B. This demonstrates that, on average, the EEG was positively modulated in the absence of LFP modulation. To investigate the role of SC in this dissociation, we again performed a GLM analysis. An example of the modeled ΔEEG for a subset of trials is shown in Figure S4C. F-statistics were significant for all but the theta and the alpha band, while values in the high-frequency range were higher compared to the control condition. The increased importance of

ΔSC can also be seen with RMSE (Figure 4D), showing a reduction of 26% in unexplained variability with the addition of ΔSC in the high-gamma range. In summary, trial-by-trial analysis of data obtained during baseline as well as the drug condition shows that a significant portion of EEG-LFP dissociations can be explained by changes in neural synchrony.

It is worth noting that although the measure of coherence is often used for measuring the degree of synchrony between neurophysiological signals, one must be cautious in interpreting its results [38,39]. We therefore used two different measures of inter-electrode synchrony and compared the results. Firstly, we band-passed filtered the LFP signals in the traditional EEG frequency bands and computed the Pearson correlation coefficient between them. The results were highly similar to those reported here, and are thus not presented. Secondly, we summed the raw LFP time series from all three intracortical electrodes prior to LFP power analysis, and compared this with the EEG. Here, the summation process minimizes contributions from non-synchronous activity, and thus provides an alternate measure of spatial synchrony. We found that this 'Mean LFP' was better correlated to the EEG compared to LFP power which was averaged over all three electrodes after spectral analysis (Figure S5A-B). These results further confirmed that the EEG indeed represents the average of temporally-synchronized sources.

Discussion

The findings presented here demonstrate how neural synchrony 'amplifies' the contribution of localized neural activity into the EEG, thus explaining the amplitude differences often observed between intracranial and surface measurements of neural activity. This offers direct experimental evidence for the long hypothesized dependence of EEG amplitude on the synchrony of neuronal sources rather than simply the strength of their activation.

Our results are in line with the modeling study of epileptic activity by Cosandier-Rimele et al. [8], who showed that when the magnitude of neural activity is held constant, increases in the degree of synchronous activity result in increasing scalp EEG. In addition, we found that if synchrony is sufficiently high, increases in EEG can also coincide with decreases in LFP activity. Interestingly, this effect was frequency-dependent. We found that trial-by-trial changes in EEG gamma power (30-100Hz) were strongly correlated to both SC and LFP power, while correlations were notably lower in the theta and alpha range (Table 1). Note, that these correlations do not reflect instantaneous, cycle-to-cycle correlations between filtered EEG and LFP signals, but rather shared fluctuations in their trial-by-trial mean amplitude and coherence. In this respect, our findings are in good agreement with intra-cortical recordings in humans and awake macaques, who show that very slow (<0.1Hz) fluctuations in the band-limited power (BLP) of high-frequency LFP remain strongly correlated across distances exceeding 10mm [17,18]. Although our observed trial-by-trial changes in mean power are not well defined in time (as inter-trial duration was dependent on animal performance), they could represent slow (<0.2 Hz) BLP modulations as reported in the aforementioned studies. The contribution of SC to the EEG was also highest in the high frequency range, (Figure 1D) while being consistently weaker in the alpha band (Figure S1, 1D, 4C). It has been shown that the amplitude of alpha oscillations in early visual regions is negatively correlated to that in higher-order regions of the IT cortex [18]. Due to the relatively large integration area of the EEG electrode, our recordings may represent a mixture of these distinct sources, resulting in a low correlation of EEG with SC in V1. This could also arise from the differential distribution of alpha sources across different

layers. Recent studies using laminar recordings of LFP in awake monkey visual cortex show that alpha-band LFP activity is concentrated in the deep granular and infragranular layers of cortex [17-20]. Conversely, the magnitude of spontaneous fluctuations in the gamma range (30-100Hz) can be up to twice as large in the superficial layers compared to deeper ones [20]. It is therefore possible that our LFP recordings, which were limited to the middle to upper cortical layers, missed a portion of deeper alpha generators, which might be closer related to activity in the surface EEG. Though technically challenging, it would be of great interest to combine multi-laminar recordings with surface EEG in order to study the contribution of synchrony across cortical layers.

Lastly, the strong relationship between SC and EEG gamma power may stem from the link between high-frequency EEG and MUA (Whittingstall, 2009). While a recent study by Ray et.al. showed that high-gamma LFP power is closely related to firing rates [22], earlier modeling work suggested that high-frequency EEG power would be more sensitive to the synchronous firing of neurons [21]. In line with these statements, we found that high-frequency EEG-LFP dissociations correlated positively with MUA synchrony and negatively with firing rates. This demonstrates that the gamma EEG signal is highly sensitive to the synchronous firing of neurons, whereas LFP power in this range mainly reflects changes in firing rates.

Regarding the impact of sensory stimulation, we observed that the effect of SC on EEG was similar across stimulus type (movie, fixation) and pharmacological condition (baseline, drug). Our results are thus not solely shaped by the visual stimulus or type of pharmamacological manipulation, and might reflect a more general phenomenon of cortical processing. It is therefore important to include the role of neural synchrony in the interpretation of EEG signals obtained in basic and clinical research. Concerning the latter, several studies have shown how various types of anesthetics reduce localized measures of neural activity (MUA, LFP) [23-25], though paradoxically increase surface EEG activity in humans [26,27]. Interestingly, it has also been shown that these types of anesthesia have the effect of synchronizing neural activity [24,26,28,29]. Kreuzer et al. [29] recorded LFPs from the somatosensory cortex of rats chronically implanted with multielectrode arrays and compared activity patterns in the awake state with those at increasing concentrations of isoflurane, enflurane and halothane. In line with our studies, they found that cortical LFP signals were more synchronous in the presence of anesthetics. Although we cannot directly compare our local lidocaine applications with these studies, they nonetheless suggest that cortical synchrony may be a key factor in explaining ‘paradoxical’ EEG amplitude changes observed under anesthesia [28].

The lidocaine-induced increase in neural synchrony raises the question about its origin. One possibility is that lidocaine simply diminishes background neural activity, which could increase the signal-to-noise ratio (SNR) of stimulus evoked-transients and result in spuriously high inter-electrode synchrony. However, we found a similar increase in SC during the fixation period, indicating that the increase in synchrony is unrelated to stimulus-selective projection neurons but rather reflects unselective mass activity. Since lidocaine more strongly affects neurons with high firing rates [12], it may particularly suppress fast-spiking interneurons [30], thus leading to a loss of controlled neuromodulation. Given that active decorrelation has been shown to be a fundamental property of intracortical processing [31,32], lidocaine infusion may disrupt this process, resulting in the observed overly-correlated network activity.

Lastly, our findings have an important implication for basic EEG studies, particularly those combining EEG with other imaging modalities such as fMRI. We have previously shown that the local application of lidocaine significantly decreases the amplitude of the BOLD signal [11], while we here demonstrate that it triggers an increase in surface EEG amplitude. This highlights the impact of neural synchrony as an important mechanism behind any potential dissociation between EEG and fMRI measurements [33-35]. A likely cause of this observation is that synchronization among a large population of neurons is less metabolically demanding [36] (though also see [37]), thus explaining why increases in EEG may appear concurrently with a reduction of the BOLD signal. Should this be the case, dissociations between EEG and BOLD may prove extremely informative in serving as a non-invasive marker for separating the effects of synaptic input (fMRI) vs. global synchronization (EEG), and potentially open a new avenue for identifying distinct neural codes used in behavioral tasks.

Figure Legends

Table 1. *Trial-by-trial fluctuations in SC and LFP power are highly correlated*. Trial-by-trial fluctuations in both SC and LFP are correlated to corresponding fluctuations in EEG. Correlations were significant for all classical EEG frequency bands ($p<0.01$) and showed strongest relations in the gamma range (30-100Hz).

Figure 1. *EEG-LFP dissociations are explained by SC.* (A) Scatter plot of trial-by-trial modulation in the high-gamma range (60-100Hz) for LFP (ΔLFP), EEG (ΔEEG) and SC (ΔSC) across all monkeys. ΔLFP and ΔEEG represent the percent change from the trial-average, while ΔSC is computed as difference (see methods). Statistical analysis shows that ΔSC is significantly higher in trials where ΔEEG is greater than ΔLFP (see results). (B) Scatter plot of trial-by-trial differences in ΔEEG and ΔLFP (ΔEEG - ΔLFP) versus ΔSC. $\Delta_{EEG-LFP}$ is positively correlated to ΔSC ($p<0.05$), indicating a relation between SC and the dissociation of EEG and LFP power. (C) An example trace of trial-by-trial fluctuations of LFP (blue), SC (black) and EEG (red). Dashed red line with open circles is the modeled EEG ($EEG_{modeled}$) using LFP and SC as regressors in a GLM. For visual purposes only, all measures were normalized to their maximum change ('Normalized Change'). (D) F-statistics obtained when comparing F-values of the full GLM to a reduced GLM (using ΔLFP as a single regressor) for all frequency bands. Stars indicate that adding ΔSC as a regressor in the GLM explained a significant amount of ΔEEG variance ($p < 0.01$) which could not be explained by ΔLFP alone (see methods). (E) When only using LFP to model the EEG (reduced model, blue bars), the mean root-mean squared error (RMSE) was consistently higher than when including ΔSC as an additional regressor (full model, red bars).

Figure 2. *Effects of lidocaine on single-trial EEG and LFP.* (A) Simultaneous recordings from two intracortical electrodes (LFP_1, LFP_2) and a single surface EEG. After lidocaine application, $LFP_{1,2}$ become more synchronized, though their amplitude is reduced. (B) Spectral power analysis of the single-trial data shown in (A) for the LFP (B) and EEG (C). Note that lidocaine slightly increases EEG power, while LFP power is reduced.

Figure 3. *Effects of lidocaine on EEG, LFP and Spatial Coherence (SC).* (A) Average lidocaine-induced changes in EEG and LFP. Results are displayed as percent change from baseline condition. (B) SC spectra before (green) and after (blue) lidocaine application (C) Lidocaine induced changes (as in A and B), for all classical EEG frequency bands. Stars indicate a statistically significant change ($p<0.01$) of EEG power. Changes in LFP and SC were significant for all frequency bands.

Figure 4. *Effects of lidocaine on ΔEEG, ΔLFP and ΔSC* (A) Scatter plot of trial-by-trial modulation in high-frequency (60-100Hz) ΔLFP and ΔEEG under lidocaine across both monkeys. The blue line shows a linear regression fit, the dashed line indicates unity (i.e. mean LFP = mean EEG). Gray circles represent trials where ΔLFP is negative and ΔEEG positive (n=307). ΔLFP and ΔEEG zero crossing is shown in green and red, respectively. Here, the linear regression crosses the ΔLFP = 0 line at ΔEEG = 32.6%. (B) EEG percent change at LFP zero crossing (as indicated by linear regression fit) in the drug condition for all frequency bands. (C) F-statistics for the addition of ΔSC into the GLM analysis in the drug condition (as in Figure 1D). (D) RMSE values for all frequency bands using ΔLFP (blue bars) or a combination of

ΔLFP and ΔSC to model ΔEEG (red bars) Addition of ΔSC into the GLM strongly reduced RMSE, especially in the high-gamma range (see also Figure 1E).

Figure S1. (A) Same analysis as in Figure 1D+E and 4C+D, though for stimulus-free baseline condition.

Figure S2. (A) Trial-by-trial correlation between MUA synchrony and the difference of ΔEEG and ΔLFP ($\Delta_{EEG-LFP}$) for all frequency bands. $\Delta_{EEG-LFP}$ and MUA synchrony are positively correlated in all frequency bands (stars indicate significance, $p<0.01$). (B) Trial-by-trial correlations of $\Delta_{EEG-LFP}$ and firing rates. Correlations are negative with higher frequencies (>15Hz).

Figure S3. (A) Lidocaine significantly reduces stimulus-induced MUA ($p<0.05$, red curve) compared to control injections of ACSF (blue curve). This lidocaine-induced reduction was moderate and comparable to MUA recordings made during baseline activity (no drug) without visual stimulation (dashed line, *'Awake Rest'*). (B) SC remains unaltered during control injections of ACSF.

Figure S4. (A) Convention is the same as in Figure 1C, though analysis is carried out on recordings referenced to a local site (see methods). A similar result was obtained when using the average LFP signal across all microelectrodes as a reference (not shown), suggesting that our results are not due to the choice of electrical reference. (B) Changes in ΔSC and ΔLFP in the drug condition are positively correlated ($p<0.01$). (C) An example trace of trial-by-trial fluctuations of LFP (blue), SC (black) and EEG (red) in the drug condition. Dashed red line with open circles is the modeled EEG ($EEG_{modeled}$) using LFP and SC as regressors in a GLM. For visual purposes only, all measures were normalized to their maximum change ('Normalized Change').

Figure S5. (A) Spectral analysis of lidocaine-triggered changes in the raw LFP signal after averaging over three microelectrodes ('Mean LFP'). The summation process minimizes contributions from non-synchronous activity, and thus provides an alternate measure of SC. Here, the lidocaine-induced reduction in LFP power is much weaker compared to single electrode LFPs (see Figure 3A) and shows a trend towards an increase with higher frequencies. The inset shows correlation of 'Single' and 'Mean' LFP to EEG. Here, the single-trial temporal correlation between the raw EEG and 'Mean LFP' (red bar) timecourse is significantly higher ($p<0.01$) compared to the LFP from a single microelectrode ('Single LFP', blue bar). (B) To show that this finding is not simply due to an increase in SNR, but the impact of synchronous activity in all three electrodes, we additionally computed trial-by-trial correlations. Trial-by-trial correlations of 'Mean' LFP power and EEG were higher compared to averaging only the power of the three electrodes ('LFP power'). This again demonstrates the importance of phase synchrony, as only averaging before spectral analysis (thus including phase information from the raw signal) yielded an increase in EEG-LFP correlation. (C) SC estimates are strongly affected, depending on the chosen window size. Shown are SC estimates before and during lidocaine application using window sizes of 256,512 and 1024ms. Low coherence values were obtained when using short time windows of 256ms (red) and highest with longer time windows of 1024ms (blue). (D) The lidocaine-induced difference in SC, as used in our study, is invariable to window size. The implication of these results is that SC differences between conditions are not substantially affected by the window size or data length used for analysis.

Reference List

1. Nunez, P. (2006). Electric fields of the brain: The neurophysics of EEG. Second edition (New York: Oxford University Press).

2. Tenke, C.E., Schroeder, C.E., Arezzo, J.C., and Vaughan Jr., H.G. (1993). Interpretation of high-resolution current source density profiles: a simulation of sublaminar contributions to the visual evoked potential. Exp. Brain Res. 183-192.

3. Steinschneider, M., Tenke, C.E., Schroeder, C.E., Javitt, D.C., Simpson, G.V., Arezzo, J.C., and Vaughan Jr., H.G. (1992). Cellular generators of the cortical auditory evoked potential initial component. Electroencephalography and Clinical Neurophysiology - Evoked Potentials *2,* 196-200.

4. Whittingstall, K., and Logothetis, N.K. (2009). Frequency-band coupling in surface EEG reflects spiking activity in monkey visual cortex. Neuron *2,* 281-9.

5. Gloor, P. (1985). Neuronal generators and the problem of localization in electroencephalography: Application of volume conductor theory to electroencephalography. Journal of Clinical Neurophysiology *4,* 327-354.

6. Cooper, R., Winter, A.L., Crow, H.J., and Walter, W.G. (1965). Comparison of Subcortical, Cortical and Scalp Activity Using Chronically Indwelling Electrodes in Man. Electroencephalogr Clin Neurophysiol 217-28.

7. Murakami, S., and Okada, Y. (2006). Contributions of principal neocortical neurons to magnetoencephalography and electroencephalography signals. J Physiol *Pt 3,* 925-36.

8. Cosandier-Rimele, D., Merlet, I., Badier, J.M., Chauvel, P., and Wendling, F. (2008). The neuronal sources of EEG: modeling of simultaneous scalp and intracerebral recordings in epilepsy. Neuroimage *1,* 135-46.

9. Telenczuk, B., Nikulin, V.V., and Curio, G. (2010). Role of neuronal synchrony in the generation of evoked eeg/MEG responses. J. Neurophysiol. *6,* 3557-3567.

10. Detsch, O., Erkens, U., Jacofsky, U., Thiel, A., Kochs, E., and Hempelmann, G. (1997). Topographical analysis of the EEG effects of a subconvulsive dose of lidocaine in healthy volunteers. Acta Anaesthesiol. Scand. *8,* 1039-1046.

11. Rauch, A., Rainer, G., Augath, M., Oeltermann, A., and Logothetis, N.K. (2008). Pharmacological MRI combined with electrophysiology in non-human primates: Effects of Lidocaine on primary visual cortex. Neuroimage *2,* 590-600.

12. Fozzard, H.A., Lee, P.J., and Lipkind, G.M. (2005). Mechanism of local anesthetic drug action on voltage-gated sodium channels. Curr Pharm Des *21*, 2671-86.

13. Logothetis, N.K., Merkle, H., Augath, M., Trinath, T., and Ugurbil, K. (2002). Ultra high-resolution fMRI in monkeys with implanted RF coils. Neuron *2*, 227-242.

14. Sheinberg, D.L., and Logothetis, N.K. (2001). Noticing familiar objects in real world scenes: the role of temporal cortical neurons in natural vision. J Neurosci *4*, 1340-50.

15. Boehnke, S.E., and Rasmusson, D.D. (2001). Time course and effective spread of lidocaine and tetrodotoxin delivered via microdialysis: An electrophysiological study in cerebral cortex. J. Neurosci. Methods *2*, 133-141.

16. Delorme, A., and Makeig, S. (2004). EEGLAB: an open source toolbox for analysis of single-trial EEG dynamics including independent component analysis. J Neurosci Methods *1*, 9-21.

17. Bollimunta, A., Mo, J., Schroeder, C.E., and Ding, M. (2011). Neuronal mechanisms and attentional modulation of corticothalamic alpha oscillations. Journal of Neuroscience *13*, 4935-4943.

18. Bollimunta, A., Chen, Y., Schroeder, C.E., and Ding, M. (2008). Neuronal mechanisms of cortical alpha oscillations in awake-behaving macaques. Journal of Neuroscience *40*, 9976-9988.

19. Maier, A., Aura, C.J., and Leopold, D.A. (2011). Infragranular sources of sustained local field potential responses in macaque primary visual cortex. Journal of Neuroscience *6*, 1971-1980.

20. Maier, A., Adams, G.K., Aura, C., and Leopold, D.A. (2010). Distinct superficial and deep laminar domains of activity in the visual cortex during rest and stimulation. Frontiers in Systems Neuroscience 31.

21. Ray, S., Crone, N.E., Niebur, E., Franaszczuk, P.J., and Hsiao, S.S. (2008). Neural correlates of high-gamma oscillations (60-200 Hz) in macaque local field potentials and their potential implications in electrocorticography. J Neurosci *45*, 11526-36.

22. Ray, S., and Maunsell, J.H.R. (2011). Different origins of gamma rhythm and high-gamma activity in macaque visual cortex. PLoS Biology *4*,

23. Hentschke, H., Schwarz, C., and Antkowiak, B. (2005). Neocortex is the major target of sedative concentrations of volatile anaesthetics: Strong depression of firing rates and increase of GABAA receptor-mediated inhibition. Eur. J. Neurosci. *1*, 93-102.

24. Greenberg, D.S., Houweling, A.R., and Kerr, J.N. (2008). Population imaging of ongoing neuronal activity in the visual cortex of awake rats. Nat Neurosci *7*, 749-51.

25. Antkowiak, B., and Helfrich-Forster, C. (1998). Effects of small concentrations of volatile anesthetics on action potential firing of neocortical neurons in vitro. Anesthesiology 1592-1605.

26. Murphy, M., Bruno, M.-., Riedner, B.A., Boveroux, P., Noirhomme, Q., Landsness, E.C., Brichant, J.-., Phillips, C., Massimini, M., Laureys, S. *et al.* (2011). Propofol anesthesia and sleep: A high-density EEG study. Sleep *3,* 283-291.A.

27. Maksimow, A., Särkelä, M., Långsjö, J.W., Salmi, E., Kaisti, K.K., Yli-Hankala, A., Hinkka-Yli-Salomäki, S., Scheinin, H., and Jääskeläinen, S.K. (2006). Increase in high frequency EEG activity explains the poor performance of EEG spectral entropy monitor during S-ketamine anesthesia. Clinical Neurophysiology *8,* 1660-1668.

28. Antkowiak, B. (2002). In vitro networks: Cortical mechanisms of anaesthetic action. Br. J. Anaesth. *1,* 102-111.

29. Kreuzer, M., Hentschke, H., Antkowiak, B., Schwarz, C., Kochs, E., and Schneider, G. (2010). Cross-approximate entropy of cortical local field potentials quantifies effects of anesthesia - a pilot study in rats. BMC Neuroscience *1,* 122.

30. Tanaka, K., and Yamasaki, M. (1966). Blocking of cortical inhibitory synapses by intravenous lidocaine [27]. Nature *5019,* 207-208.

31. Cohen, M.R., and Maunsell, J.H. (2009). Attention improves performance primarily by reducing interneuronal correlations. Nat Neurosci *12,* 1594-600.

32. Wiechert, M.T., Judkewitz, B., Riecke, H., and Friedrich, R.W. (2010). Mechanisms of pattern decorrelation by recurrent neuronal circuits. Nat. Neurosci. *8,* 1003-1010.

33. Nunez, P.L., and Silberstein, R.B. (2000). On the relationship of synaptic activity to macroscopic measurements: does co-registration of EEG with fMRI make sense? Brain Topogr *2,* 79-96.

34. Yesilyurt, B., Whittingstall, K., Ugurbil, K., Logothetis, N.K., and Uludag, K. (2010). Relationship of the BOLD signal with VEP for ultrashort duration visual stimuli (0.1 to 5 ms) in humans. J Cereb Blood Flow Metab *2,* 449-58.

35. Meltzer, J.A., Fonzo, G.A., and Constable, R.T. (2009). Transverse patterning dissociates human EEG theta power and hippocampal BOLD activation. Psychophysiology *1,* 153-162.

36. Buzsáki, G., and Draguhn, A. (2004). Neuronal olscillations in cortical networks. Science *5679,* 1926-1929.

37. Torrealdea, F.J., D'Anjou, A., Graña, M., and Sarasola, C. (2006). Energy aspects of the synchronization of model neurons. Physical Review E - Statistical, Nonlinear, and Soft Matter Physics *1,*

38. Guevara, M.A., and Corsi-Cabrera, M. (1996). EEG coherence or EEG correlation? Int J Psychophysiol *3*, 145-53.

39. Ramírez, D., Via, J. and Santamaría, I. Paper presented at ICASSP, IEEE International Conference on Acoustics, Speech and Signal Processing - Proceedings.

Table 1

Freq.Band	δ	θ	α	β	Low γ	High γ
$r_{EEG,LFP}$	0.27	0.23	0.19	0.33	0.43	0.62
$r_{EEG,SC}$	0.22	0.24	0.15	0.19	0.25	0.54

Figure 1

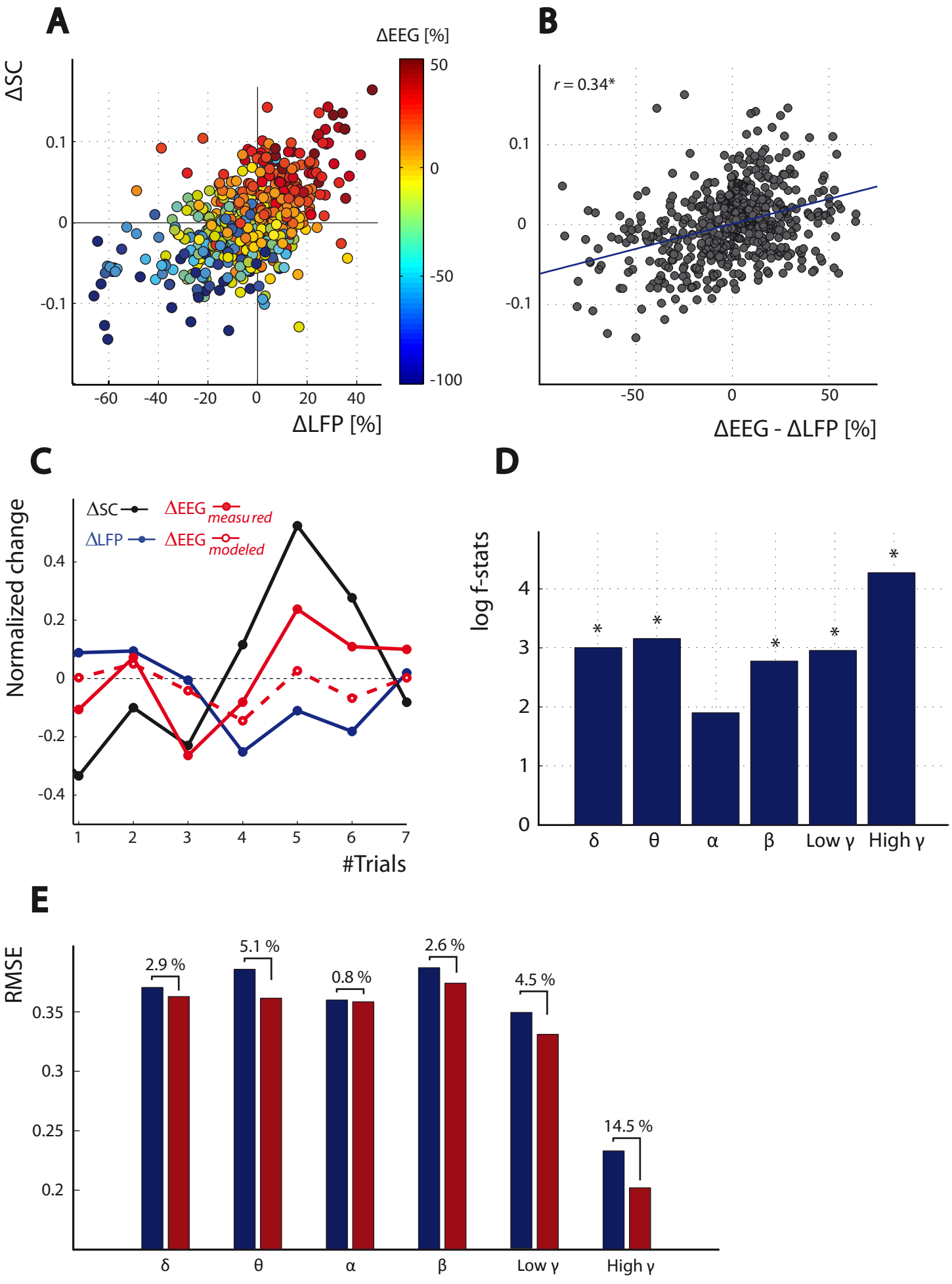
A
ΔEEG [%]
50
0
-50
-100
ΔSC
0.1
0
-0.1
-60
-40
-20
0
20
40
ΔLFP [%]
B
r = 0.34*
0.1
0
-0.1
-50
0
50
ΔEEG - ΔLFP [%]
C
ΔSC
ΔEEG measured
ΔLFP
ΔEEG modeled
Normalized change
0.4
0.2
0
-0.2
-0.4
1
2
3
4
5
6
7
#Trials
D
log f-stats
4
3
2
1
0
*
δ
θ
α
β
Low γ
High γ
E
RMSE
0.35
0.3
0.25
0.2
2.9 %
5.1 %
0.8 %
2.6 %
4.5 %
14.5 %
δ
θ
α
β
Low γ
High γ

Figure 2

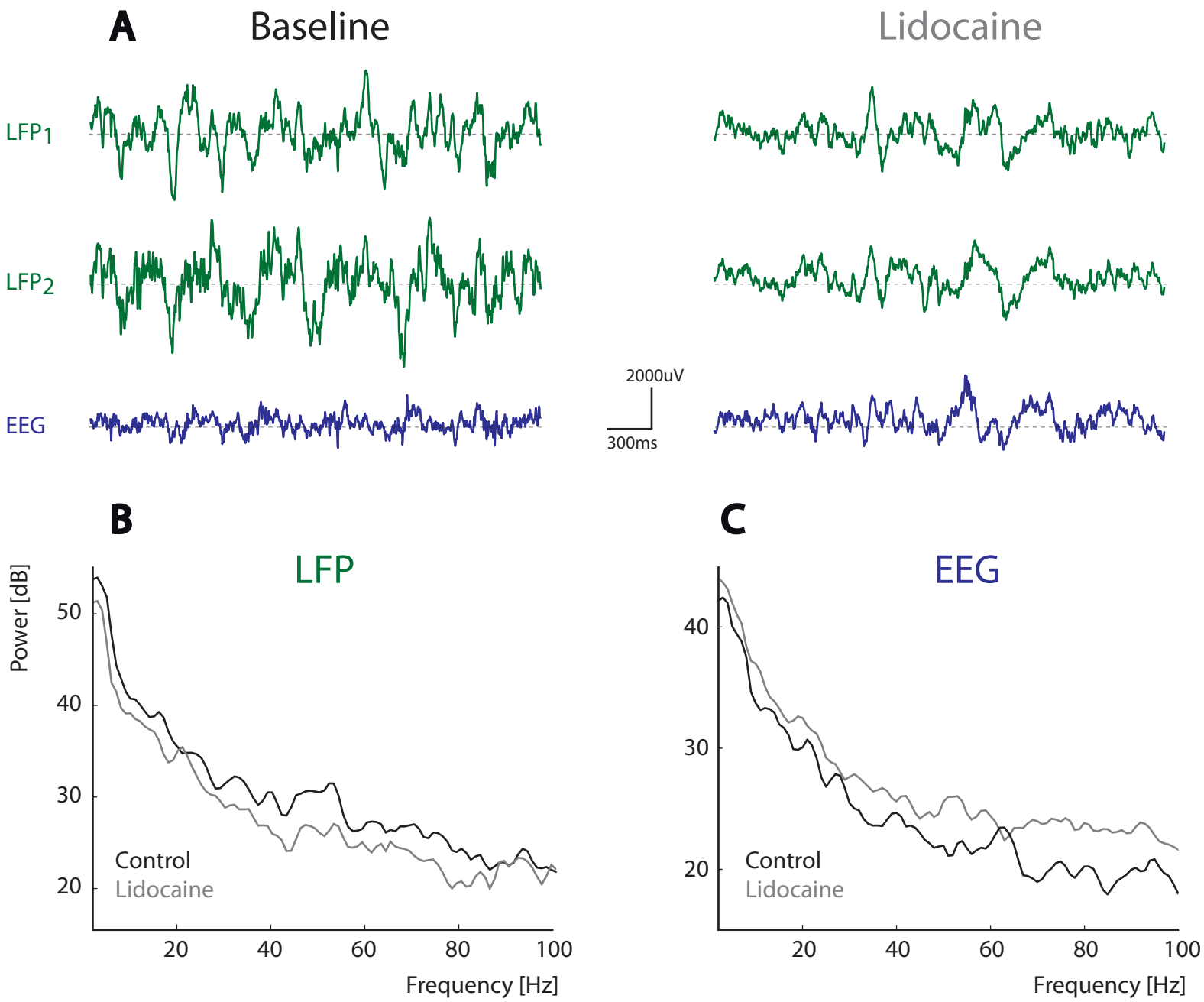
A
Baseline
Lidocaine
LFP1
LFP2
EEG
2000uV
300ms
B
LFP
Power [dB]
50
40
30
20
Control
Lidocaine
20
40
60
80
100
Frequency [Hz]
C
EEG
40
30
20
Control
Lidocaine
20
40
60
80
100
Frequency [Hz]

Figure 3

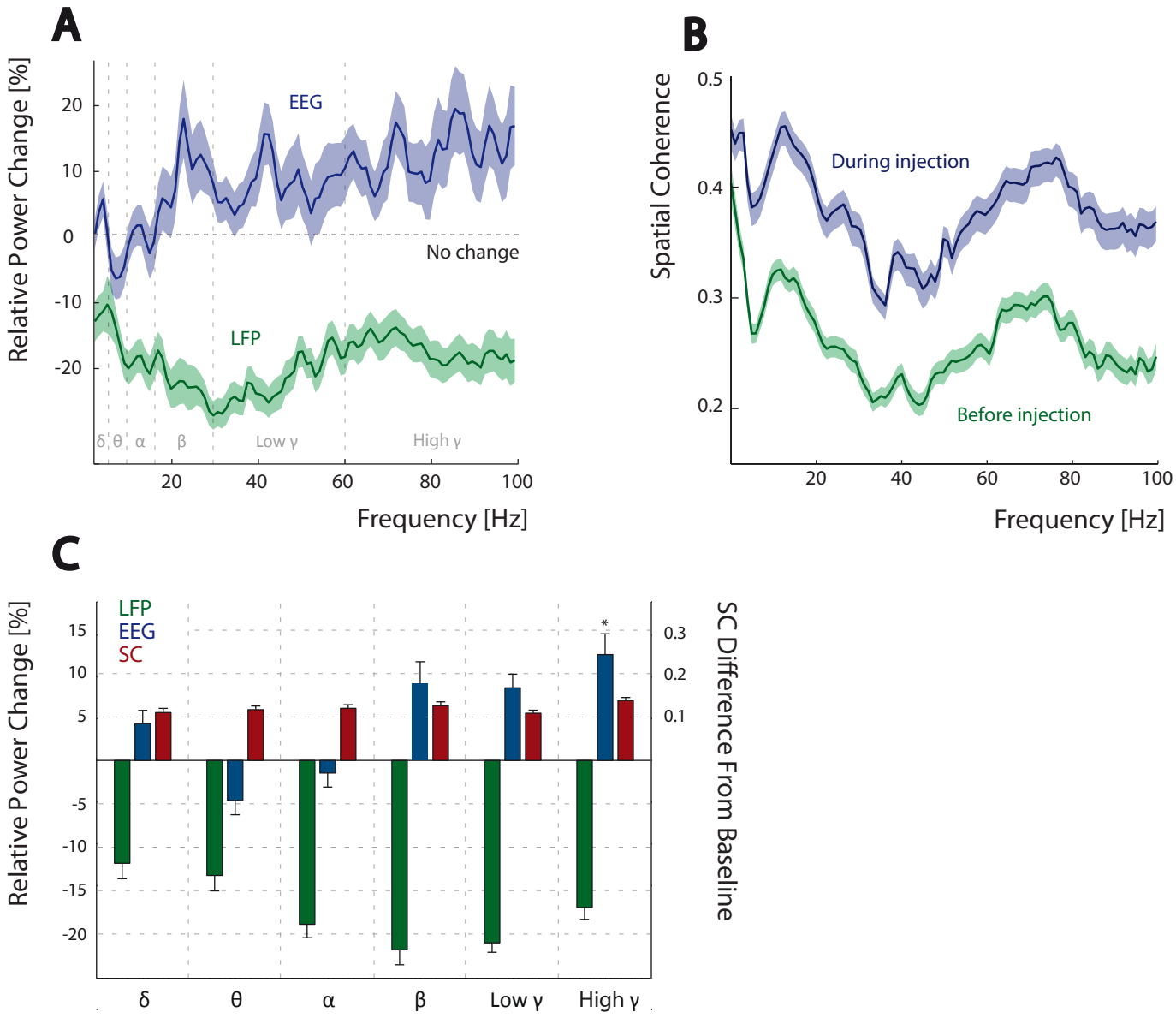
A
Relative Power Change [%]
EEG
LFP
No change
δ θ α β Low γ High γ
Frequency [Hz]
B
Spatial Coherence
During injection
Before injection
Frequency [Hz]
C
Relative Power Change [%]
LFP
EEG
SC
SC Difference From Baseline
δ θ α β Low γ High γ

Figure 4

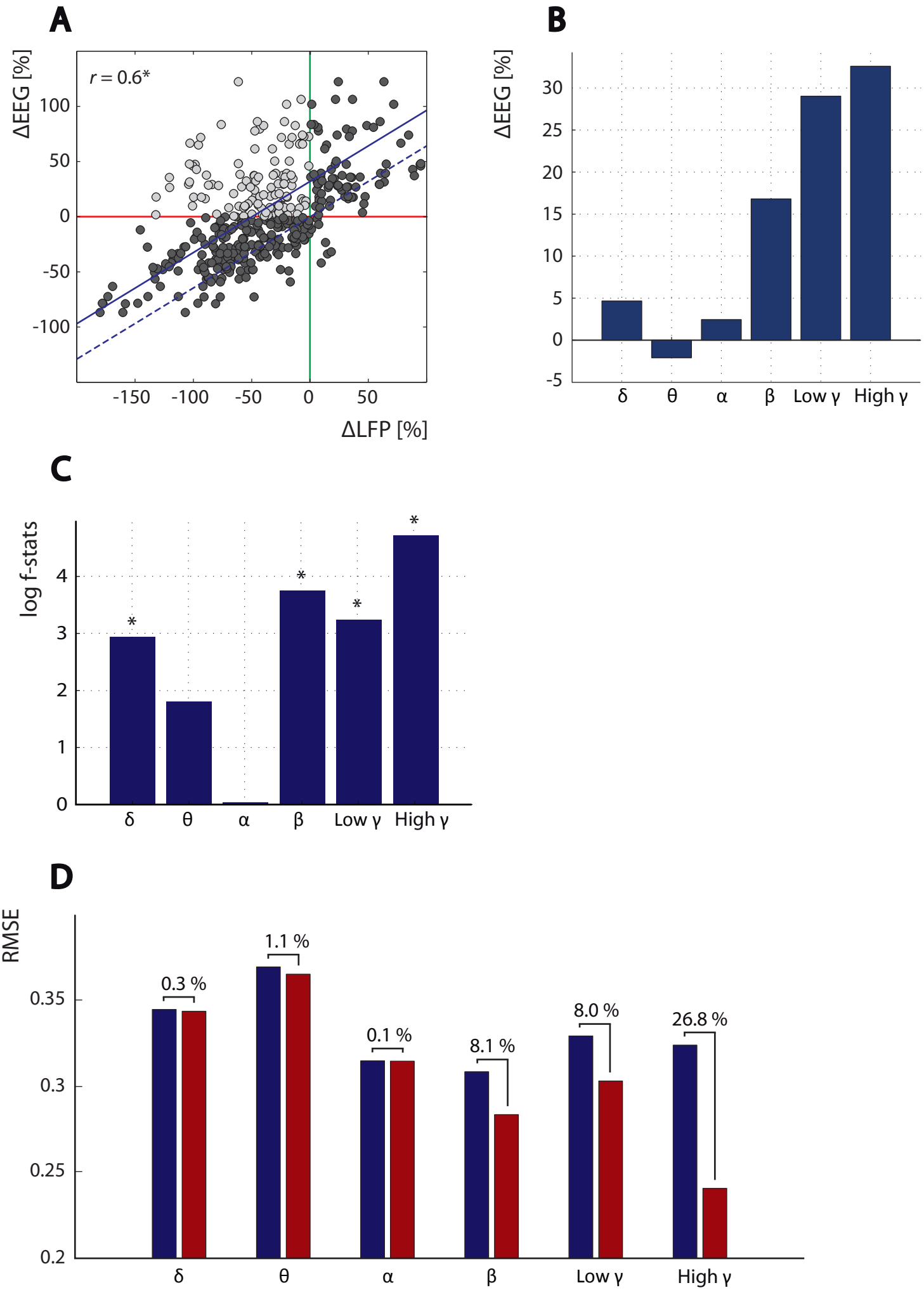
A
r = 0.6*
ΔEEG [%]
ΔLFP [%]
100
50
0
-50
-100
-150
-100
-50
0
50
B
ΔEEG [%]
30
25
20
15
10
5
0
-5
δ
θ
α
β
Low γ
High γ
C
log f-stats
4
3
2
1
0
*
δ
θ
α
β
Low γ
High γ
D
RMSE
0.35
0.3
0.25
0.2
0.3 %
1.1 %
0.1 %
8.1 %
8.0 %
26.8 %
δ
θ
α
β
Low γ
High γ

Figure S1

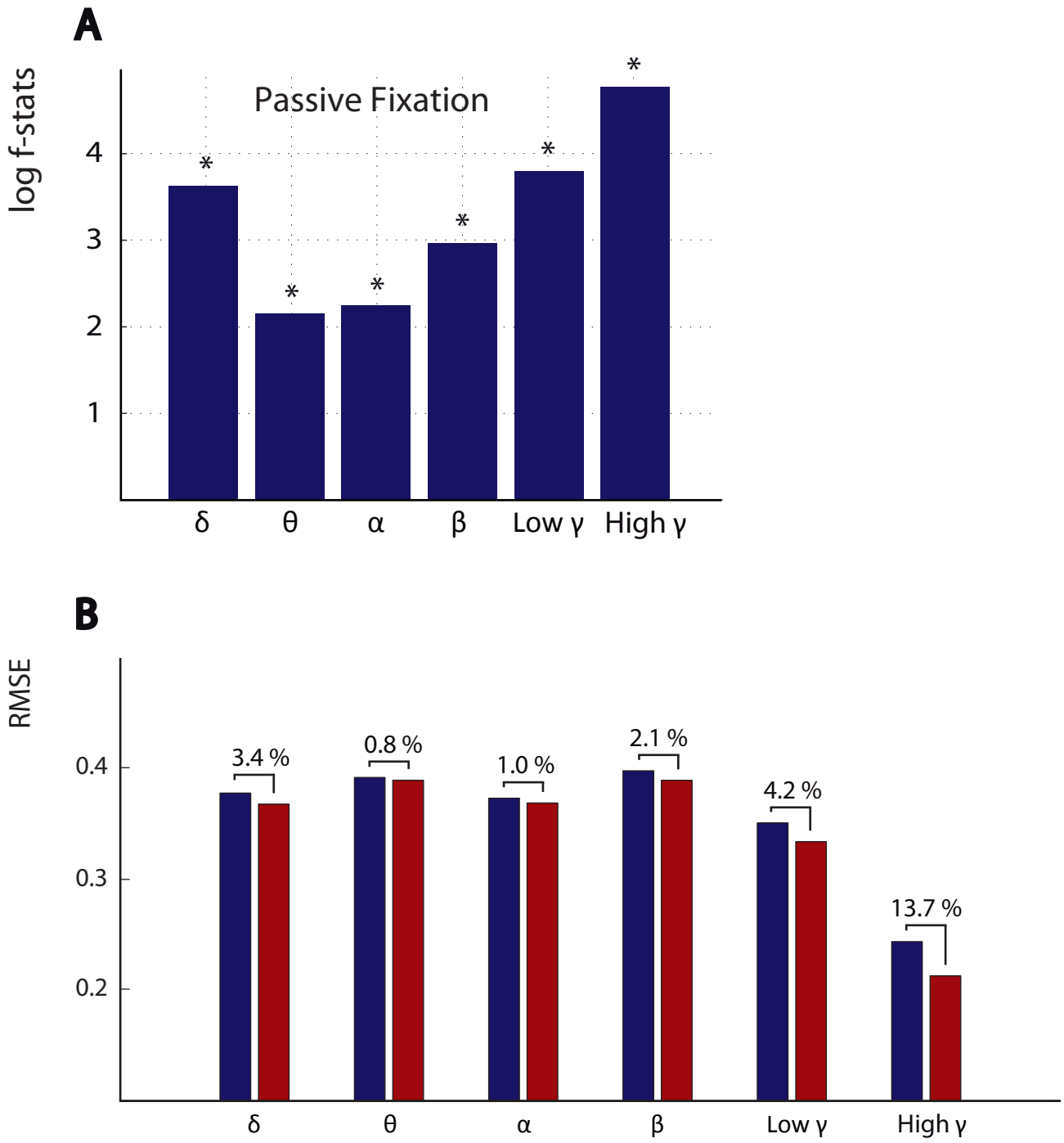
A
log f-stats
Passive Fixation
4
3
2
1
δ
θ
α
β
Low γ
High γ
B
RMSE
0.4
0.3
0.2
3.4 %
0.8 %
1.0 %
2.1 %
4.2 %
13.7 %
δ
θ
α
β
Low γ
High γ

Figure S2

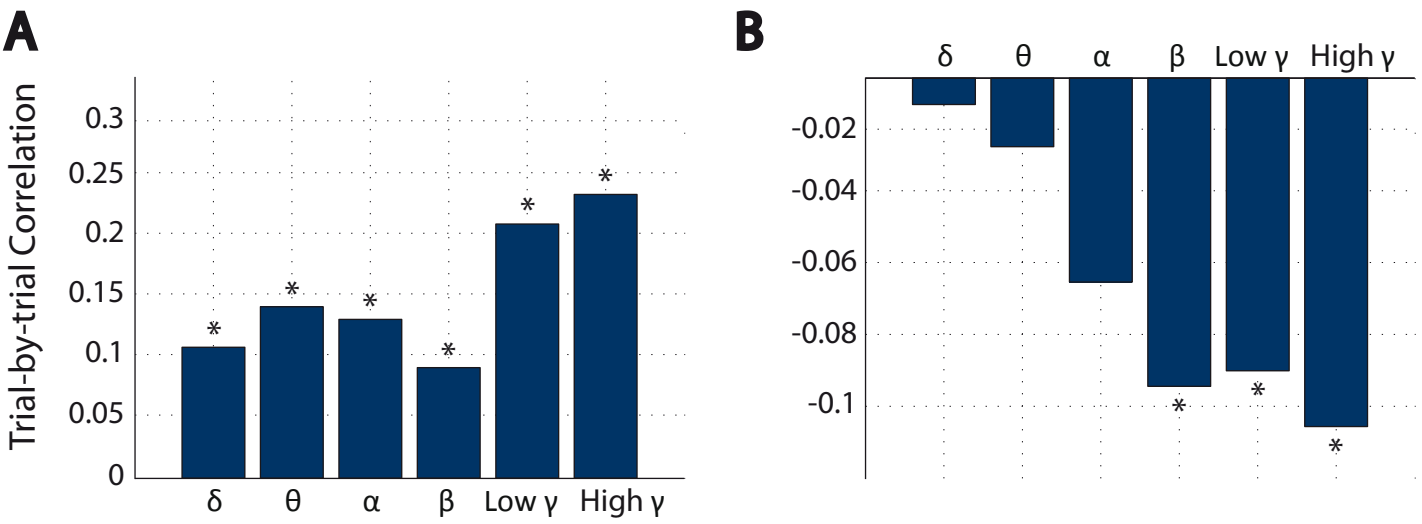
A
Trial-by-trial Correlation
0.3
0.25
0.2
0.15
0.1
0.05
0
δ
θ
α
β
Low γ
High γ
B
δ
θ
α
β
Low γ
High γ
-0.02
-0.04
-0.06
-0.08
-0.1

Figure S3

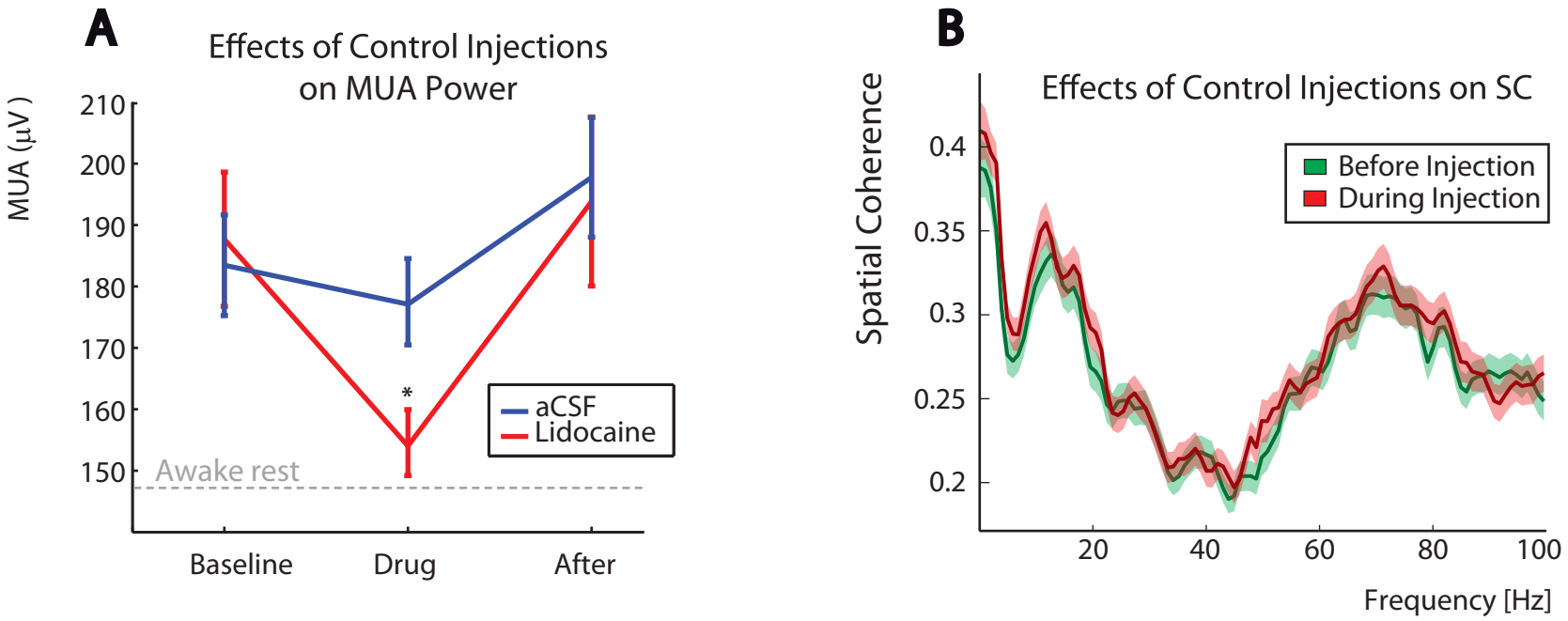
A
Effects of Control Injections
on MUA Power
MUA (μV)
210
200
190
180
170
160
150
Awake rest
*
aCSF
Lidocaine
Baseline
Drug
After
B
Effects of Control Injections on SC
Spatial Coherence
0.4
0.35
0.3
0.25
0.2
Before Injection
During Injection
20
40
60
80
100
Frequency [Hz]

Figure S4

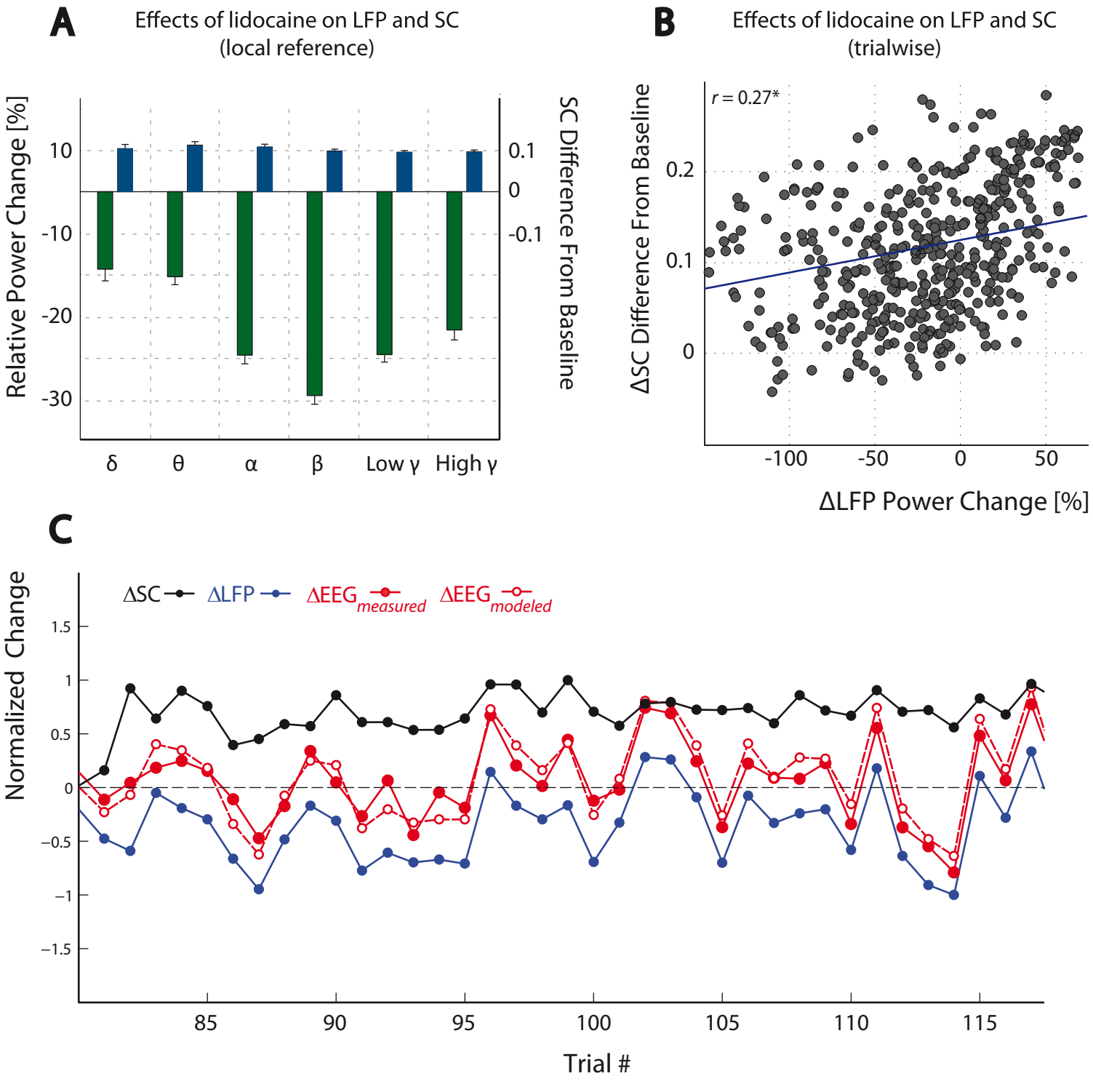
A
Effects of lidocaine on LFP and SC
(local reference)
Relative Power Change [%]
SC Difference From Baseline
10
-10
-20
-30
0.1
0
-0.1
δ
θ
α
β
Low γ
High γ
B
Effects of lidocaine on LFP and SC
(trialwise)
r = 0.27*
ΔSC Difference From Baseline
0.2
0.1
0
-100
-50
0
50
ΔLFP Power Change [%]
C
ΔSC
ΔLFP
ΔEEG measured
ΔEEG modeled
Normalized Change
1.5
1
0.5
0
−0.5
−1
−1.5
85
90
95
100
105
110
115
Trial #

Figure S5

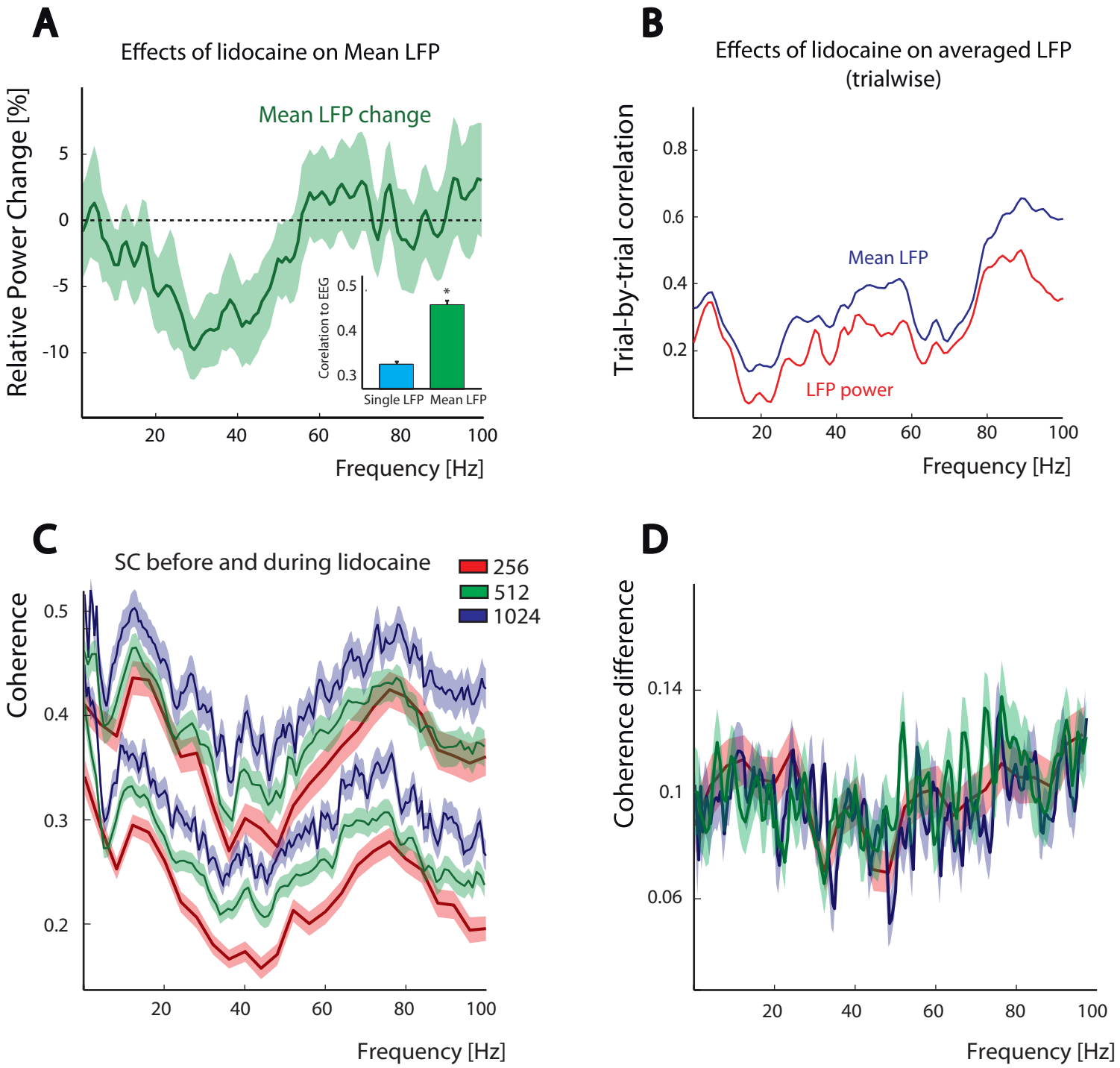
A
Effects of lidocaine on Mean LFP
Mean LFP change
Relative Power Change [%]
5
0
-5
-10
20
40
60
80
100
Frequency [Hz]
Corelation to EEG
0.5
0.4
0.3
*
Single LFP
Mean LFP
B
Effects of lidocaine on averaged LFP
(trialwise)
Trial-by-trial correlation
0.8
0.6
0.4
0.2
Mean LFP
LFP power
20
40
60
80
100
Frequency [Hz]
C
SC before and during lidocaine
256
512
1024
Coherence
0.5
0.4
0.3
0.2
20
40
60
80
100
Frequency [Hz]
D
Coherence difference
0.14
0.1
0.06
20
40
60
80
100
Frequency [Hz]